SURFACE PHOTOVOLTAGE STUDIES OF ENVIRONMENTAL INFLUENCE ON CHARGE DYNAMICS IN NANOSTRUCTURED SILICON

by

PUSKAR RAJ CHAPAGAIN

Master of Science, 2009
University of Minnesota
Duluth, MN

Submitted to the Graduate Faculty of College of Science and Engineering
Texas Christian University
in partial fulfillment of the requirements
for the degree of

Doctor of Philosophy

December 2015

SURFACE PHOTOVOLTAGE STUDIES OF ENVIRONMENTAL INFLUENCE ON CHARGE DYNAMICS IN NANOSTRUCTURED SILICON

by
Puskar Raj Chapagain

Dissertation approved:

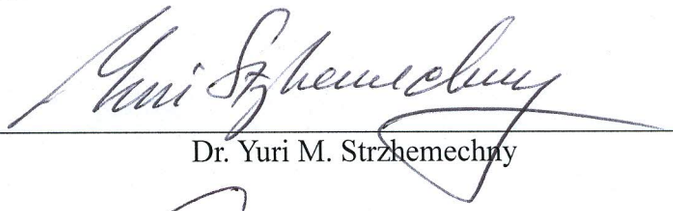

Dr. Yuri M. Strzhemechny

Dr. Zygmunt Gryczynski

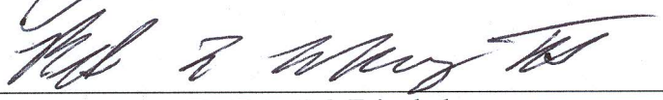

Dr. Peter M. Frinchaboy

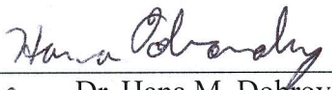

Dr. Hana M. Dobrovolny

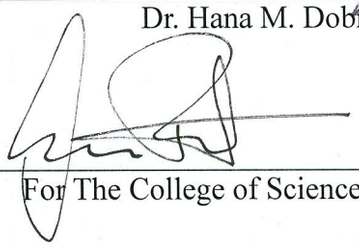

For The College of Science and Engineering

Acknowledgements

I would like to express my deepest gratitude to my advisor Dr. Yuri Strzhemechny for continuous support to my research, his guidance, patience, motivation, and immense knowledge.

I am also thankful to all of my lab partners and fellow graduate students for their valuable suggestions. Thanks to D. Yale, D. Carroll and G. Katchinska for their help in repairing and maintaining lab equipment.

I would also like to thank our collaborators; Dr. Petra Granitzer and Dr. Klemens Rumpf (University of Graz, Austria) for providing nanoporous silicon samples, Dr. Jeff Coffer (TCU Chemistry Department) for silicon nanotubes, Dr. Wieslaw Strek (Polish Academy of Sciences, Wroclaw, Poland) for graphene-based composites and Dr. Vadym Mochalin (Drexel University, PA) for nanodiamond samples.

Lastly, I would like to thank my family for their support and encouragement.

Contents

List of Figures

List of Tables

List of Abbreviations

CPD – Contact Potential Difference

GC – Graphene Based-Composite

NPS – Nanoporous Silicon

SCR – Space Charge Region

SEM – Scanning Electron Microscopy

SNT – Silicon nanotubes

SPV – Surface Photovoltage

TEM – Transmission Electron Microscopy

UHV – Ultra High Vacuum

Chapter 1

1. Introduction

The interest in nanoscale materials is driven by the uniqueness of phenomena occurring at this scale and the ensuing novel applications of these materials. In recent years, meso- and nanostructured silicon systems have become, among others, the focus of scientific and technological attention due to their emerging and potential use in biophysics, energy production/storage, industrial chemistry, gas sensors, optical detectors and luminous sources [1-5].

Due to the reduction in size, the properties of nanostructures are different from those of bulk materials sharing largely the same composition and microscopic structure. In particular, the surface-to-volume ratio increases dramatically and the surface effects become dominant. At the free surface of a semiconductor/dielectric crystal, due to the termination of the lattice, electronic states are created in the gap which are related to (a) intrinsic defects such as dangling bonds, kinks, vacancies, etc. and (b) extrinsic defects, such as sub-surface impurities as well as chemi- and physisorbed atoms and molecules. The presence of surface states induces drift- and diffusion-driven charge transfer between the bulk and the surface, which in turn modifies such surface electronic characteristics as the surface band bending, the surface carrier density and the surface state density [6]. Thereby, physisorption, chemisorption or desorption of environmental species at the surface are among the key processes affecting surface's electronic structure.

The surface band bending usually refers to the changes in the energy offset of the band structure at the surface. One way to monitor these changes is by means of photo-excitation, specifically for materials suitable for applications in photodetectors, photovoltaics, photocatalytic and photochemical devices. The photo-absorption is accompanied by charge

transfer from the surface to the bulk or vice-versa. The optimization of charge transfer processes at the surface by manipulation of the electronic structure is therefore a subject of great interest [7]. In this work, we investigate the influence of the environment on the surface band bending of illuminated surface of primarily a nanoporous silicon (NPS), as well as some other nanostructured materials.

NPS is an intricate network of nanoscale pores on the surface of silicon. A large interior surface area and porosity are two major features which make NPS suitable for device applications. In this regard the important figures of merit are the photoresponse, the surface conductivity and its type (*n*-type vs. *p*-type). As the silicon material is lost during the pore formation, it is believed that the NPS becomes depleted of the charge carriers possibly leading to flattening of the bands at the surface, which in turn can alter the surface photoconductivity [8]. It is necessary therefore to gauge the reaction of the surface conductivity in NPS to light. Since the surface of NPS is sensitive to the environment [9-11], it would be practical to understand the mechanisms through which the surface potential barrier of NPS is affected by the ambient pressure. Elucidating these phenomena in a wide range of pressures between the atmospheric pressure and high vacuum could be valuable for the potential application of NPS as gas sensors. The pressure of the system can significantly influence, among others, the interaction between the NPS surface and adsorbed species. For a given temperature and pressure, the rate of physisorption is many times faster than the chemisorption process. Thus there is a possibility of coexistence of multiple processes in the surface photoresponse of NPS occurring on different time scales and in different ambient pressures. Such findings could help explicating the roles of intrinsic and/or extrinsic surface states in the surface transport properties of NPS.

The performance of a gas sensor might be significantly affected by its response and the recovery times, and their dependence on stimulation by light. Therefore it is important to know

the typical ranges of values of these times in NPS. Of particular interest in our studies is detection of multiple components in the photo-induced charge recombination processes (e.g., relatively fast transient processes on a time scale of few seconds vs. much slower ones, e.g. thousands of seconds) for light-irradiated NPS in different environments. Moreover, studies of the ambient-dependent surface photoresponse can address another important performance parameter of a gas sensor, the reversibility, i.e., the ability of the sensing material to return to its original state after detection. We in our studies tackle this issue via studies of NPS surface photoreactivity by cycling it between vacuum and non-vacuum environments.

The photoconductivity processes could be affected not only by the ambient pressure but also by the type of the gas environment that the surface is exposed to. In order to investigate this aspect, systematic experimental studies of NPS are performed in our work employing variation of the ambients.

In our studies, for the photoexcitation of the NPS surfaces, we use mostly polychromatic illumination containing both super-bandgap and sub-bandgap photon energies. To further differentiate between dissimilar surface charge transport processes affected by adsorption/desorption we also employ monochromatic super- and sub-bandgap illumination for selective excitation of these processes.

The surface photoresponse could be affected not only by the excitation wavelength but also by the excitation intensity. By observing the rate at which the surface potential responds to changes in light intensity, we can gain insight of the dynamics of the photon-induced electronic transitions as the initial part of the response is dominated by optically stimulated carrier migration whereas the later part is dominated by thermally mediated processes. The rate of change of the surface barrier immediately after the onset of irradiation for most semiconductors in a bulk form was found to be linearly proportional to the illumination intensity [12], most

likely related to the fact that, as a rule, the bulk of the specimen can provide an essentially infinite supply of charges to the surface. Whether the same physical picture holds true for a nanoscale material, such as NPS, has not been adequately studied. Therefore in our work we look into this issue by carefully monitoring the initial photoresponse of the NPS surface to the incident illumination.

In certain applications the NPS pores could incorporate non-silicon containing fillers, e.g., metal nanoparticles. Such fusion of two different materials may give rise new electrical properties. In this work thereby we investigate photo-generated charge recombination processes in NPS embedded with metal nanoparticles in different environments.

Most of the measurements reported here were performed on NPS specimens. In order to understand whether the results observed for NPS are rather generic to nanoscale materials or specific to NPS we ran complementary experiments, similar to the ones discussed above, on silicon nanotubes (SNT) and graphene-based composites (GC) in different ambients.

In our studies to investigate all the phenomena of interest we utilized primarily an experimental technique known as surface photovoltage (SPV) a non-destructive and a highly surface-sensitive probe, the details of which will be discussed in the sections to follow.

1.1. Surface Band Bending

The free surface of a semiconductor can be defined as the boundary between the solid and its ambient. Since some of the surface atoms have an incomplete coordination number, this may cause a lattice rearrangement and a greater reactivity at the surface as compared to the bulk. Surface defects may give rise to almost discrete electronic states inside the semiconductor bandgap (e.g., the unpaired electronic vacancies in the dangling bonds of the surface atoms). As a result, the charge transfer becomes possible between the bulk and the surface states leading to a

surface band bending (cf. Fig. 1). Let us assume that the surface states are half filled and are located approximately in the middle of the gap of an undoped semiconductor (E_c and E_v are the bottom of the conduction band and the top of the valence band, respectively). In an undoped semiconductor the Fermi level of the bulk (E_F (bulk)) lies at the middle of the gap and thus no charge transfer occurs between the bulk and the surface – the so called surface flat band configuration (Fig. 1(a)). If the semiconductor is *n*-type, E_F (bulk) is located close to the bottom of the conduction band, enabling thus the bulk electrons to transfer to the surface states until E_F (bulk) is equal to E_F (surf) (Fig. 1 (b)). When the equilibrium is reached, the energy bands in this *n*-type semiconductor are bent upward near the surface (Fig. 1 (c)).

1.2. Effects of Environment on Nanoscale Surfaces

Surfaces of nanostructured materials could be extremely sensitive to atoms or molecules coming into their proximity, some of which may attach themselves to the surface. The process of attachment of environmental species to semiconductor surfaces is called adsorption while the process of their detachment is called desorption. Many factors may strongly affect the adsorption and desorption phenomena, such as the nature of the ambient, the type of the semiconductor, the initial surface band bending, as well as the temperature and the pressure of the environment. Environmental species could significantly alter the surface and near-surface electronic structure leading to a modified surface charge dynamics. For example, they can be bound by the surface defects and other adsorption sites thus generating new gap states or modifying the existing ones. Furthermore, at many semiconductor surfaces it is common to observe formation of a surface dipole layer. Its origin is in the "leaking out" of the electron density outside of surface boundary. It is natural to expect that the surface dipole layer might be also directly affected by the environment. Since some adsorbed species could have their own

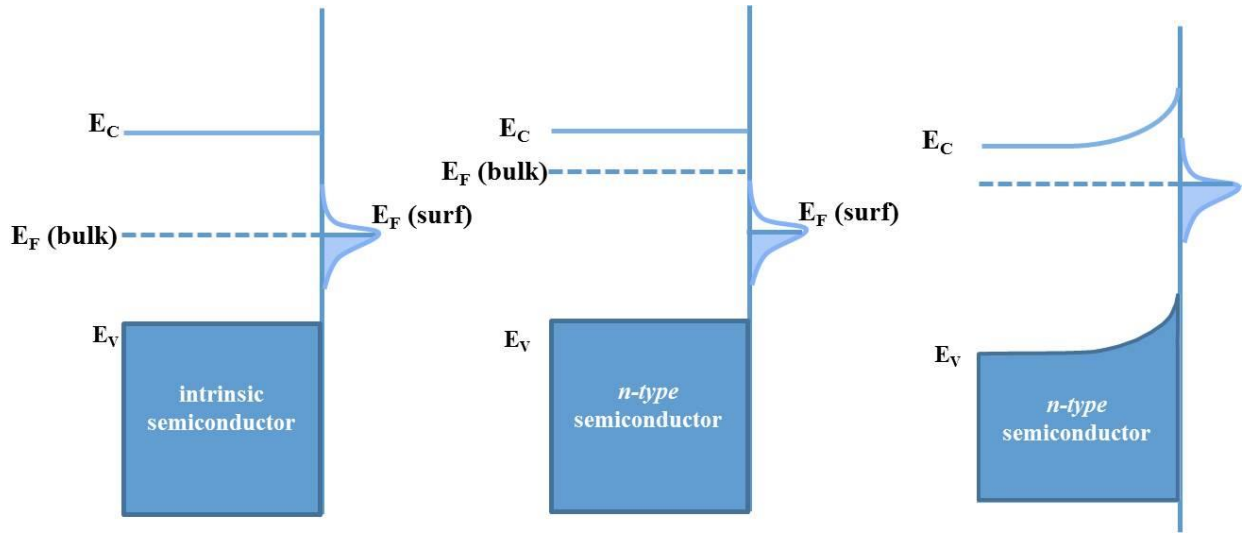

Figure 1 Schematic of surface band bending of clean semiconductor surface: (a) intrinsic semiconductor-flat band situation; (b) *n*-type semiconductor in non-equilibrium condition; (c) *n*-type semiconductor in equilibrium condition [13].

dipole moments, this would provide an additional contribution to the surface polarity. Interaction between dipoles, their formation and annihilation may also modify the surface charge dynamics. A significant amount of charge transfer may occur during the conversion of the physisorbed environmental species into chemisorbed ones or vice versa, leading to the change in the surface band bending.

Interaction of light with semiconductor surfaces, in the presence of a certain gas, may significantly change both adsorption and desorption. For example, light could stimulate the physi-/chemi- and chemi-/physi- conversions. The illumination-induced charge exchange between the intrinsic surface states and the adsorbed species could lead to the additional change in the surface band bending. Charge exchange with foreign species is a rather slow process. On the other hand removal of many of the physisorbed species from the surface can be achieved by evacuation. It is quite natural to expect a different behavior of the surface in a gaseous environment versus vacuum. Thereby, controlling the surface electronic structure by illumination in different ambients could be very beneficial, e.g. in gas sensor applications.

1.3. Nanoporous Silicon

Silicon is the most used material in modern electronic devices, and the demand for small-size devices drives the downscaling of silicon dimensions. Although the bulk form of crystalline silicon is extremely valuable for electronic applications, its usefulness for optical, magnetic or biophysical applications is rather limited. However, when the characteristic dimensions of silicon are reduced to nanoscale, dramatic changes are observed in its properties, opening a broad range of new nanotechnology applications. Because of light emitting properties and biocompatibility, nanostructured silicon is becoming a material of choice for optoelectronics and biomedical applications [14-15].

In general, porous silicon grown by anodization of a silicon wafer is a versatile material which can exhibit different morphologies depending upon the doping concentration of the wafer and other growth parameters. The investigated NPS samples were grown by anodization of highly *n*-doped (100) silicon (10^{19} cm^{-3}) in an aqueous hydrofluoric acid solution (courtesy of Dr. Petra Granitzer and Dr. Klemens Rumpf, University of Graz, Austria). The pores thus formed on the surface of silicon revealed an average diameter of 60 nm and a mean distance between the pores of 45 nm as shown by scanning electron microscopy (SEM) (Fig. 2 (a)). By varying the current density and the electrolyte concentration, NPS of different morphologies can be obtained. Nickel particles were electrochemically deposited within the pores of the bare NPS [16]. Fig. 2 (b) shows an SEM image of a Ni-filled NPS sample with deposits of approximately 100 nm in size.

Porous silicon was first synthesized in 1956 by Uhlir during electropolishing of silicon [17]. Since then, this material has not attracted significant attention until the discovery of its visible light emitting properties observed on anodized *p*-type silicon [18]. Since then extensive investigations of NPS luminescence have been carried out with a multiplicity of possible mechanisms proposed to explain the observed behavior. It is well known that the luminescence efficiency in conventional bulk silicon is very low, primarily due to its narrow indirect bandgap. The emission from nanoscale silicon is possible because of the reduction of dimensions, and consequently the increased uncertainty of the momentum vector. This effectively makes the bandgap pseudo-direct, allowing the electron-hole pairs to recombine [19]. Thus efficient red luminescence has been attributed to the 2D quantum confinement within silicon quantum wires leading to a broadening of the bandgap [20]. The blue-green emission has been attributed to direct transitions in nanometer sized Si crystallites [21], defects in SiO_2 [22], thin silicon

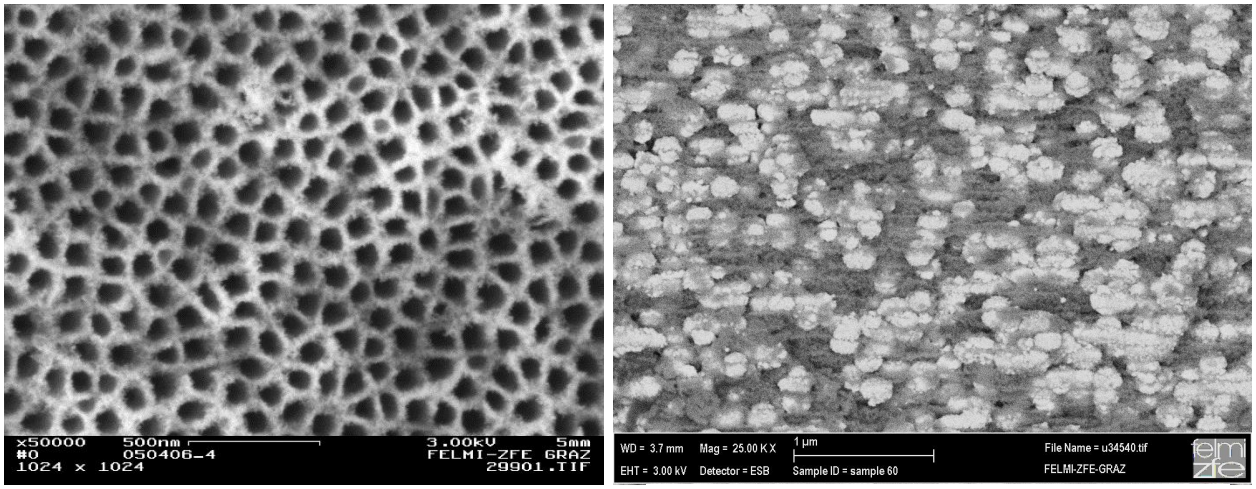

(a) Top view of pristine NPS (b) Cross-section of Ni-filled NPS

Figure 2 (a) Top view of pristine NPS with pore-diameter ~ 60 nm, distance between pores ~ 45 nm and thickness of porous layer ~ 35 µm. (b) Cross-sectional region of Ni-filled NPS.

quantum wires [23], surface states of silicon nanoparticles [24], siloxene-like clusters [25] or to OH groups adsorbed on structural defects in SiO_2 [26].

The relatively wide bandgap of porous silicon, as measured by different optoelectronic probes such as photoluminescence, electroluminescence and photoabsorption is still a subject of debate [27-30]. Generally two models are used to explain this bandgap broadening phenomenon. The first one is based on the radiative recombination of quantum-confined electrons and holes in columnar structures or wires associated with the creation of pores and the other model is based on the presence of hydrogen or siloxene-like complexes at the porous silicon surface [31]. In addition to optical techniques, electrical methods have been used to investigate the properties of porous silicon [32], all pointing to the bandgap broadening.

Not only the interaction of photons with the surface of NPS play an important role in the surface optoelectronic properties, but the surface can also be influenced by its chemical environment. Atoms or molecules of gas from the environment can physisorbed, chemisorbed or desorbed from the surface of NPS. NPS has drawn considerable attention because of the huge values of the surface-to-volume ratio as well as porosity (the fraction of the volume occupied by the pores with respect to the volume of the material), both of which render this material suitable for solar cells [33], sensors [34], and biological probes [35]. Thus it is interesting to understand how charge dynamics of illuminated surface is affected by different environments.

NPS oftentimes contains a very thin layer of native oxide, adding an extra surface, the SiO_2/Si interface. A large variety of extrinsic and intrinsic states at both the SiO_2 surface and at the interface between Si and SiO_2 has been reported in the literature (for example [36], [37]). When the surface of NPS is illuminated, the charge transfer could occur via many of these states, and the rate of this transfer may occur on different time scales depending on the channel. For example, for the surface-adsorbed species it could take a longer time as the bulk charge has to

overcome the high near-surface barrier. Moreover, the pressure of the environment determines the interaction between adsorbed species and NPS. At high pressures the surface adsorbates which tend to leave the surface are continuously colliding with atoms or molecules of the gas. As a result, these species are brought back to the surface and temporarily physisorbed to the surface whereas in high vacuum the physisorbed atoms or molecules are released from the surface during evacuation. Adsorption/desorption processes of foreign species at the surface can significantly modify the existing surface states and affect the surface charge dynamics. *Thus in this paper we investigate the influence of the ambient pressure on the surface electronic structure of NPS, and the surface band bending in particular, during photostimulation*.

Studies of the surface transport properties in different gaseous ambients can help establish performance benchmarks for potential applications of NPS in optoelectronic gas sensors. It could also allow better understanding of the separate roles played in the photo-induced charge exchange by the Si/SiO_2 interface and NPS free surface, as well as finding the reactivity and photochemistry of the NPS surface. Moreover, determining the response and recovery times in light and dark would be beneficial for improving performance of NPS-based optoelectronic gas sensors in applications.

Previously only a few studies on the subject were carried out, separately either in vacuum [38] or air [39, 40], and thus there is a significant shortage of comparative studies between vacuum and various non-vacuum environments, which motivated us to perform experiments on the NPS surface response to different ambient gases. In ref [40], an abrupt change in surface voltage was observed when traces of methanol and ammonia were introduced into dry air at normal temperature and pressure. This change was attributed to the photoinduced transitions from and to the surface states generated by the gas species. However, this work could not explain the similarity of the observed behavior in the dark and under illumination. In a different

report, SPV measurements on NPS on a substrate and in a free-standing form were carried out in vacuum using pulsed laser to characterize processes occurring on rather short time scales (within a few seconds) [41]. For the free standing samples the barrier height was found to be correlated with porosity. The samples with a low porosity revealed a two-fold change in the photoresponse resulting in both fast and slow processes whereas the samples with a high porosity revealed only the slow process. The fast process was attributed to the drift of carriers at the space charge layer whereas the slow process was assigned to diffusion. Another investigation on the topic in NPS indicated that the excess carrier recombination at the boundary of the porous layer and the substrate contribute to both fast and slow processes [39]. In our work we perform systematic measurements involving variation of multiple experimental parameters to elucidate the influence of ambients on the light-stimulated surface charge dynamics in NPS in order to formulate a robust model describing studied phenomena.

For the photovoltaic types of applications of NPS, it is necessary to determine such physical quantities as the excess carrier mobility, the recombination lifetime, the absorption coefficient, and the band gap of the material. Among these quantities, the photo-carrier recombination lifetime plays an important role in determining the efficiency of a solar cell because it limits the proportion of photo-generated charges collected by the electrodes. The recombination lifetime of photo-excited carriers is defined as the time between light absorption and recombination. In general, large recombination times are desirable for solar cells [42]. However, measurements of these times in such nanostructured materials as NPS are challenging because of the indirect bandgap, small film thickness and porosity. Generally the carrier lifetime could be affected by the presence of interfaces, doping, carrier density, etc. Therefore, employment of SPV, a contactless, non-destructive and highly surface-sensitive technique is

most adequate for determining the recombination lifetimes and the bandgap in such delicate and thin layered material as NPS.

In many cases, loss of silicon during the anodization process results in the several orders of magnitude decrease of the electrical conductivity in the host silicon material. Numerous works [44-48] attributed this to a substantial loss of free charge carriers in NPS. Such loss could result in some cases in the flattening of the band edges at the surface and a disappearance of the surface photoresponse. Therefore, for a good control of the sensing behavior it is important to know the surface conductivity type of NPS. It has been found that the conductivity type in porous silicon could be different from that of the original bulk sample [49]. *In this regard, one of the questions arising in our studies is about the conductivity type of the studied NPS specimens*. As the electronic properties of porous silicon could be very sensitive to environmental gases [50], the adsorbates may also change the type of surface conductivity. For example, when traces of NO_2 and NH_3 are introduced onto a *p*-type surface of NPS a dramatic change is observed, most likely due to hole trapping [51]. In this report, the transient response in the gas ambient revealed a sharp increase and a quick response on the rising front, with a slower component that never reached saturation. During evacuation, a response similar but opposite to that in the case of the gas insertion was observed. Such anomalous behavior has not been studied in detail and has not been adequately explained. In our work we address such anomalies and incorporate their explanation into our model.

In recent years luminescence properties of NPS covered with thin insulting layer have been actively investigated. However, the photo-transport properties of these systems have been considered in very few works. In particular, the surface band bending related to the slow relaxation time is still not clearly understood. Charge trapping with relaxation times of the order of several minutes and longer was detected in oxidized porous silicon [38]. Both positive and

negative surface bending was detected when the samples were irradiated with photon of different energies. The opposite nature of band bending was attributed to the changes of the electron/hole trapping by surface states following thermal annealing of the porous silicon. Photoconductivity [52] and photovoltage [53] of metal/NPS junctions in the visible spectral range also revealed multiple relaxation times. For example, a barrier change in the junction [54] was associated with the slow relaxation process. As a rule, metal contacts affect photoresponse detrimentally while the mechanisms leading to the slow relaxation time are still unclear, while little attention has been paid to the role of the absorbed species remaining at the free surface of NPS. To fill this gap, in our work we investigate whether the fast photoresponse mechanism is related to the intrinsic states and slow response to the extrinsic states.

Another factor that may control the surface photoresponse is the photon energy(ies) of the incoming radiation. Surface charge saturation can be achieved by using both super- and sub-bandgap excitation. In the case of a sub-bandgap illumination, direct excitation of the surface states takes place and it depends only on the optical cross-sections of the states. As a result, optical processes dominate the thermal ones yielding a fast response. In the case of a super-bandgap excitation, the surface states are not excited directly, rather their population is modified via trapping of photo-induced excess carriers from the bands. Thus, in this case the energy positions of the surface states and their thermal cross-sections (which control thermal generation/recombination) may compete with the optical processes [6]. As a result we may obtain a coexistence of multiple components in the surface charge dynamics occurring on different time scales. Although multi-component response was observed in GaN [55], $SrTiO_3$ [56], $LaAlO_3$ [57], GaP [58] during the irradiation by either poly- or mono-chromatic light separately, no studies were performed to make a comparison between such excitations for the same material, and NPS is no exception in this regard. *In our work we investigate the effects of a*

monochromatic super-bandgap and sub-bandgap excitation (and their comparisons to the case of panchromatic excitation) on the surface band bending in NPS for different ambients. These studies provide additional information on the predominant mechanisms of the studied phenomena since they can separate contributions from intrinsic vs. extrinsic states, and also from the free NPS surface vs. the interface with the native oxide.

Along with the excitation wavelength, it has been found that the light intensities differing by orders of magnitude can significantly affect the dynamic of the surface photoresponse [58]. Different processes contributing to the photo-induced charge separation at a given wavelength are indeed affected by the illumination intensity, and one way to elucidate its effect is to monitor the initial rate at which the surface reacts to the onset of illumination. The response of the light-induced excess carriers is much faster than that due to thermal emission. As the initial response of the surface is due to purely optical excitation processes, it determines the speed of the charge separation in a semiconductor. In the case of common bulk semiconductors, the surface can receive charge from an essentially infinite reservoir of the bulk region. Whether this applies to nanostructured materials, with a significantly reduced bulk charge reservoir, has yet to be determined. Since in many cases charge dynamics in nanoscale material is significantly different from that of bulk semiconductors, it would be important to study the variation of the initial change in potential barrier in NPS vs. illumination intensity. In previous studies on the bulk semiconductors such as GaP [12], GaN [55], ZnO [59], CdS [60], it was found that the immediate response of surface potential change always varies linearly with the illumination intensitiy. *In this project, we investigate how the variation of illumination intensity affects the initial rate of change of the surface band bending in NPS*. While interpreting multiple charge recombination processes in bulk semiconductors, the surface is considered to be a major contributing factor and the most common mechanism for a photo-induced charge separation is

the drift of excess carriers due to an electric field present in the near-surface region. However, the change in the surface potential barrier could be also affected by a non-uniform absorption giving rise to diffusion which may also cause the charge separation. These two processes may occur simultaneously in a way such that their superposition would suppress the overall charge separation efficiency.

By embedding the pores of NPS with magnetic nanoparticles such as Ni and Co, it is possible to integrate the properties of nano-fillers with those of the semiconducting silicon which could be useful for dual sensory/spintronic [61] usage. *In this regard, an important question arises of what role if any may magnetic metal nano-fillers play in the surface photoresponse of such NPS-based composite material*. We thus performed appropriate studies of metal-infused NPS in vacuum and non-vacuum environments to compare the observed behavior with that of pristine NPS.

With all the issues listed above, it is obviously important to understand *whether the properties of NPS investigated here are generic for a wide class of nanostructured materials (including nanostructured silicon) or specific and maybe unique for NPS synthesized via anodization of bulk silicon*. To answer this question we studied the role of the ambient on the surface electronic structure of some other nanomaterials subjected to photostimulation. Among those materials were silicon nanotubes (SNT) and graphene-containing composites (GC). Below is the brief description of these samples as well as some rationale for employing them in our experiments.

SNT used in our studies was grown by the sacrificial template method (courtesy of Dr. Jeffery Coffer, Department of Chemistry, TCU). First, ZnO nanowires were grown on *p*-type wafers. Silicon was deposited on the surface of the ZnO nanowires using chemical vapor deposition of silane at 500°C and the ZnO core was removed by etching with HCl and NH_3 [62].

By varying the growth parameters, the nanotubes of different wall thickness and morphology were obtained. The cylindrical structures grown on the top of a silicon substrate are vertically aligned with a variable diameter and morphology whose dimensions are listed in Table 1.

Table. 1 Description of the studied SNT

Wall thickness	**Internal diameter**	**External diameter**	**Standard deviation**
~ 10 nm	~ 50 nm	~ 70 nm	± 2 nm
~ 25 nm	~ 35 nm	~ 85 nm	± 6 nm
~ 50 nm	~ 35 nm	~ 135 nm	± 10 nm

The diameters of these tubes are very small (a few hundred nanometers) compared to the length of the tubes (a few microns). Schematic of tube arrangement and a transmission electron microscopy (TEM) image of SNT with the largest diameters are as shown in Fig. 3 (a) and Fig. 3 (b), respectively. SNT are the material of choice for many new and potential optical and electrical applications because of the quasi-1D structure, large surface area and possible quantum confinement effects [63].

For example, as of today, SNT have found applications in photovoltaics [64], battery technology [65], hydrogen storage [66], and nanoscale drug delivery [67]. Because of the nanometer-size inter-tube separation, the morphology of SNT is similar to that of NPS. Since NPS has been already found to be electrically conductive, photoactive and sensitive to environment, one might expect that SNT could also be useful for gas sensing properties. *Thus in our work we studied the sensitivity of SNT to the ambient conditions, analogous to the one discussed in detail for NPS*.

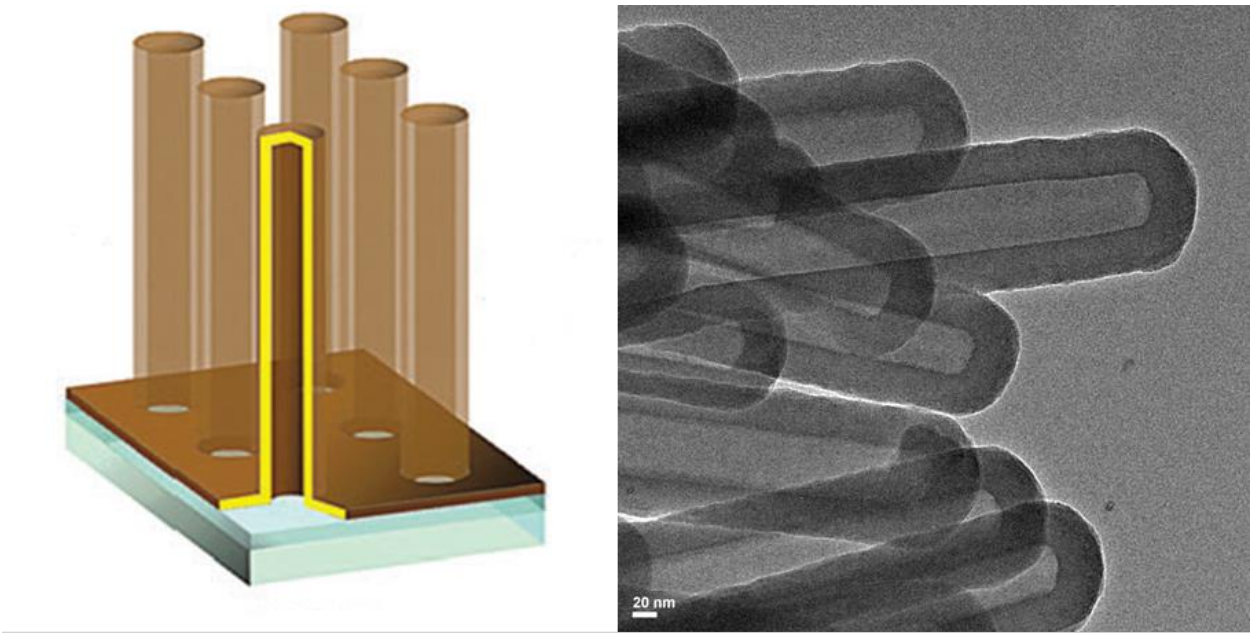

(a) (b)

Figure 3 (a) Schematic diagram of SNT sample grown by sacrificial template method. (b) TEM images of SNT with external diameters of (b) external diameter 135 nm [62].

One of the most interesting properties of SNT is photoconductivity which makes them suitable for applications in photodetectors and photovoltaics. Photoconductivity of SNT may be affected by the dimensions of the tube. The reduction in diameter of a nanoscale material commonly results in the increase of the surface state density thereby affecting mobility and diffusion length of minority carriers [69-70]. Thus correlating geometrical structure with surface-related optoelectronic properties would be quite informative. *In particular, an interesting question to tackle would be: does the SNT diameter affect its surface photovoltage?*

Another nanoscale material chosen for comparative studies was a graphene-based composite (GC) prepared by stacking 4-5 layers of commercially available nanoplatelets (courtesy of Dr. Wieslaw Strek, Institute of Low Temperatures and Structural Research of Polish Academy of Sciences, Wroclaw, Poland) (Fig. 4). Each nonoplatelet shares high surface area (600-750 m^2g^{-1}) with average thickness of 8 nm. The GCs were synthesized in the form of circular pellets as follows. First, cold pressing (at 0.2 GPa) was applied and circular pellets of diameter 6 mm and thickness 2 mm were obtained. These pellets were kept in calcium carbonate toroid and annealed by a heating source while keeping a thin layer of boron nitride between the source and the sample. Then a high pressure of 8 GPa was applied to each pellet under 500°C for 1 min. The GCs were then polished to remove the traces of boron nitride from the sample surface [71].

In general, graphene is a 2D network of sp^2 hybridized carbon atoms whereas GC consists of mixed hybridization of sp^2 and sp^3 along with the specific oxygen groups which may give extra properties that are not found in graphene. The presence of such functional groups containing oxygen in the basal plane and the edges provides the interaction sites for different organic and inorganic materials to GC [72, 73].

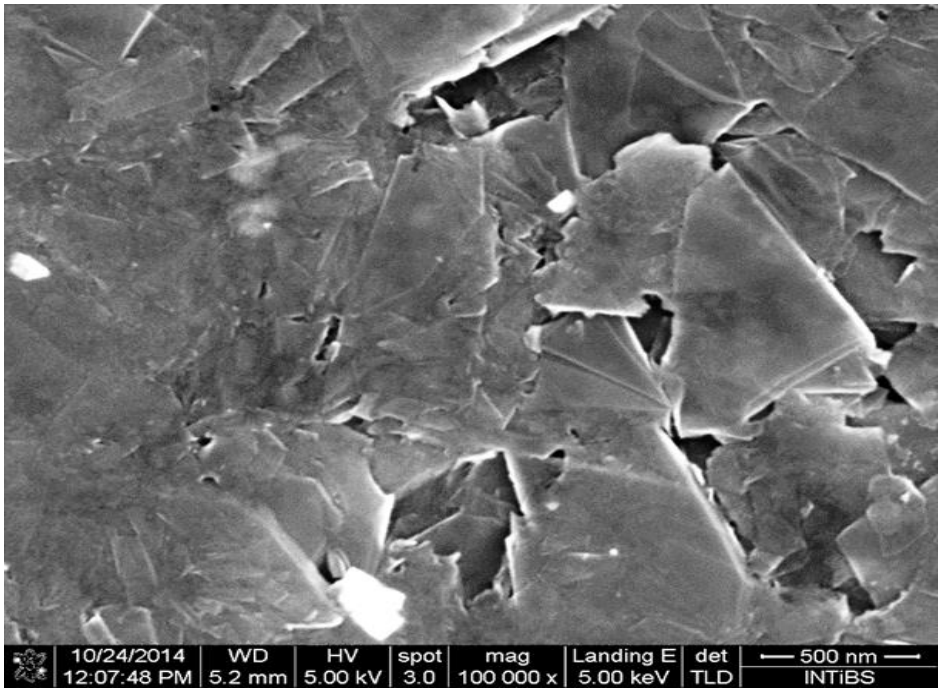

Figure 4 SEM of top surface of GC.

Application of many 2D nanostructures in gas sensors has gained a tremendous interest because of their high performance [74]. Particularly, the so called graphene oxide (GO) and reduced graphene oxide (rGO) have become promising materials for sensing because of the oxide-containing functional groups providing sites for physi- or chemisorption of foreign species when exposed to the environment [75]. Previous studies have revealed that the sensing mechanism in graphene-based materials is influenced not only by the defects and the functional groups in GO but also by the pristine region of the graphene [76]. The fast response to conductance change was attributed to the adsorption to sp^2-bonded carbon during gas introduction, whereas the molecular interaction with vacancies, structural defects, and oxygen functional groups is responsible for the slow response. Other experiments on GO have also proved that it could be a promising gas sensor to detect H_2 [77], NH_3/NO_2 [78], CO [79], etc. In all these reports the change in resistance or conductance was monitored in the presence and absence of a gas in proportion to the concentration. Most of research mentioned here has been performed for GO and rGO, and almost none on the optoelectronic behavior of graphene-containing composite materials in any environments, thus many questions about such phenomena remain essentially open. On the other hand, GC could be a cheap and efficient alternative to GO or rGO. In the present study, we employed white light to elucidate the role of surface species adsorbed at functional groups by performing separate experimental studies in nitrogen gas and in vacuum. The transport of excess carriers to/from the GC surface promotes the adsorption/desorption of foreign species, and therefore opens the potential usage of GC in optoelectronic gas sensors.

Chapter 2

2. Experimental

2.1. Basic Principles of Surface Photovoltage (SPV)

In SPV experiments one monitors the changes in the surface potential due to the illumination either vs. the incident light wavelength (SPV spectroscopy) or vs. time (transient SPV). In this work we used primarily the transient SPV mode to investigate the surface band bending of nanoscale silicon in different ambients. In the process of obtaining SPV transients, the surface is irradiated either with super-bandgap illumination (photons of energy greater than or equal to the bandgap) or sub-bandgap illumination (photons of energy smaller than the bandgap) to equilibrate the surface potential in light, and then the illumination is turned off, leaving the surface potential to saturate in the dark. In the super-bandgap SPV, the transition of photo-induced carriers from band-to-band is the dominating process whereas band-to-trap (trap-to-band) transitions are the dominating process in the sub-bandgap SPV. In both cases the overall surface charge is changing and an SPV signal is observed.

There are several methods for measuring the surface potential. In our experiments, we used so called Kelvin probe method. The working principle of the Kelvin probe relies on the change in the surface band bending equivalent to the change in the surface work function. The parallel plate arrangement of a reference metallic electrode (Kelvin probe) and a sample measures a contact potential difference (CPD = – SPV) between them, which is defined as: $V_{CPD} = \frac{W_1 - W_2}{-e}$ where W_1, W_2 are the work functions of the reference electrode and the sample, and e is the elementary charge. When the reference electrode is connected to the sample surface, an electrical field is generated between them due to the mismatch in their Fermi energy levels.

Fig. 5 (a) shows the energy band diagrams of the probe and sample surface when they are separated by a finite distance. In this situation vacuum levels are aligned with each other but Fermi levels are different. As soon as an electrical contact is made, the Fermi levels will align via electron current flow from the lower work function to the higher, and the system will reach equilibrium (Fig. 5 (b)). Both surfaces will be charged, with finite V_{CPD} aligning the Fermi levels yet vacuum levels are no longer the same. An electric field will appear at the junction due to V_{CPD}. This field can be nullified by applying an external bias (V_{DC}) equal and opposite to V_{CPD} (Fig. 5 (c)). Within this arrangement, the Kelvin probe vibrates near the top surface of the sample generating capacitance and current in the external circuit. The external compensating dc bias aligns the probe and the samples' vacuum levels nullifying the current in the external circuit. Thus, the applied dc bias is equal and opposite to V_{CPD}.

2.2. Photo-Induced Charge Separation at Nanoscale Surfaces

Physical mechanisms governing generation of SPV in nanoscale materials are very complex because of a large surface area, high absorption coefficient, modified width of space charge region (SCR), complex geometry of the nanostructure, relatively small volume of material, etc. However, even in nanoscale systems the near-surface electric field is rather appreciable due to surface-trapped charges and the excess carriers drift playing a major role in the surface band bending [80], which is similar to the SPV normally generated in a bulk material.

Let us consider the surface of an *n*-type semiconductor as shown in Fig. 6. In equilibrium, electrons from the conduction band are trapped at the surface states. Due to the transfer of charge per unit area into the surface states Q_{ss}, a positive charge per unit area Q_{sc} is

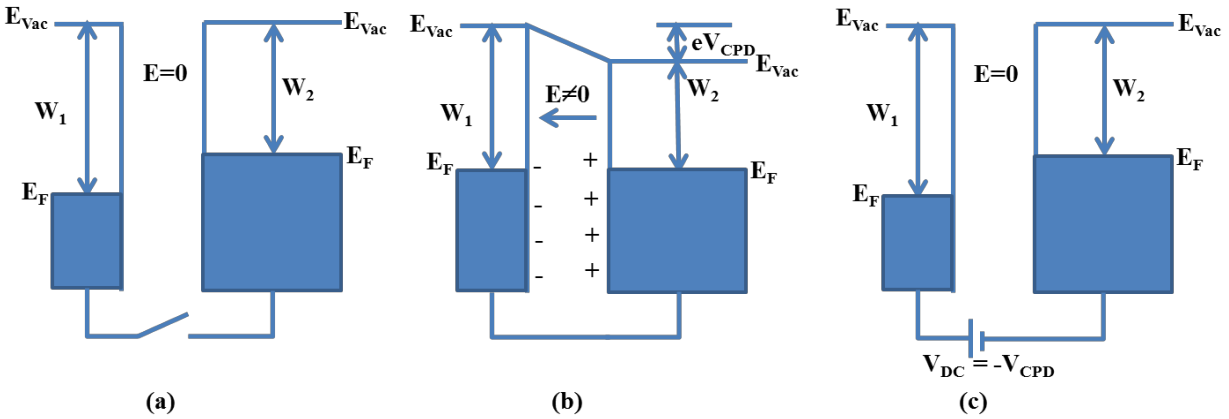

Figure 5 Energy band diagrams of two materials having different work functions (a) without contact, (b) with external electrical contact, where *E* is electrical field between plates and (c) with external bias (V_{DC}). W_1 and W_2 represent Fermi levels of Kelvin probe and sample, respectively.

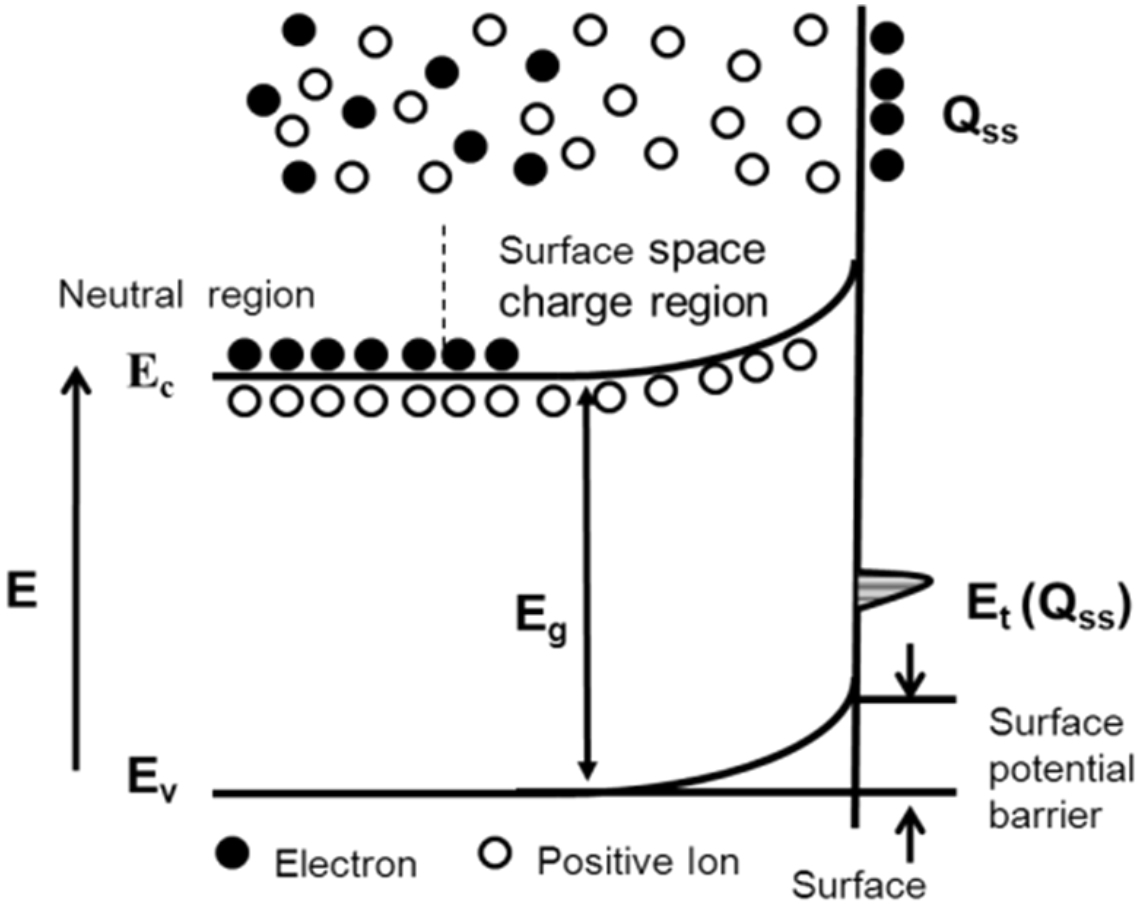

Figure 6 Energy band diagram of *n*-type semiconductor showing surface states (E_t) trapping surface charge (Q_{ss}), forming space charge region and surface potential barrier formed by surface band bending [81].

created in the near-surface region known as SCR. The conservation of charge requires that

$$Q_{ss} + Q_{sc} = 0 \qquad (1)$$

As a result, an electric field will appear directed from the bulk towards the surface preventing the further flow of electrons towards the surface. Due to the presence of a non-zero electric field there will be a non-zero electric potential barrier at the surface known as the surface potential, V_s. Thus, in equilibrium, the semiconductor bands will bend upward near the surface by eV_s relative to the bulk. Since both Q_{ss} and Q_{sc} depend on V_s, by solving equation (1), we can obtain the value of V_s.

2.3. Dependence of Q_{ss} on V_s

Let us assume that N_t is the number of available surface states per unit area, n_t – the electron occupation measured in charge carriers per unit area. Then the hole occupation in charge carriers per unit area will be given by $Q_{ss} = e(N_t - n_t)$ for donor-type surface states. Taking into the account the degeneracy of states, the effective surface states lie above the Fermi-level (E_F) of the bulk. In the presence of a surface band bending, the energy interval between the surface states and the Fermi level changes from its previous value in the absence of the band bending $(E_t - E_F)_0$, as shown in Fig. 7. It can be shown that

$$n_t = N_t\left(\frac{1}{1+\exp\left[((E_t - E_F)_0 - eV_s)/kT\right]}\right)$$

$$Q_{ss} = eN_t\left(1 - \frac{1}{1+\exp\left[((E_t - E_F)_0 - eV_s)/kT\right]}\right) \qquad (2)$$

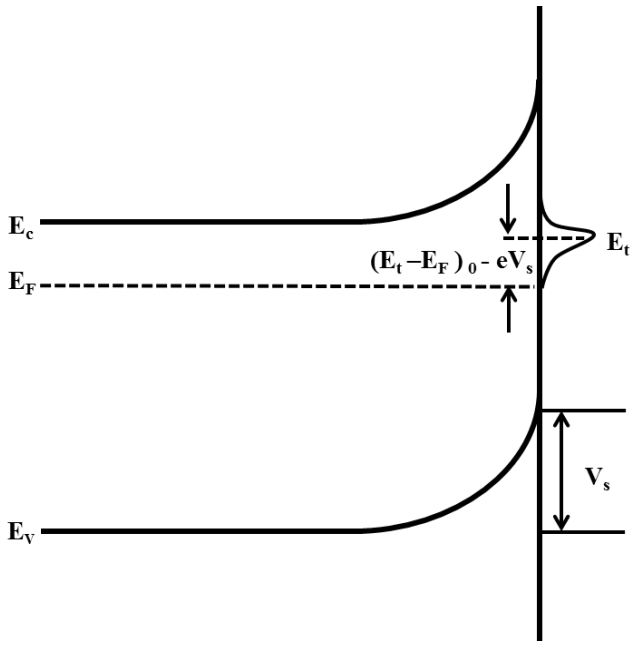

Figure 7 Energy band diagram of semiconductor showing surface potential barrier, surface states and Fermi level.

Similarly, for acceptor-type surface states

$$Q_{ss} = -eN_t\left(\frac{1}{1+\exp\left[((E_t - E_F)_0 - eV_s)/kT\right]}\right) \tag{3}$$

2.4. Dependence of Q_{sc} on V_s

Case I: Equilibrium Conditions

Let us consider a *p*-type semiconductor with both donor and acceptor states [82]. The relation between potential V and charge density ρ is given by Poisson's equation,

$$\frac{d^2V}{dx^2} = -\frac{\rho(x)}{\varepsilon} \tag{4}$$

Here ε is the permittivity of the material and $\rho(x) = e\left[N_D - N_A + p(x) - n(x)\right]$, where N_D and N_A are the donor and acceptor charge densities whereas $p(x)$ and $n(x)$ are the hole and electron densities, respectively, at SCR. In the bulk, $V = 0$ and $\rho(x) = 0$ thus

$$N_D - N_A = n_b - p_b$$

and

$$\frac{d^2V}{dx^2} = -\frac{e}{\varepsilon}\left[n_b - p_b + p(x) - n(x)\right] \tag{5}$$

The relationship between the electron and hole densities at SCR vs. that in the bulk is given by Boltzmann's statistics as follows (assuming $\Omega = \frac{eV}{kT}$):

$$n(x) = n_b e^{\Omega} \tag{6}$$

$$p(x) = p_b e^{-\Omega} \tag{7}$$

Combining (5)-(7), one obtains

$$\frac{d^2V}{dx^2} = -\frac{e}{\varepsilon}\left[p_b\left(e^{-\Omega} - 1\right) - n_b\left(e^{\Omega} - 1\right)\right] \tag{8}$$

Using $\frac{d^2V}{dx^2} = \frac{1}{2}\frac{d}{dx}\left(\frac{dV}{dx}\right)^2 \frac{dx}{dV}$ and $E = -\frac{dV}{dx}$ and integrating equation (8) from bulk towards the surface, we obtain:

$$\int_0^{E_s} d(E^2) = -\frac{2e}{\varepsilon}\int_0^{V_s}\left[p_b\left(e^{-\Omega}-1\right)-n_b\left(e^{\Omega}-1\right)\right]dV$$

$$E_s = \pm\left[\left(\frac{2kT}{\varepsilon}\right)\left\{\left(e^{-\Omega}+\Omega-1\right)+\frac{n_b}{p_b}\left(e^{\Omega}-\Omega-1\right)\right\}\right]^{\frac{1}{2}} \tag{9}$$

Applying Gauss' law, it can be shown that

$$Q_{sc} = -\varepsilon E_s = \mp\frac{\sqrt{2}\varepsilon_s kT}{eL_D}F\left(\Omega,\frac{n_b}{p_b}\right), \tag{10}$$

where $L_D = \sqrt{kT\varepsilon_s / e^2 p_b}$ is the Debye screening length for holes and the space charge function in equilibrium is

$$F\left(\Omega,\frac{n_b}{p_b}\right) = \left[\left(e^{-\Omega}+\Omega-1\right)+\frac{n_b}{p_b}\left(e^{\Omega}-\Omega-1\right)\right]^{\frac{1}{2}} \tag{11}$$

Substituting relation (2) and (10) into (1) and solving the resulting equation we can get the value of V_s. Graphically one can plot both Q_{ss} and Q_{sc} with respect to the surface potential and the intersection of the curves will give the value of the surface potential as shown in Fig. 8.

From the Q_{sc} vs. V_s curve, we can clearly distinguish three different regions: accumulation (the density of the majority carriers at the surface is greater than its value in the quasi-neutral bulk), depletion (the density of the majority carriers at the surface is smaller than the equilibrium value but greater than that of the minority carriers at the surface) and inversion (the density of the majority carriers at the surface is smaller than that of the minority carriers at the surface). It is worth noting the following:

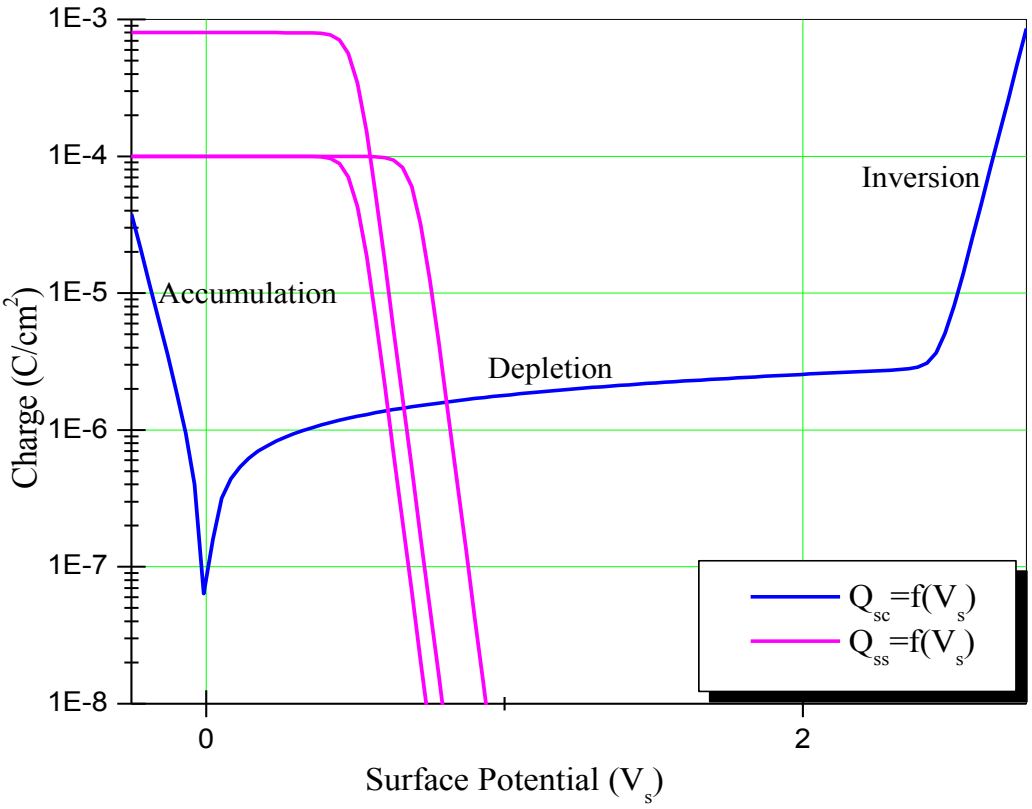

Figure 8 Plot of Q_{ss} and Q_{sc} with respect to V_s.

i. The accumulation region is characterized by positive charges in the SCR. In this case Q_{sc} is positive, $p_b >> n_b$ and the band bending is upward so V_s is negative. Thus, the space charge function F is dominated by the first exponential term and $Q_{sc} \approx \exp(eV_s / 2kT)$.

ii. The inversion region is characterized by negative charges in the SCR. In this case Q_{sc} is negative, $n_b >> p_b$ and the band bending is downward while V_s is positive. Now F is dominated by the fourth exponential term and $Q_{sc} \approx \exp(eV_s / 2kT)$.

iii. For the depletion region, Q_{sc} is negative, $p_b >> n_b$, and the band bending is downward so that V_s is positive. In this case, F is dominated by the second term and $Q_{sc} \approx \sqrt{|V_s|}$

It is important to know whether the given surface is on the accumulated, inverted or depleted type as the SPV response is significantly affected by the type of the surface chosen. The surface band bending is less sensitive to accumulated surfaces than to depleted or inverted surfaces. In the case of an accumulated surface, the photo-generated minority carriers are swept towards the bulk, where they can easily recombine with the majority carriers. However, in the case of the depleted or inverted type, the excess minority carriers are directed towards the surface, where the probability of their recombination is negligible as there is a low concentration of the majority carriers. Thus, the sample with the accumulated type of surface exhibits a small change in the surface band bending due to illumination. Fig. 9 below shows the different surfaces of an *n*-type semiconductor.

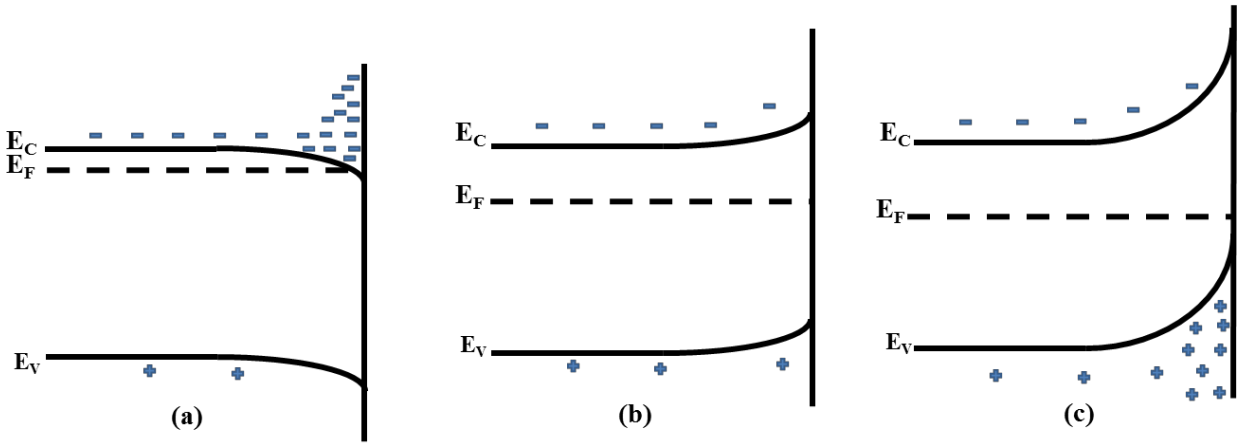

Figure 9 Energy band diagrams for *n*-type semiconductor with (a) accumulated, (b) depleted and (c) inverted surface types.

Case II: Non-Equilibrium Conditions

When the semiconductor surface is illuminated by light, extra carriers are generated and the system tends to deviate from the equilibrium conditions. The excess carriers at a given time recombine to re-establish the thermal equilibrium. The manner in which the thermal equilibrium is re-established is of a fundamental importance for the operation of semiconductor devices. Below we consider modification of the theory outlined above for the non-equilibrium situation, for both super- and sub-bandgap illumination.

Super-Bandgap SPV

In the super-bandgap SPV, photons of energy $h\upsilon \geq E_g$ (E_g being the energy gap) are used to excite the semiconductor and the redistribution of the excess carriers occurs (i) under the electric field in the SCR and (ii) by trapping. Fig. 10 shows the super-bandgap process for a depleted surface of an *n*-type semiconductor, in which even under the equilibrium conditions (dark), the bands bend upward in the vicinity of the surface due to the charge exchange between bulk and surface (thus a non-neutral SCR). The vertical axis measures the energy whereas the horizontal axis measures the position from the surface. Hereinafter we will use the following notations: E_t as the energy of a trap state, E_c – the energy of the conduction band minimum and E_v – the energy of the valence band maximum. In Fig. 10 (a), excess electron-hole pairs are generated in the SCR under illumination. Holes move towards the surface and electrons move towards the quasi-neutral bulk due to the electric field present in the SCR, which is directed from the bulk toward the surface. The holes coming into the vicinity of the surface recombine with the electrons in the surface states. This makes the surface positively charged, and the electronic bands bend down at the surface (SPV increases). In Fig. 10 (b), the trapping of electrons and

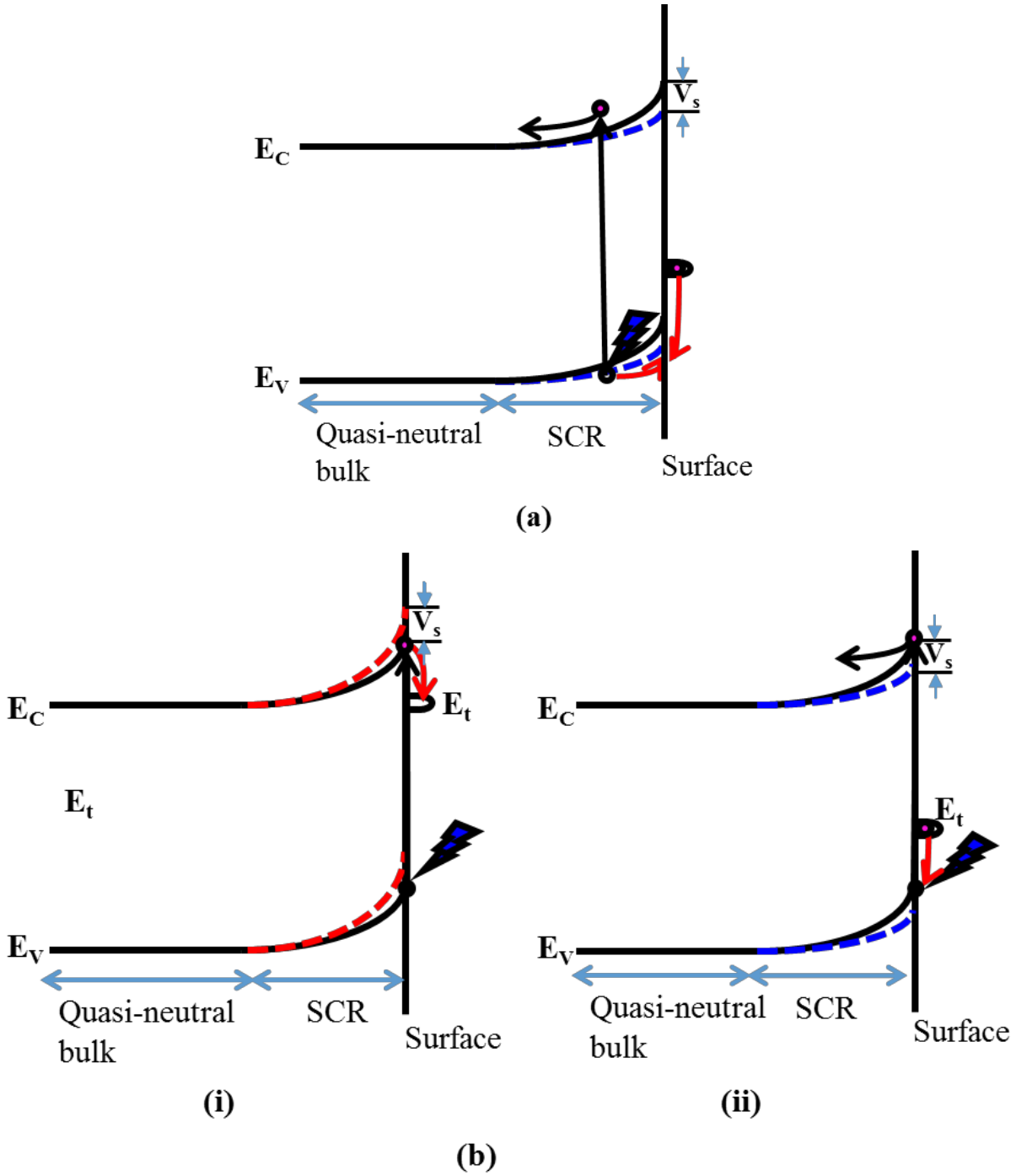

Figure 10 Super-bandgap SPV: (a) induced by charge separation in electric field; (b) produced by trapping of (i) electrons and (ii) holes. Solid and dashed lines represent band positions in dark and under illumination correspondingly and surface potential, $V_s = V_s$ (dark) – V_s (light) [83].

holes is shown. The surface band bending increases through electron trapping as a negative charge at the surface increases (SPV decreases). The trapping of holes depletes the surface charge and reduces the amount of band bending. The latter trapping mechanism is more likely as holes always tend to accumulate at the surface due to the electric field. In order to have electron trapping, there should be a sufficient diffusion of holes toward the bulk and/or a significant charge recombination in SCR.

Sub-Bandgap SPV

For the sub-bandgap SPV, energy of excitation $h\upsilon < E_g$ is sufficient to generate transitions of electrons from and to localized states, causing a change in the surface charge density and the surface band bending. Again, we consider a depleted surface of an *n*-type semiconductor. Upon illumination by photons with energy of $h\upsilon \geq E_c - E_t$, the electrons are excited from the trap states to the conduction band. This depopulates the surface states and the surface becomes less negative. SCR is now less-depleted and the band bending decreases as shown in Fig. 11 (a). If photons of energy $h\upsilon \geq E_t - E_v$ are employed, the electrons jump from the valence band to the surface states, thus increasing the band bending and decreasing the SPV signal as shown in Fig. 11 (b).

Under non-equilibrium conditions due to irradiation, the excess charge carriers generated in the SCR change the value of Q_{sc} significantly from its equilibrium value. In this case, the equilibrium Fermi level departs from the equilibrium value within the SCR, but farther away from the SCR the effect of illumination is practically negligible. For this situation we have to use the concept of the quasi Fermi levels. The excess carrier recombination time is longer than the time interval between carrier collision and relaxation. This means that before the

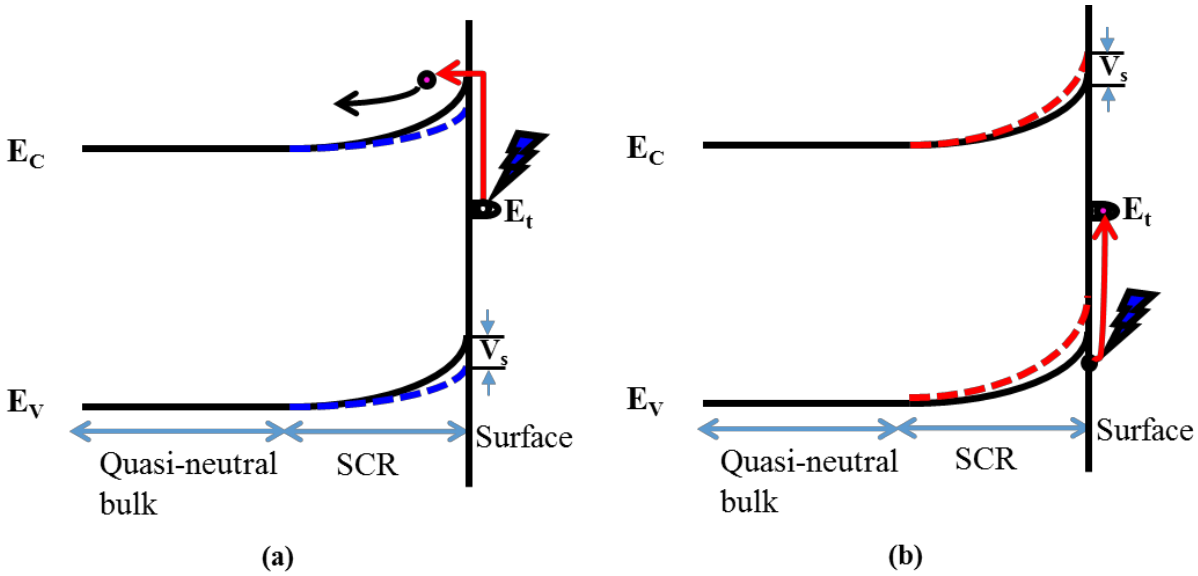

Figure 11 Sub-bandgap SPV (a) brought by depopulating surface states and (b) produced by populating surface states [83].

recombination takes place, the excess carriers collide with the crystal lattice many times prior to coming to equilibrium. Even though electrons and holes are not in equilibrium, the system as a whole is approximately in a state of thermal stability known as a quasi-thermal stability. Therefore, the conduction band electron system and the valence band hole system do not share the same Fermi level and split into their own Fermi levels known as the quasi-Fermi levels for electrons (F_n) and holes (F_p). The separation of the quasi-Fermi levels $F_n - F_p$ is a measure of the deviation from equilibrium (in equilibrium $F_n = F_p = E_F$). Since the recombination at the surface is larger than in the bulk, the effective excess carrier density at the surface is greatly reduced in comparison to the bulk. This may cause the quasi-Fermi levels to deviate less from equilibrium closer to the surface than at the SCR edge [84]. As a result the quasi-Fermi levels in the SCR acquire a bump-like shape, as shown in Fig. 12. Quantitative description of the quasi-Fermi levels is rather complicated mathematically, so some approximations have to be made in order to simplify the calculations. Following [6] we assume that:

i. The quasi Fermi levels are flat throughout the SCR.
ii. The diffusion length of the charge carriers and the absorption length of light are much greater than the width of the SCR.
iii. The recombination current in the SCR must not be too large and the depletion of carriers may not be too extreme.

Using the flat quasi-Fermi level approximation, the non-equilibrium charge densities are given by Boltzmann's statistics:

$$n^*(x) = n_b^* e^{\Omega} \tag{12}$$

$$p^*(x) = p_b^* e^{-\Omega} \tag{13}$$

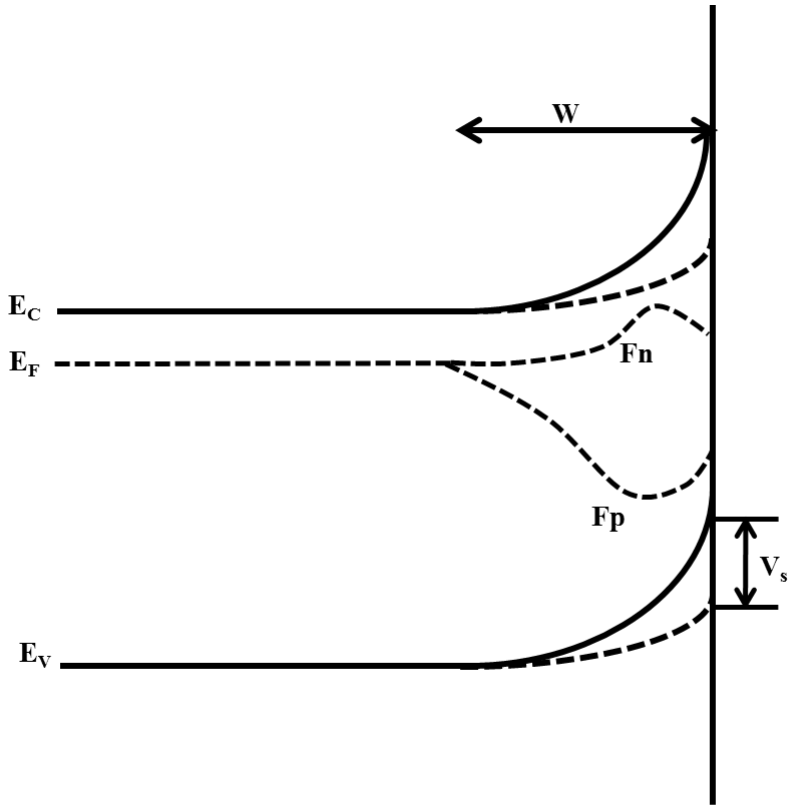

Figure 12 Quasi Fermi levels in SCR of width (*W*) [84].

where n_b^* and p_b^* are the non-equilibrium densities at the edge of the SCR region and

$$n^*(x) = n_b + \delta n \tag{14}$$

$$p^*(x) = p_b + \delta p \tag{15}$$

Here n_b, p_b are the equilibrium charge densities and δn, δp are the excess charge densities.

For a *p*-type semiconductor, applying Poisson's equation, one obtains

$$\frac{d^2V}{dx^2} = -\frac{e}{\varepsilon}\left[n_b - p_b + p^*(x) - n^*(x)\right] = -\frac{e}{\varepsilon}\left[n_b - p_b + p_b^* e^{-eV/kT} - n_b^* e^{eV/kT}\right]$$

Integrating the above relation from the surface towards the bulk and assuming the potential at infinity to be zero, we can find the electric field at the surface E_s. Applying Gauss' Law

$$Q_{sc}^* = -\varepsilon_s E_s = \mp \frac{\sqrt{2}\varepsilon_s kT}{eL_D} F^*\left(\Omega^*, \frac{n_b}{p_b}, \Delta_n\right) \tag{16}$$

where $L_D = \sqrt{kT\varepsilon_s / e^2 p_b}$; the injection ratio $\Delta_n = \frac{\delta n}{n_b} = \frac{n_b^* - n_b}{n_b}$ and

$$F^*\left(\Omega^*, \frac{n_b}{p_b}, \Delta_n\right) = \left[F^2\left(\Omega^*, \frac{n_b}{p_b}\right) + \frac{n_b}{p_b}\Delta_n\left(e^{-\Omega^*} + e^{\Omega^*} - 2\right)\right]^{\frac{1}{2}} \tag{17}$$

so that

$$F\left(\Omega^*, \frac{n_b}{p_b}\right) = \left[\left(e^{-\Omega^*} + \Omega^* - 1\right) + \frac{n_b}{p_b}\left(e^{\Omega^*} - \Omega^* - 1\right)\right]^{\frac{1}{2}} \tag{18}$$

The variation of Q_{sc} and Q_{sc}^* with respect to the surface potential is shown in Fig. 13. Substituting relation (2) and (16) into (1), and solving we can obtain V_s.

From relation (16), we see that the surface band bending occurs due to the presence of a net change in carriers due to illumination-the injection ratio, Δ_n. For most of the time the

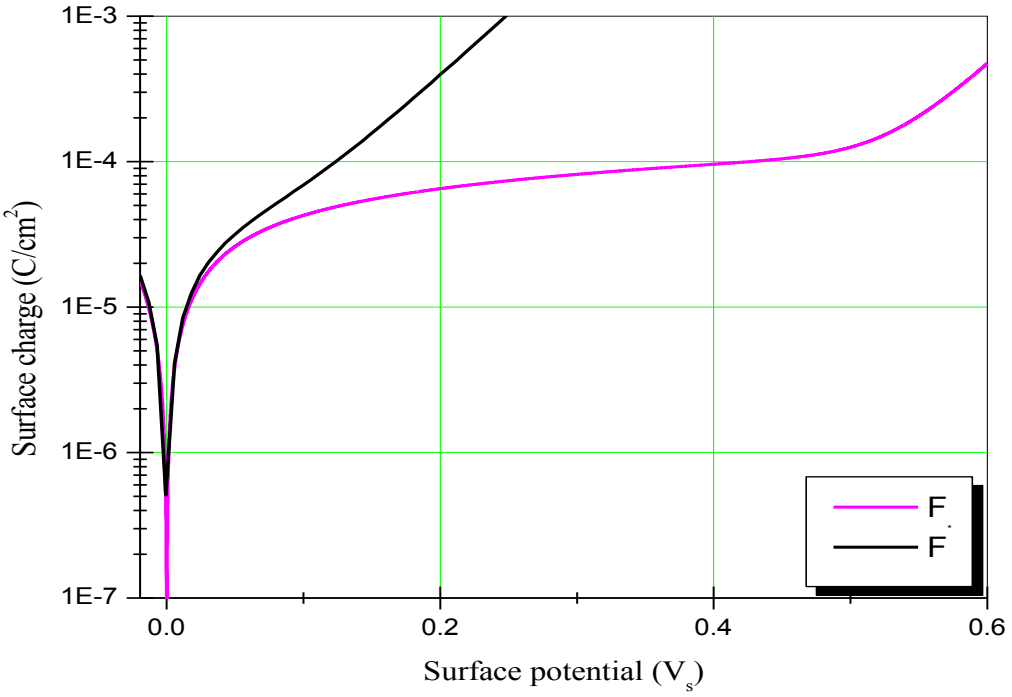

Figure 13 Plot of Q_{sc} as function of surface potential.

surface band bending results from the change in the surface charge. However, the dependence of the surface space charge Q_{sc} on the injection ratio (Δ_n) shows that even the redistribution of carries in the SCR, without changing the space charge can also generate the band bending known as the barrier SPV. A fixed surface space charge implies that $Q_{sc} = Q_{sc}^* \Rightarrow F^*\left(\Omega^*, \frac{n_b}{p_b}, \Delta_n\right) = F\left(\Omega^*, \frac{n_b}{p_b}\right)$. Solving this equation we get $V_s^* - V_s$ which is SPV. F^* is always greater than F because of extra term containing Δ_n. F^* could return to its equilibrium value F, if $|V_s|$ decrease upon illumination. Thus in the absence of a change in the surface charge, illumination always tends to decrease the band bending. Physically, the photo-induced carriers partially screen the fixed surface state charge, thereby reducing the band bending. This is a very simplified model which is rather difficult to achieve experimentally.

2.5. Mechanisms behind SPV Transients with Multiple Components

As we mentioned above, in order to obtain the SPV transients the surface is first allowed to saturate in light, and then the illumination is cut off to monitor the surface potential reaching equilibrium in the dark. The rate of change of the surface charge density depends on the optical generation and recombination. If the generation is significantly greater than the recombination, the dynamics of such processes can be approximated by exponential time dependencies, similar to those of a capacitor charging/discharging in a single-loop RC-circuit with connected or disconnected emf (Fig. 14).

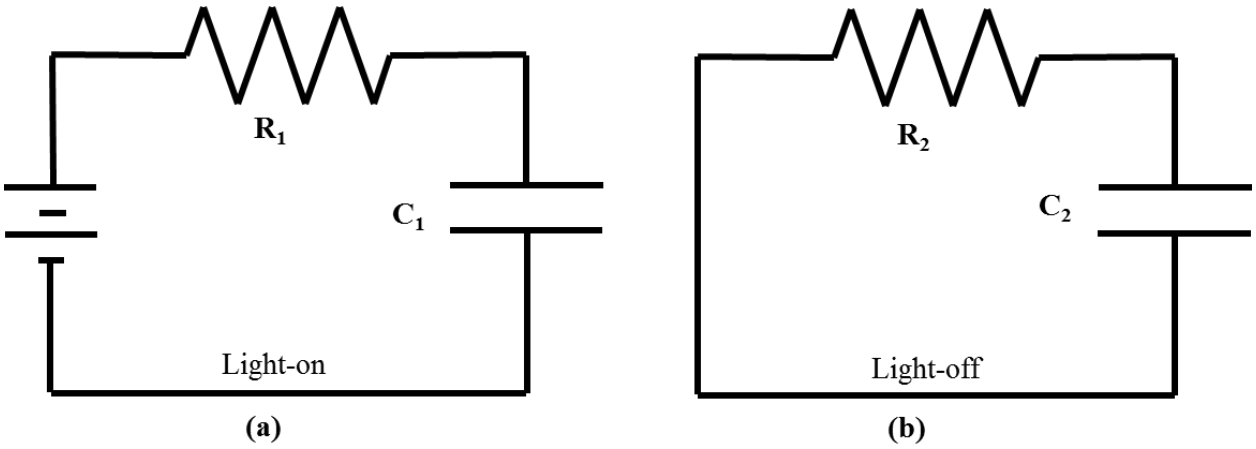

Figure 14 Simple approximations showing model of (a) charging and (b) discharging of capacitor in presence and absence of irradiation.

We use such model to approximate the time dependencies of CPD response as shown in Fig. 15 (a), (b), and we will use a term 'single-process' or 'trivial' transient. On the other hand, in certain SPV transient measurements during illumination or in the dark, one can observe a behavior that cannot be adequately matched by the curves similar to Fig 15 (a). In such cases when transients acquire a more complex shape, an adequate fit may involve superposition of several different functional dependencies, oftentimes with dissimilar characteristic time scales. It is natural to expect that such dependencies reflect co-existence of several different charge recombination processes. In such case we will use a term 'multiple-process' or 'non-trivial' transient. When plotted on a logarithmic time scale, such curves can better reveal processes dominating in different time ranges, apparent by e. g., a conspicuous change in the slope. An example of a transient with multiple processes is illustrated in Fig. 15 (c), which reveals at least two (or more) processes during the light-on event. Here a fast component is followed by a slower tail (or more tails). The presence of the fast and slow components shows that at least two different types of charge recombination process are responsible for the observed behavior.

2.5.1. Origins of Multiple Characteristic Times

The change in surface potential, V_s (Δ_n) is determined by the charge exchange between the surface states and the bulk. Dynamics of the surface states depends mainly on the capture cross-section of the surface states which in turn depends on the occupation of available energy states and the energy position of these states with respect to the Fermi level. If the thermal energy is the only energy source, then the occupation of the states varies depending on their energy position relative to the Fermi level, which in turn will determine the different times of

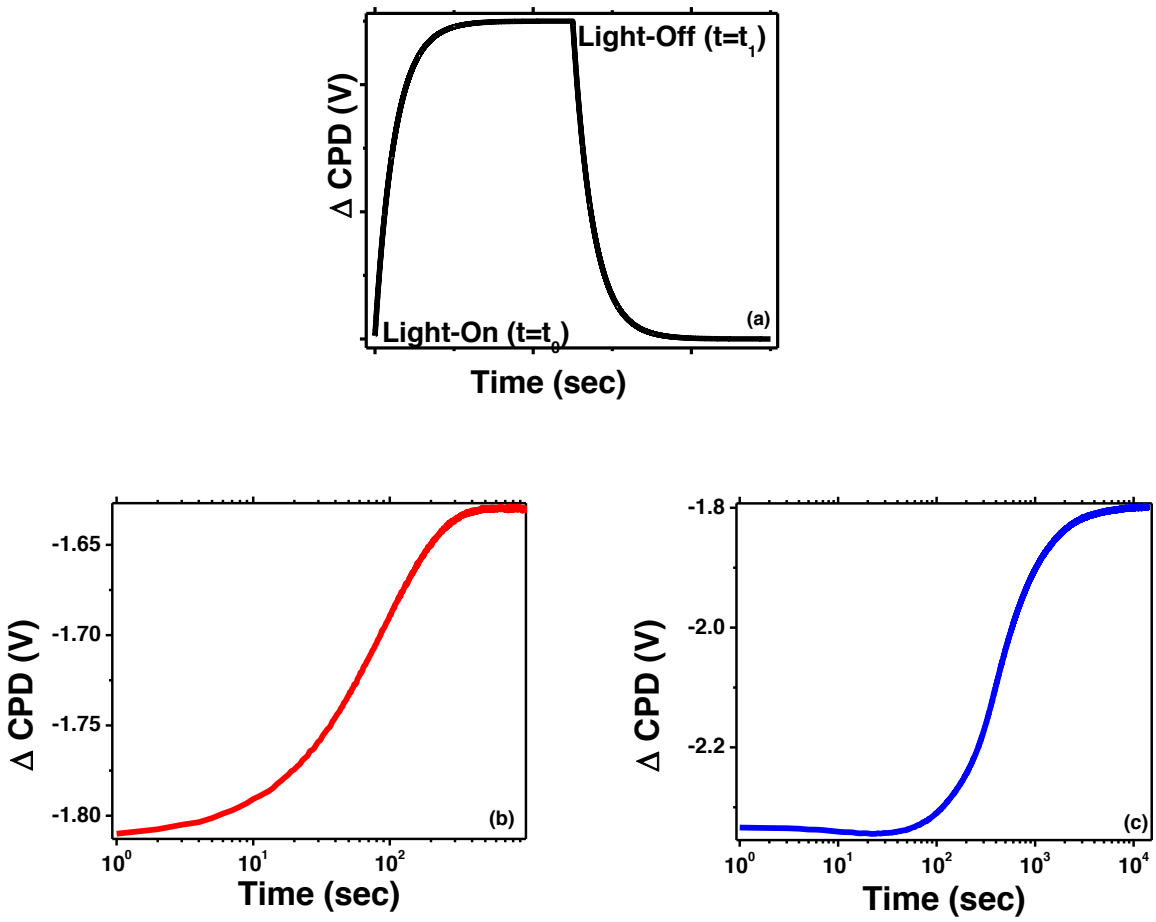

Figure 15 (a) SPV transients during light on and off cycles, (b) light-on part of transient with single process on logarithmic time scale, (c) light-on part of multiple processes on logarithmic time scale.

charge exchange between the surface and the bulk in dark. Depending on the types of states involving in charge transfer, SPV signal may exhibit different time dependencies. The surface states can be categorized as relatively fast or slow depending on the rate of change of the charge in the surface states in response to illumination. Sometimes at the semiconductor surface, for example, covered with an oxide layer, there are states formed also at the semiconductor-oxide interface. These states are in a close contact with the bulk, and can attain equilibrium within a relatively short period of time, thus they could be referred to as the fast states. Another type of states, usually referred to as the slow states, exists within or at the top of the oxide layer. These states may be formed either by adsorbed ambient species or defects in the oxide region.

Thereby, within a relatively simple approximation, the change in the surface photovoltage V_s can be modelled as a parallel RC network with the photon energy as a source, where R is the resistance due to surface recombination and C_{sc} is the capacitance due to the surface SCR (Fig. 16).

The characteristic time associated with this circuit arrangement is given by [85]

$$\tau = RC_{sc} \tag{19}$$

$$\text{where, } R = \frac{1}{s_n dn_s} = \frac{1}{c_n N_t (e^2/kT) n_b \exp(eV_s/kT)} \tag{20}$$

Here s_n is the surface recombination velocity, dn_s – the change in the surface electron density, c_n – the energy-dependent capture cross-section and N_t – the surface charge density.

The capacitance due to the SCR can be calculated as

$$C_{sc} = \left| \frac{dQ_{sc}^*}{dV_s^*} \right| \tag{21}$$

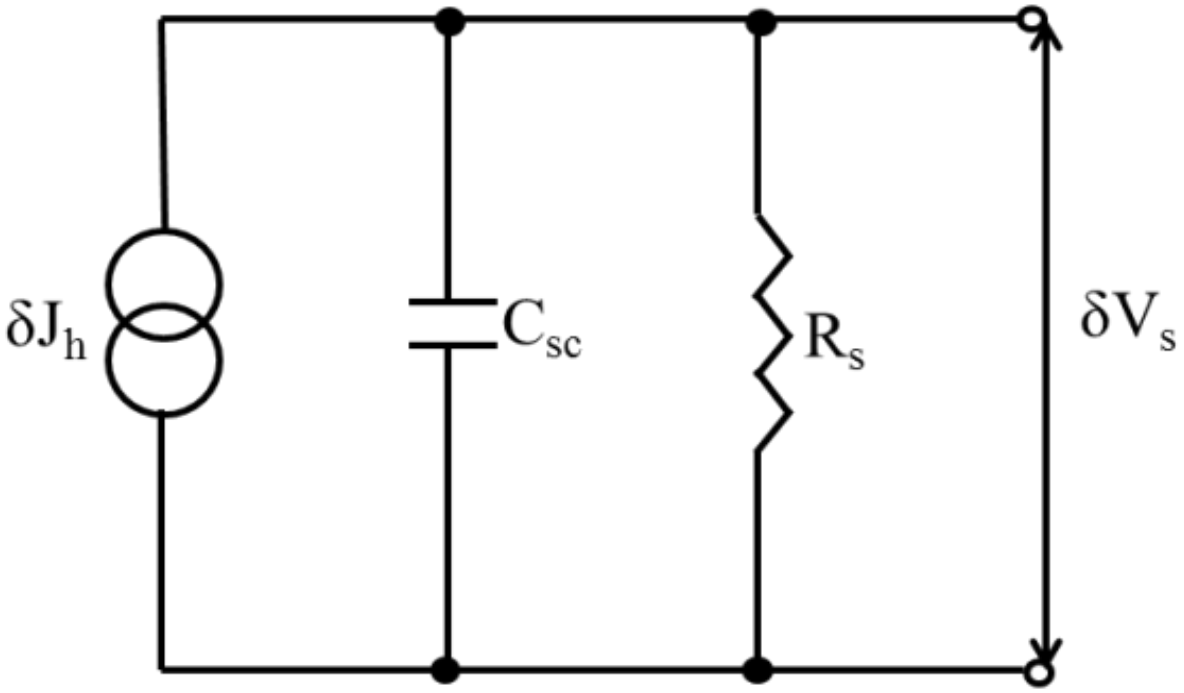

Figure 16 Model circuit diagram showing output voltage as surface photovoltage in parallel with an RC circuit [85].

$$C_{sc} = \frac{\varepsilon}{L_D} \frac{(e^{-eV_s^*/kT} + 1) + \frac{n_b}{p_p}(e^{-eV_s^*/kT} - 1) + \frac{n_b}{p_p}\Delta_n(e^{eV_s^*/kT} - e^{-eV_s^*/kT})}{\sqrt{2[(e^{-eV_s^*/kT} + eV_s^* - 1) + \frac{n_b}{p_p}(e^{eV_s^*/kT} - e^{-eV_s^*/kT} - 1) + \frac{n_b}{p_p}(e^{eV_s^*/kT} + e^{-eV_s^*/kT} - 2)]}} \tag{22}$$

Thus the characteristic time now becomes

$$\tau = \frac{C_{sc}}{c_n N_t (e^2/kT) n_b \exp(eV_s/kT)} \tag{23}$$

From equation (23), it is clear that the charge equilibration rates are related to the change in the capture cross-section, the density of the surface states, the bulk electron concentration and the surface photovoltage. The greater is the capture cross-section, the faster is the relaxation time because a small change in the surface quasi-Fermi level is enough for the surface state to become populated. The larger is the surface state density the faster is the relaxation time, because more charge transfer from the surface to the bulk is necessary to reach equilibrium and thus a larger SPV is obtained. This in turn increases the value of the exponential cofactor in the denominator and thus decreases the magnitude of the relaxation time. In addition, a lower bulk electron concentration results in a faster relaxation time: the smaller is the bulk charge, the more difficult is to screen the surface departure from equilibrium, and hence a larger SPV is needed to change the bulk charge distribution. This also increases the exponential cofactor and reduces the characteristic time.

There are several mechanisms responsible for the generation of non-trivial SPV transients. Among them are:

a. Presence of both fast and slow surface states;

b. Bulk-related phenomena such as the Dember effect;

c. Charge exchange between the surface and the adsorbed species;

d. Photochemical reactions associated with the surface dipole.

We will discuss each of these processes separately.

2.5.1.a. Presence of Both Fast and Slow Surface States

Transients with multiple components can be obtained for semiconductors in which both fast and slow surface and near-surface states are present. SPV transients in the presence and absence of illumination with fast and slow components are illustrated in Fig. 17 (a). The time constant for the slow process appears to be 2-3 orders of magnitude lower than that for the fast process.

Let us consider a depleted surface of an *n*-type semiconductor. As mentioned earlier, for the depleted type of a surface, the space charge varies as a square root of the surface potential ($Q_{sc} \approx \sqrt{|V_s|}$). The variation of Q_{sc} with respect to V_s during illumination and in the dark is shown in Fig. 17 (b) by two parabolic curves, which represent the depletion regions of Fig. 8. Starting with the light-on event, the initial band bending of an *n*-type semiconductor occurs due to the generation of excess electron-hole pairs at the surface SCR upon illumination of the super-bandgap. Excess electrons migrate towards the bulk and excess holes towards the surface under the influence of the electric field that exists in the SCR, which is directed towards the surface. Presence of the excess holes near the surface makes the surface positive. Oftentimes the photo-induced carriers screen the surface state charge thereby reducing the surface band bending. During this process the amount of charge in the surface states remains the same. This process is often referred to as the barrier SPV. As a result, the surface band bending decreases, the

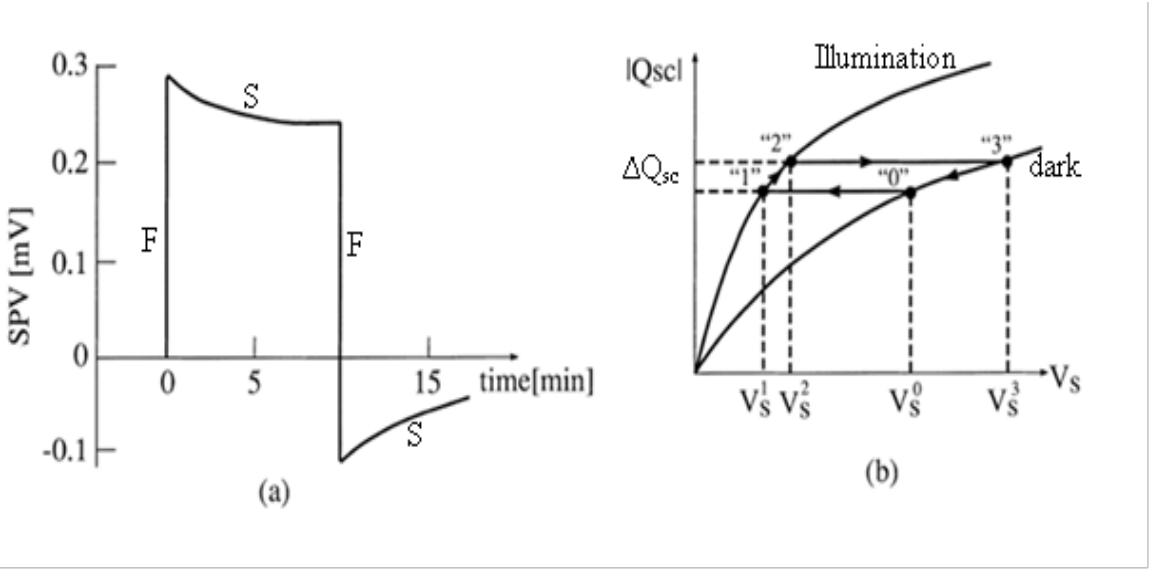

Figure 17 (a) Illustration of fast (F) and slow (S) SPV transients. (b) Charge dynamics vs. SPV diagram illustrating transients in (a) [86].

corresponding SPV increases and the system reaches state "1" in Fig. 17 (b). Since no change in the surface charge has taken place during this process, it is represented as a horizontal transition in Q_{sc} versus V_s curve. The next process is a capture of electrons by the surface traps, which is accompanied by an increase in the band bending and a decrease in SPV. This is represented as an increase in the surface charge in the illumination curve "1-2" and the system now reaches a steady quasi-equilibrium state "2" in Fig. 17 (b). The fast process and the slow processes occur simultaneously and the competition between these processes is responsible for the fast and slow SPV transients. During the light-off event, the relaxation of the barrier SPV takes place first and the band bending increases. As a result, SPV decreases and the system goes to a non-equilibrium state "3" in Fig. 17 (b). Since this decay process occurs at a fixed value of the surface charge, it can be represented as a horizontal transition. The recovery of the thermodynamic equilibrium between the surface traps and the quasi-neutral bulk by releasing captured electrons is followed by a decrease in the band bending and increase in SPV. The depopulation of the surface states by the ΔQ_{sc} amount takes place at "3-0" and the system returns back to the initial state "0" in the dark.

2.5.1.b. Dember Effect

Another mechanism that could be responsible for multi-component SPV transients is the Dember effect. This effect is observed when the incident light produces a non-uniform carrier generation and recombination provided that the mobilities of electrons and holes are different. Suppose a depleted surface of an *n*-type semiconductor (with the thickness greater than the absorption length of light) is excited with super-bandgap photons. Due to illumination a concentration gradient of excess carriers is generated from the near-surface region towards the

bulk. The presence of the concentration gradient will cause electrons and holes to diffuse along the direction of the incident light with different rates because of their unequal mobilities. When the excess carriers diffuse, there is always a possibility of trapping of one type of carrier which is closer to the surface. In the meantime, the separation of electrons and holes under diffusion builds an electric field directed from surface towards bulk. Under this electric field, the excess charges start to drift in the direction opposite to that of the diffusion current. The drifting holes are now driven deeper into the sample whereas the drifting electrons move towards the surface and are trapped at the surface states. Even though the diffusion and the trapping occur simultaneously, they occur on different time scales resulting in non-trivial transients. Since the mobility of electrons is greater than the mobility of holes, electrons diffuse faster towards the bulk than the holes. In general, the charge centers for electrons and the holes separate under concentration gradients and, on average, the holes are closer to the surface. This brings more positive charge to the surface or hole trapping sites and the surface band bending decreases. On the other hand, trapping or bringing the electrons closer to the surface under the influence of the electric field results in more negative charge at/near the surface and hence the band bending increases.

2.5.1.c. Charge Exchange between Surface and Adsorbed Species

Transients produced by processes occurring on different time scales could also be observed in a semiconductor due to photoinduced adsorption (e.g., in ambient air). When the semiconductor is excited with the photons above the bandgap, electron-hole pairs are generated in the near-surface region by interband transitions. The excess carriers drift due to the electric field present in the surface barrier. For the *n*-type semiconductor considered here, the electrons are swept into the quasi-neutral bulk region and the holes – into the surface region. The flux of

holes coming towards the surface recombines with electrons in the surface states, thus depleting the surface charge and reducing the surface band bending (Fig. 18 (a)). The reduction in the surface barrier allows electrons from the bulk tunnel into the surface region as the barrier is lowered and they may become trapped by the adsorbates on the surface. This makes surface negatively charged accompanied by an increase in the barrier height (Fig. 18 (b)). The charge exchange between the adsorbed species and the semiconductor depends on the electron affinity of these species and the work function of the material. The work function of a semiconductor is defined as the amount of energy required to remove a surface electron from the Fermi level into vacuum and electron affinity is the total barrier that an electron from the conduction band has to overcome to reach vacuum. If the adsorbed species have greater electron affinity than the work function of the semiconductor, electrons may transfer from the semiconductor to the adsorbed species. Oxygen, for example, is one of the most electronegative elements, so electrons are rather easily transferred to the oxygen-covered surface. The latter process is slower than the surface recombination of electrons with the accumulated holes because the transfer of electrons has to overcome the barrier under the thermal excitation [87].

2.5.1.d. Photochemical Reactions Associated with Surface Dipole

In addition to the surface states there is another factor associated with the free surface which could contribute to non-trivial transients – the surface dipole. The electron wave function, which is periodic inside the semiconductor, may "leak out" from the free surface as shown in Fig. 19. As a result, a negatively charged layer is formed outside and a positively charged layer inside the surface. The doubly-charged layer thus formed over the depth of several atomic monolayers is known as a microscopic surface dipole.

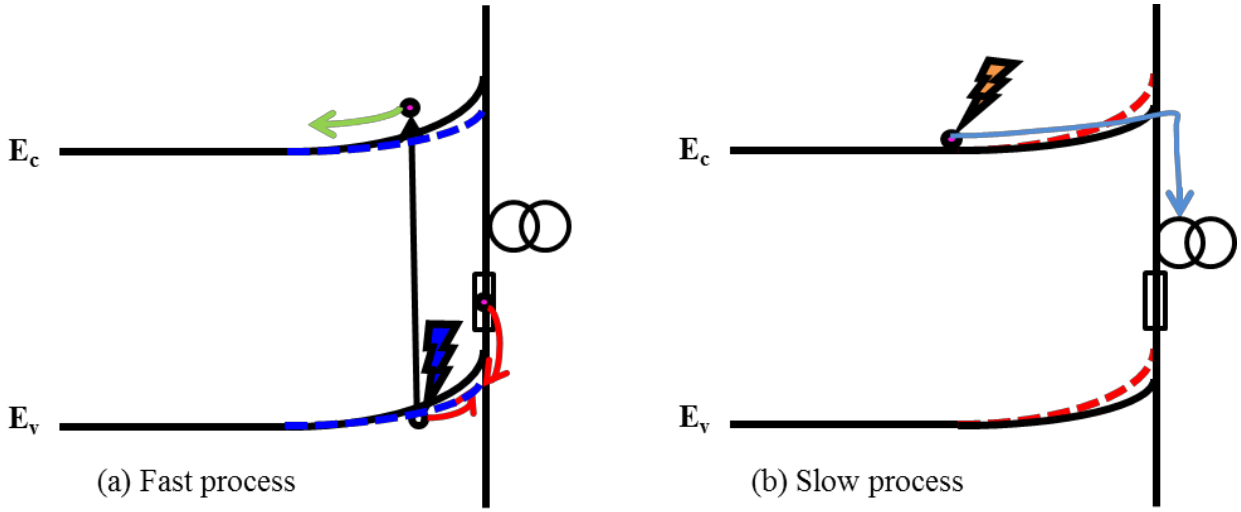

Figure 18 Surface band bending in *n*-type semiconductor covered with adsorbates. (a) Fast process due to recombination of surface states electrons with accumulated holes and (b) slow process due to bulk electron trapping by surface species.

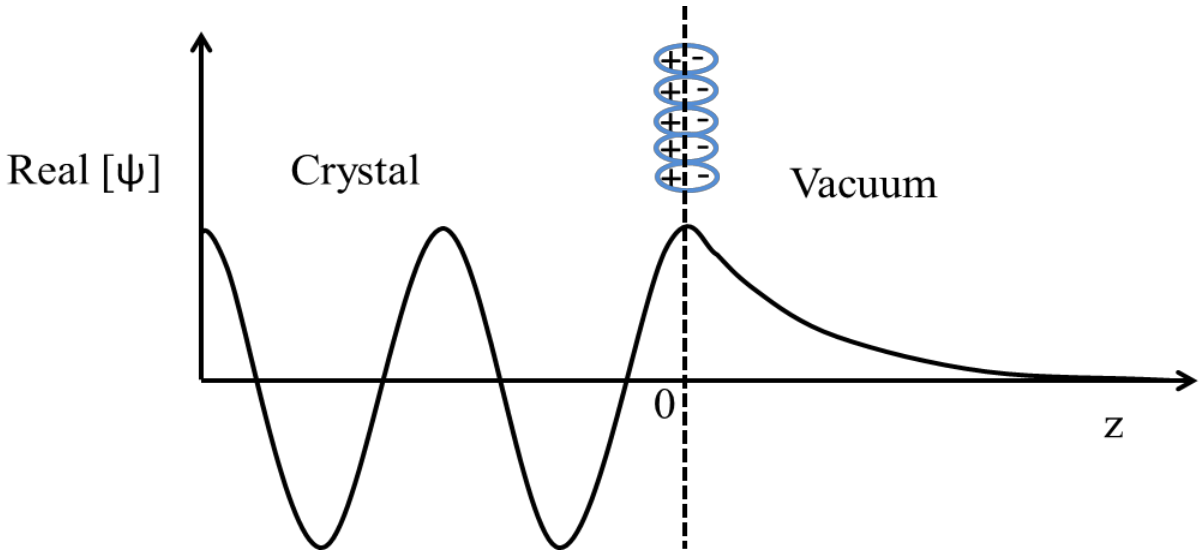

Figure 19 "Leaking out" of tail of electron wave function gives rise to surface dipole [88].

The dipole thus created at the surface produces an electric field toward vacuum and opposes the motion of electrons from the surface into the vacuum. Due to this electric field, a potential barrier is created for electrons equal to the electron affinity, which we will denote as χ. Besides spilling out of the otherwise periodic wave function, the surface dipoles can arise due to the relaxation and reconstruction processes of the crystal lattice at the surface. In general, during reconstruction, a rearrangement of surface atoms occurs in order to reduce the total energy of the system. Because of the reconstruction some of the surface atoms are displaced inwards and some outwards, and the dipole layer is created as a result. Presence of absorbed environmental species may also impact the reconstruction, affecting in turn the electron affinity and the surface band bending.

In the case of an adsorbate-covered surface, charge transfer can occur between the semiconductor and physisorbed atoms or molecules, resulting in a chemisorption of these species which will also affect the surface band bending and oftentimes induce charge transfer within the chemical bonds thus creating additional surface dipoles. This in turn may change the work function and create a step in the vacuum level as shown in the energy band diagram for a semi-conductor surface covered with adsorbates (Fig. 20 (b)).

Since the presence of dipole directly affects the work function, let us express the work functions for a clean and an adsorbate-covered semiconductor surface as

$$W_s = (E_c - E_F)_b + eV_s + \chi \tag{24}$$

$$W_s^{'} = (E_c - E_F)_b + eV_s^{'} + \chi^{'} \tag{25}$$

where χ and $\chi^{'}$ are the electron affinities without and with the surface dipole whereas V_s and $V_s^{'}$ are the band bending without and with the dipole present, respectively.

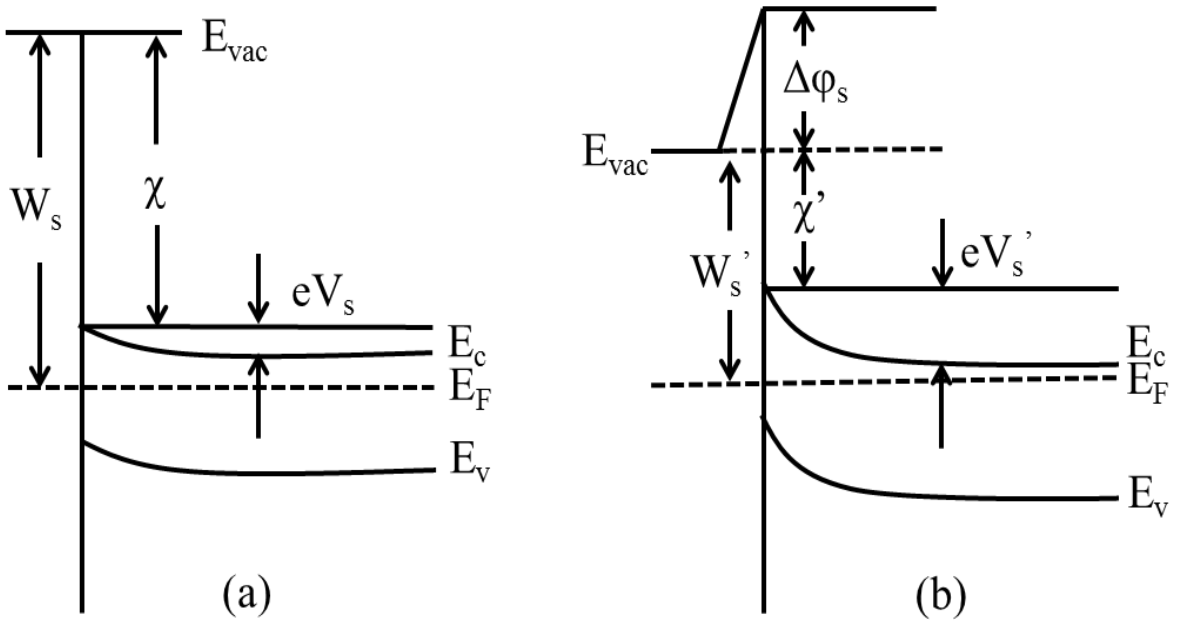

Figure 20 Energy band diagram of (a) clean semiconductor surface (b) semiconductor surface covered with absorbed species [89].

The change in the surface work function due to the dipole contribution $\Delta\phi_s$ is given by

$$\Delta W_s = W_s - W_s^{'} = e(V_s - V_s^{'}) + (\chi - \chi^{'}) = e\Delta V_s + e(\Delta\phi_s) \quad (26)$$

This relation suggests that the surface work function may change due to the modified surface band bending, surface dipole, or both. The surface band bending can change due to a charge transfer from the surface to the bulk or vice-versa whereas the surface dipole may change due to the formation/annihilation of dipoles and/or a change in the ordering of the surface.

Fefer, *et al*. [90] designed an experiment where an optical "probe beam" was used in addition to ultraviolet (UV) light ($h\nu \geq E_g$) to monitor a photo-induced chemical reaction due to dipoles. Pulses of a probe beam were used simultaneously while monitoring the surface work function continuously with UV light. A plot of the surface work function versus time was obtained which could be visualized as the envelope of the probe pulses or spikes on the top of a regular UV light transient, as seen in Fig. 21. The envelope formed by spikes was compared to the regular UV transient and the contribution of the dipoles was obtained as

$$e(\Delta\phi_s) = \Delta W_s - e\Delta V_s . \quad (28)$$

The following three scenarios were observed:

1. The spike-envelope may follow the original shape of the work function. In this case, the height of the spikes remains the same so that the band bending is zero (i.e., $\Delta V_s = 0$) and $e(\Delta\phi_s) = \Delta W_s$. This implies that the chemical reaction takes place during illumination and the change in the work function is due to the change in the surface dipole only as seen in Fig. 21 (a).

2. The spike-envelope may remain constant and the height of the spikes changes with time such that ΔV_s is not zero, i.e. the chemical reaction brings the change in the band bending and not in the surface dipole. ΔW = change in spikes height as seen in Fig. 21 (b).
3. When the spike-envelope and the height of the spikes are different from cases (i) and (ii), we conclude that the surface reaction changes both the surface dipole and the surface band bending as seen in Fig. 21 (c).

In addition to the processes described above, other electronic transitions may take place under super and sub-bandgap excitation, which can possibly impact the surface band bending of the material. Fig 22 (a) shows one of the possibilities where photo-induced electrons are excited from impurity levels to the conduction band and then swept into the bulk. The separation of electrons and positively charge impurities, which are closer to the surface than the electrons create a macroscopic dipole with a field opposite to the SCR, thereby decreasing the surface band bending. Fig. 22 (b) shows the excitation of electrons from the valence band to the bulk trap states. The holes are transported to the surface by the field present in the SCR. There they recombine with the electrons in the surface states and reduce the surface barrier. The third possibility shown in Fig. 22 (c) illustrates the intra-band transition due to the absorption by free electrons in the conduction band which excites the electrons to higher levels within the conduction band. The excited electrons are able to overcome the surface potential barrier and get trapped into surface states increasing the band bending.

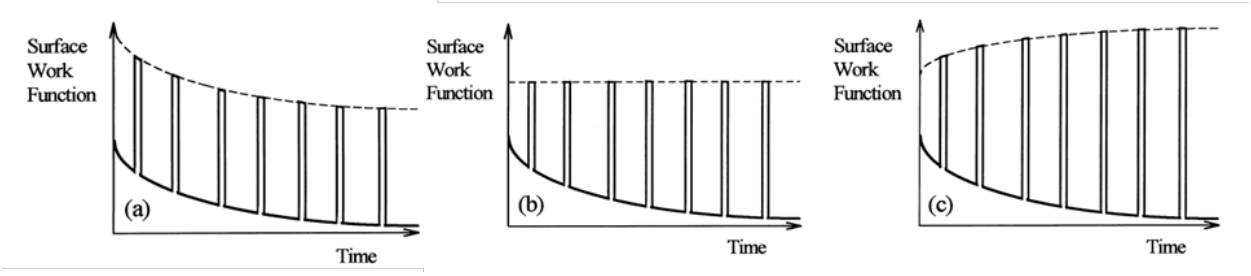

Figure 21 Changes in work function due to (a) change in the surface dipoles, (b) change in band bending and (c) change in both surface dipoles and band bending [90].

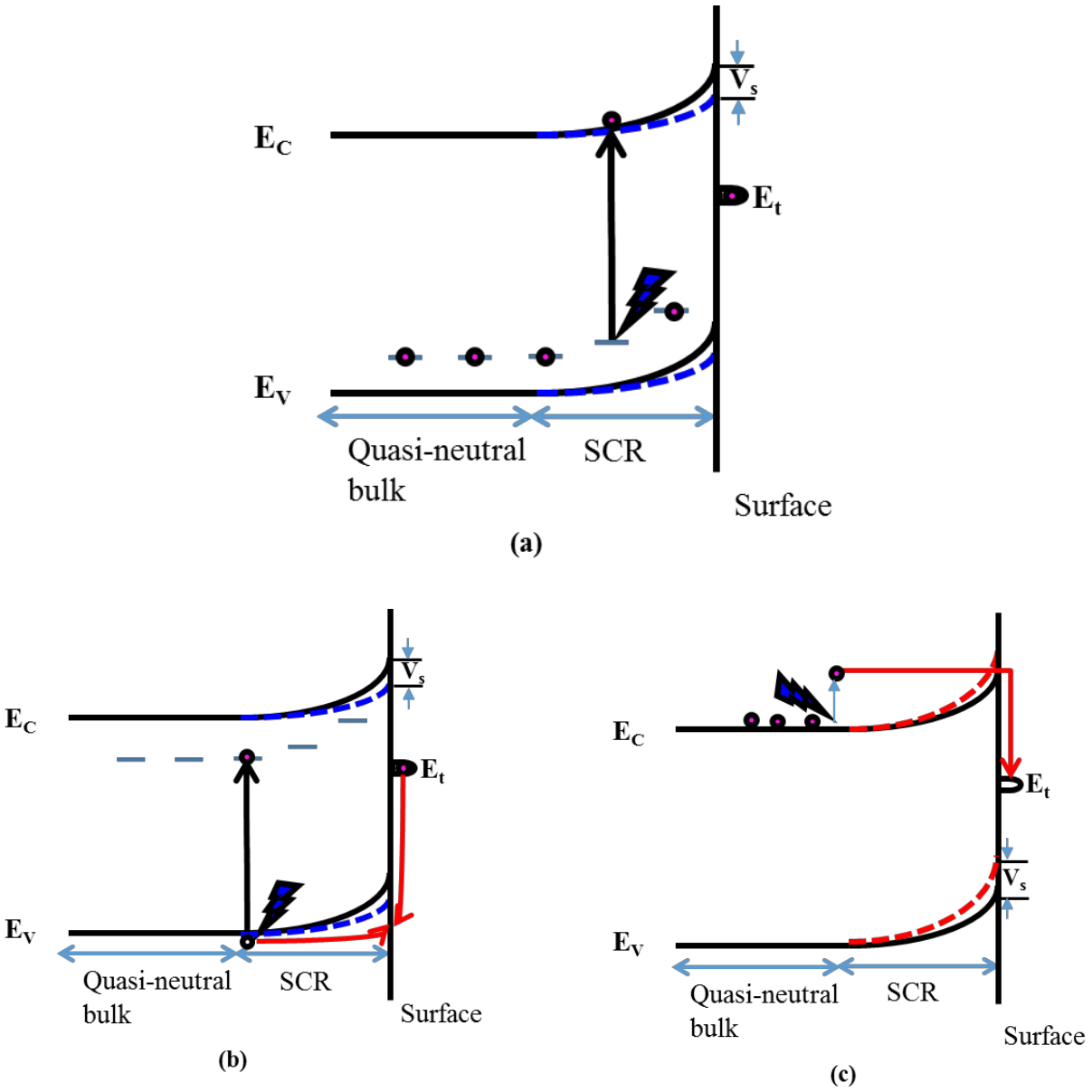

Figure 22 Some possible interfering processes affecting surface band bending of material. Transitions from (a) impurity level to conduction band (b) valence band to bulk traps and (c) intra-band transition within conduction band [91].

2.6. Effects of Pressure as well as Light Wavelength and Intensity on Surface Band Bending

The time evolution of surface band bending in nanoscale materials could be affected by several experimental parameters such as the duration of the surface exposure to the dark before illumination, temperature and pressure of the environment, the wavelength and intensity of the light. The pressure of the system plays an important role in the interaction of the illuminated surface and the surface adsorbed species. In the gaseous ambient the species which tend to leave the surface are in a continuous collision with the gas particles and may return back to the surface and become temporarily physisorbed at the surface. Therefore the density of the physisorbed species remains constant at a given pressure. In the meantime the charge exchange between the physisorbed species takes place resulting in the chemisorption of the physisorbed species. For a given temperature and pressure, the rate of physisorption is many times faster than that of the chemisorption process which would affect the surface band bending. In the case of high vacuum, some of the physisorbed species are removed from the surface during evacuation. In this case, the charge exchange between the adsorbate and the surface becomes significantly different affecting the band bending as well.

The excitation wavelength also plays a significant role in the multi-component SPV processes. Within a sub-bandgap excitation, the incident light directly populates or depopulates the surface states thereby changing the potential barrier. This process directly depends on the effective target area of the surface states excited by the photons. This may generate a single SPV process. For a super-bandgap SPV the surface states are modified by the photo-induced minority charge carriers drifting to the surface due to the field present in the surface region. The majority carriers then are removed away from the surface. At the same time, because of the reduction of

the barrier, the same majority carriers can be brought to the surface via thermal mechanisms. The surface band bending depends on the effective capture area of the majority carriers, which in turn depends on the energy separation of the surface states from the band edges. This may generate multiple charge recombination processes in transient SPV.

The surface band bending may be also influenced by the excitation intensity. This means that the processes happening on the different time scales are directly affected by the light intensity of a given wavelength. The rate of change of the surface potential barrier is directly related to the rate of change of the surface charge density. One of the easiest ways to find the rate of charge transfer to the surface states is to monitor the onset slope of an SPV transient. The initial portion of the transient is generated due to an immediate response to photons whereas the later part may acquire substantial contributions from the thermal processes. Thus monitoring the dependence of an onset slope of transient SPV processes on the excitation intensity could provide insight of the carrier dynamics of the surface states participating in the optical transitions in the absence of interference by thermal excitation, adsorption/desorption etc. Fig. 23 and 24 show the variation of the onset slope as a linear function of the illumination intensity observed for bulk semiconducting CdS and GaN. From the slope of these dependencies one can extract such surface-related parameters as the depletion width, the initial barrier height in the dark, the surface state density, etc. In the case of bulk materials the linear behavior is very common whence the charge supply to the surface states is provided by the underlying bulk. However, in the case of nanoscale materials, the surface-to-volume ratio increases with the decreasing characteristic dimensions, and the physical properties of the system are no longer dominated by the bulk of the material but primarily by the surface. Thus it is interesting to test whether the linear dependence of the SPV onset on the illumination intensity, typical for bulk materials, is still valid for the nanoscale materials.

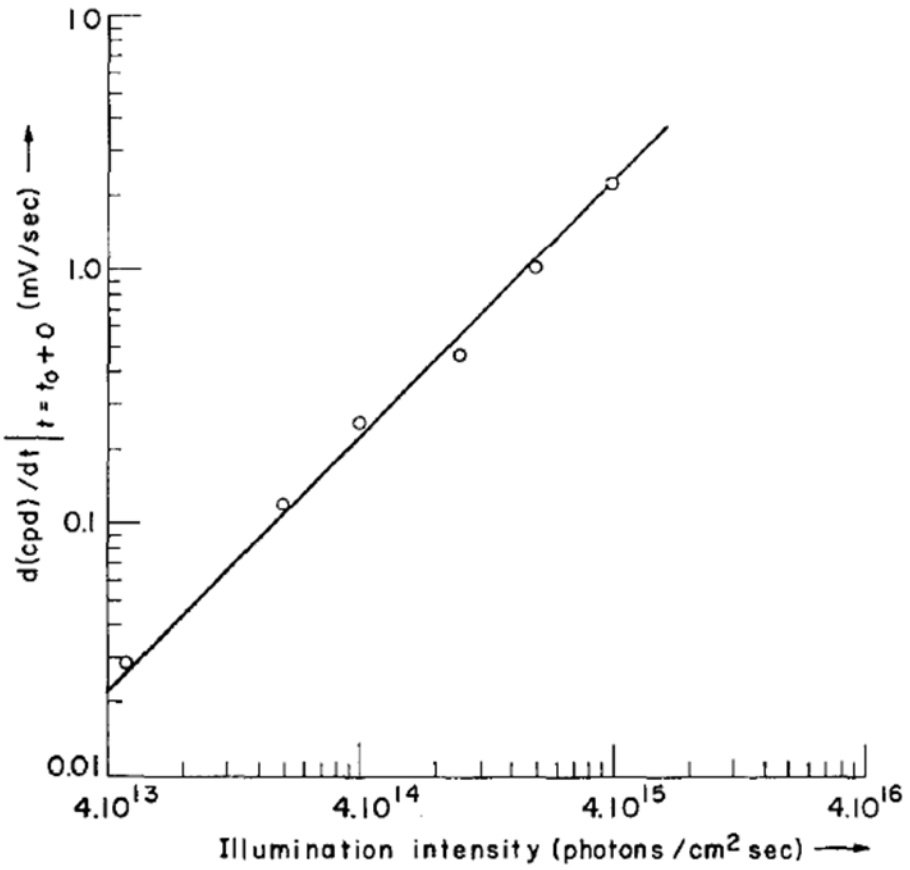

Figure 23 Onset slope of SPV transient vs. illumination intensity observed for CdS [60].

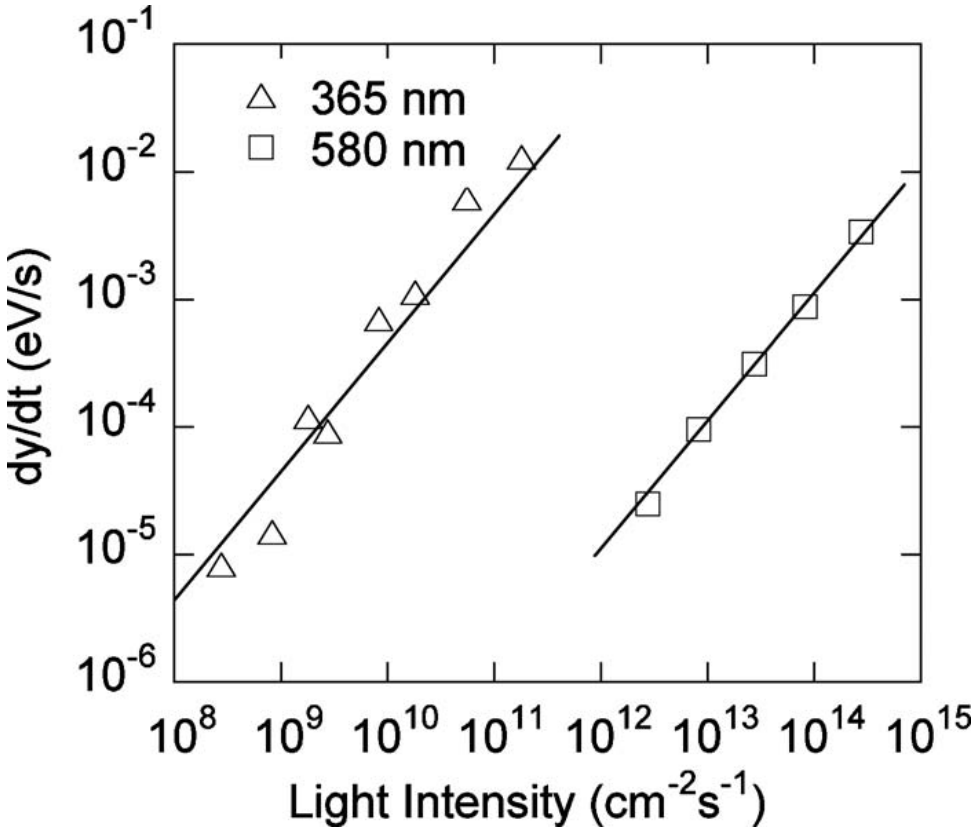

Figure 24 Onset slope of SPV transient vs. illumination intensity observed for GaN [55].

2.7. Experimental Setup

As mentioned earlier, for our studies we employ primarily SPV transients. Here we provide a brief description of our SPV experimental setup.

All the transient SPV experiments in different environments are performed in a ultra high vacuum (UHV) chamber. The pressure inside the chamber can be varied between atmospheric and ~ 2×10^{-7} Torr. In order to enhance the signal-to-noise ratio in different ambiences, we isolate the vacuum chamber from vibrations of all mechanical pumps by turning them off during data acquisition and the vacuum conditions maintained in the characterization chamber only by the ion-pump. We use a Besocke Kelvin probe S which is fixed inside the characterization chamber. The Kelvin probe consists of a vibrating gold mesh with a circular shape having a diameter of ~ 2.5 mm. The vibration frequency of the probe is ~ 250 Hz and the vibration amplitude is ~ 1 mm. During operation the sample is placed ~ 1-2 mm away from the probe. The sample is mounted on

a sample holder with its top surface facing both the illumination and the Kelvin probe. The motion of the sample-holder is provided by the XYZ-manipulator attached. Most of the time all the samples have Ohmic contacts, deposited at their top surfaces and occasionally at the back surfaces, to be connected to a common ground during the experiments.

The experimental setup for transient measurements is shown in Fig. 25. All the necessary optical instruments and components except the sample and the Kelvin probe are mounted *ex-vacuo*. For illumination, we use a white light source of a 30 W halogen lamp, and for intensity dependent, we employ a LHRR-2000 HeNe laser (wavelength 632 nm) and a CW Kimmon IK5452R-E HeCd laser (wavelength 442 nm and 332 nm) whose intensities are controlled by a neutral density filter. Light collected from this source is fed directly onto sample surface via an

optical fiber bundle with a transmission range of 160-1200 nm. A LabView program is used to record the change in CPD as a function of time during the light-on and dark intervals. Throughout the experiment, a complete blockade of other external light sources is maintained to prevent possible leakage of stray light inside the chamber.

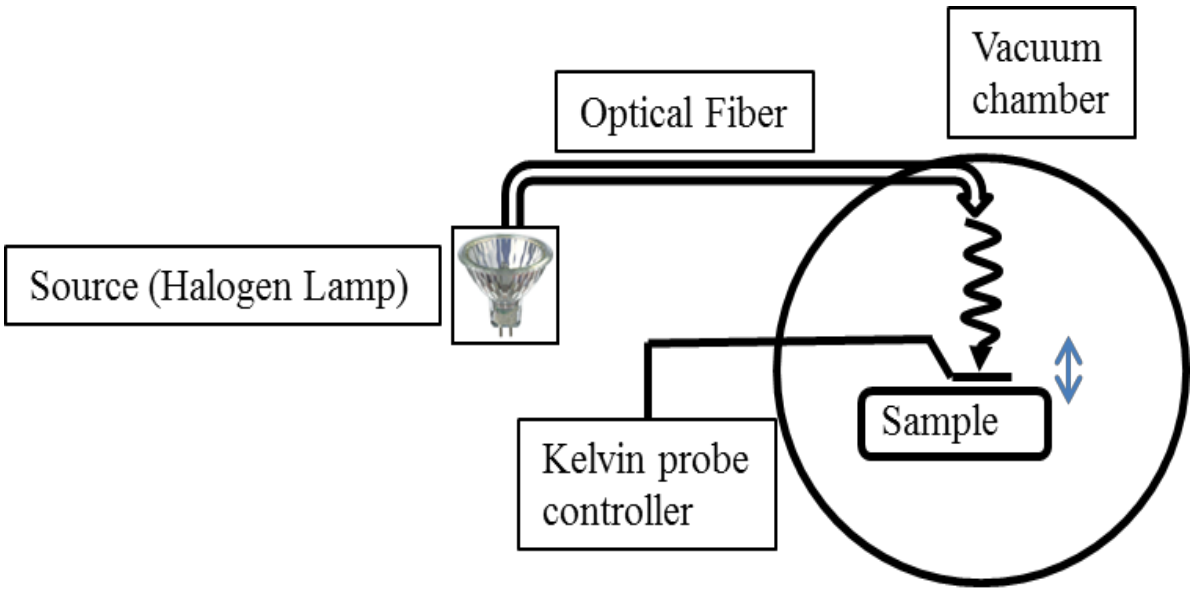

Figure 25 Experimental arrangement for transient SPV measurements.

Chapter 3

3. Results and Discussion

3.1. Effects of the ambient on the surface band bending in NPS

As mentioned above, our prime experimental probe was the time-dependent SPV performed in different environments, such as N_2, and in high vacuum (10^{-7} Torr). During the transient SPV measurements, we first monitored the change of the CPD between the Kelvin probe and the sample due to the illumination (e.g., with white polychromatic light) allowing the surface to reach equilibrium in light. The surface was then allowed to relax in the dark, and this was again monitored through the CPD reaching saturation. Prior to turning on the illumination the samples were kept in darkness for an extended time to ensure the initial surface charge equilibrium.

SPV transients observed for the pristine NPS in different environments are illustrated in Fig. 26 and 27. These results were obtained first in N_2 gas at a pressure comparable to the atmospheric pressure, and then the experimental chamber was evacuated to 10^{-7} Torr to record transients in vacuum. One can clearly see distinct signal spikes immediately after turning the light on and off in both vacuum and nitrogen gas.

These spikes occur on a time scale different from the time scale over which the super-bandgap saturation is achieved. In order to compare processes occurring on different time scales it is convenient to plot the SPV transient curves on a logarithmic time scale. As a result, more informative plots are produced (Fig. 28), with the curves revealing both fast and slow

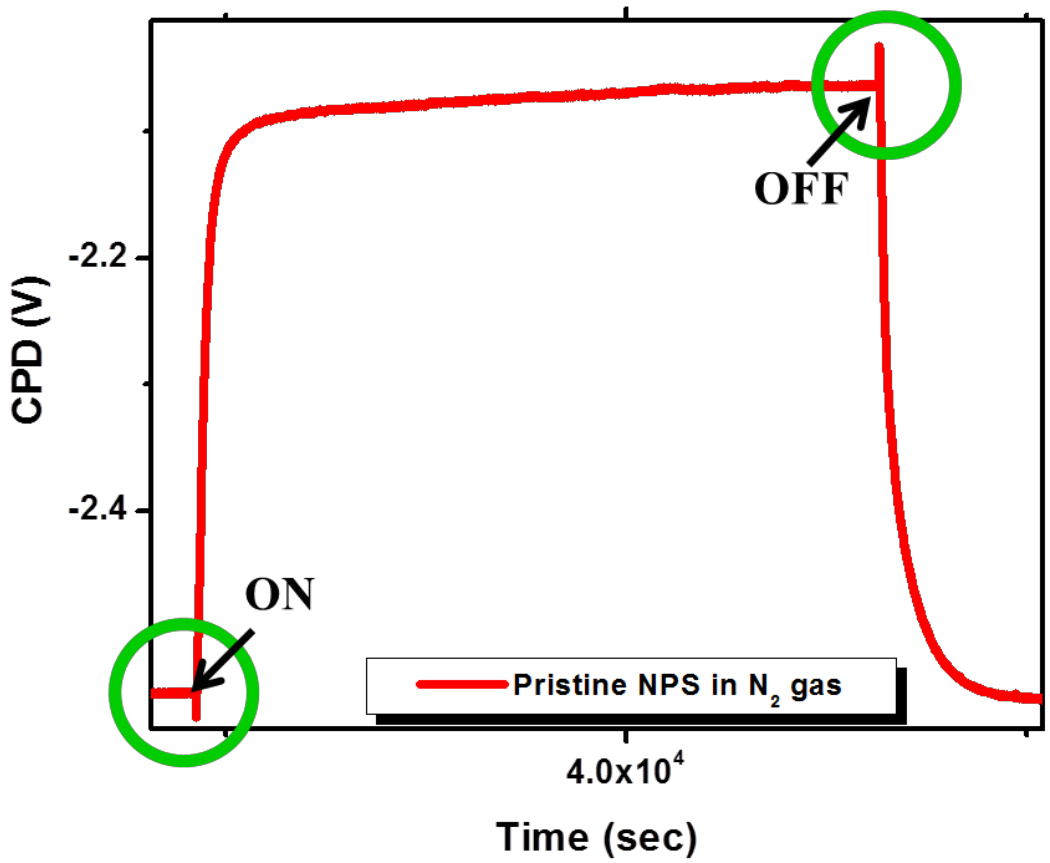

Figure 26 CPD during illumination and in dark on linear time scale for NPS in N_2 gas.

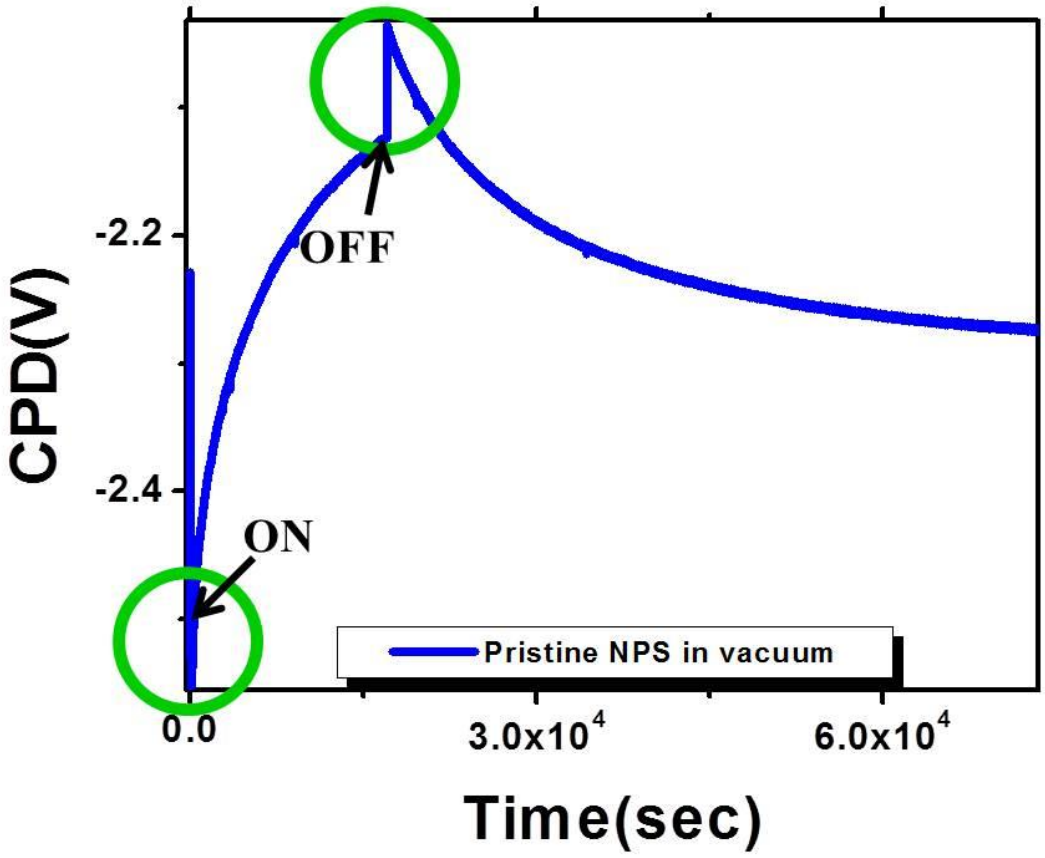

Figure 27 CPD during illumination and in dark on linear time scale for NPS in vacuum.

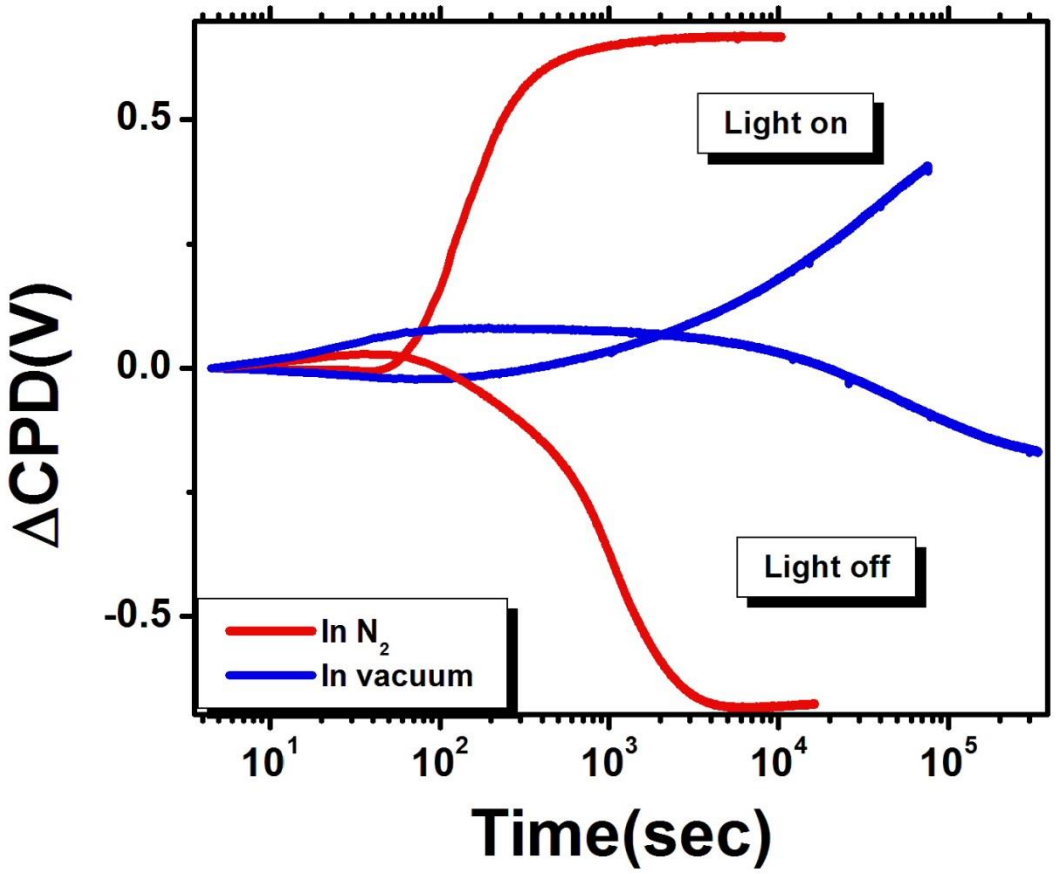

Figure 28 SPV transients on logarithmic timescale revealing fast and slow processes during illumination and in dark.

components. The change of the CPD for the slow process is opposite to that of the fast one. The characteristic time scale for the initial fast processes during both the light-on and light-off processes is of the order of tens of seconds, whereas the slower saturation process lasts for thousands of seconds. Transients with fast and slow characteristic times have been commonly observed in different semiconductors [6]. A comprehensive theoretical treatise of multicomponent SPV was presented in refs. [92] for wide-bandgap materials such as GaN. According to the authors of this model, the fast and slow components arise due to an internal mechanism associated with the surface/interface states and an external mechanism related to the ambient environment. We assume that such model could be applicable to describe phenomena observed in our experiments. Let us consider a surface band diagram of NPS with a thin native oxide layer on the silicon surface as shown in Fig. 29. In a gaseous environment during illumination of NPS the charge transfer due to the internal and external mechanisms occurs simultaneously but on different time scales resulting in multicomponent transients. Since the fast process is present in both environmental conditions, we believe that it is associated with the charge recombination within NPS. The slow process in vacuum is weaker in comparison to the gaseous environment implying that it may be related to the physisorbed species that are already present at the surface of NPS. The fast process during the light-on transient could be related to the drift of the excess electrons in Si towards the bulk and excess holes towards the Si/oxide interface due to the electric field in the surface space charge region. The surface recombination of the electrons in the trap states at the interface with the incoming holes from the Si side may lead to the initial decrease of the CPD in the light-on transient (Fig. 29). The decrease in the band bending reduces the depletion width and the barrier height. More electrons can now cross the barrier,tunnel through the oxide layer and become captured by the species at the free surface possibly converting them into chemisorbed. This increases the negative charge at the free

surface and consequently the band bending yielding a slow increase in the CPD of the light-on transient (Fig. 30). Since the chemisorption is a very slow process, it is quite obvious that some surface absorbed species contribute to the charge transfer mechanism related to the slower component. It has been reported that when the surface of NPS is exposed to air it can adsorb water, CO_2, H_2, O_2, N_2, F, siloxene-complexes, CH_3, etc. [5]. The rate of desorption of these species depends on the temperature and pressure of the environment. The difference in the adsorption/desorption rates of those different species present at the free surface may be the reason behind the observation of very slow SPV processes.

On the other hand, when a similar measurement was performed in vacuum, slow component became weak and required very long time to saturate in comparison to the case of N_2 gas. We suggest that in vacuum a substantial amount of the physisorbed species could be removed from the surface during evacuation. There still might be some of them remaining on the surface and being responsible for trapping the charges from the bulk, thus contributing to the weaker slow component observed in vacuum during the light-on process.

Testing of this general idea was carried out by running the transient SPV experiments similar to the described above with the ambient pressure of the nitrogen environment as a variable. Fig. 31 shows the effects of the ambient pressure of nitrogen on the surface band bending during the light-on interval. The pressure was changed from experiment to experiment starting from atmospheric and then incrementally reduced to high vacuum. Prior to each transient SPV measurement, the chamber pressure was monitored to stabilize for about 5 hours in the dark while observing the surface potential. Our results demonstrated that the rate of charge transfer during the fast process was approximately the same for all the ambient pressures whereas a significant change could be observed for the slow charge recombination processes,

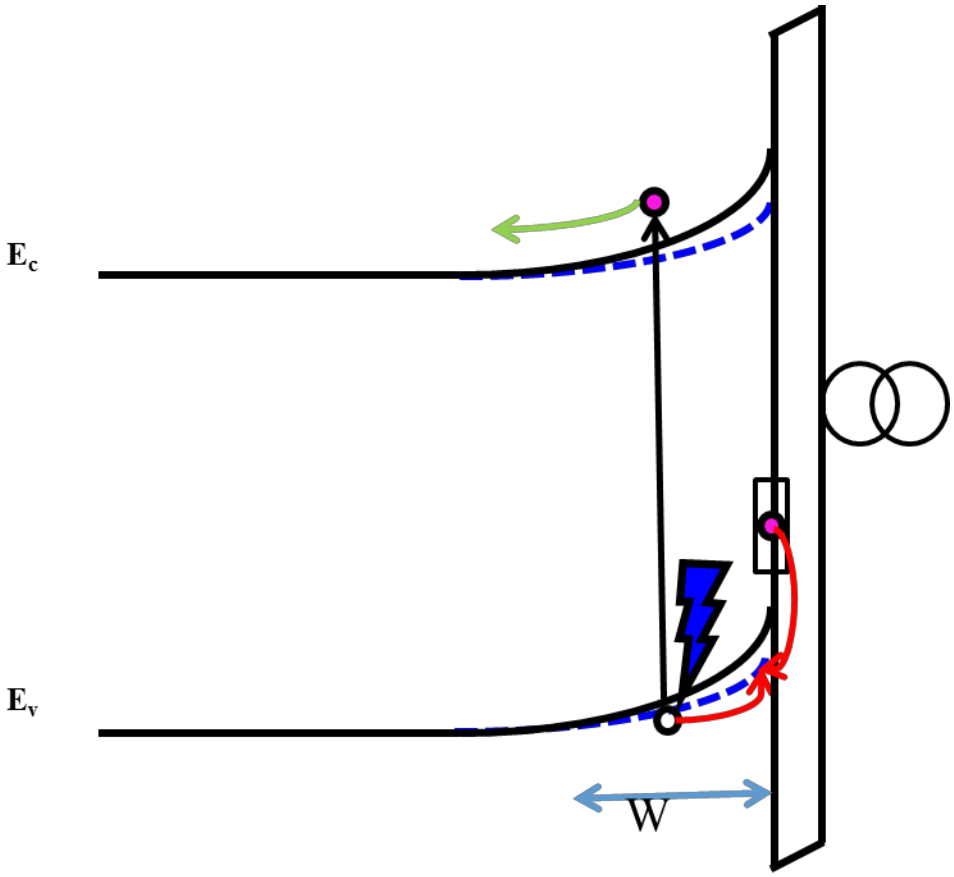

Figure 29 Model band diagram for NPS surface illustrating a fast (dominated by photo-assisted processes) charge redistribution occurring during light-on SPV transient in different environments.

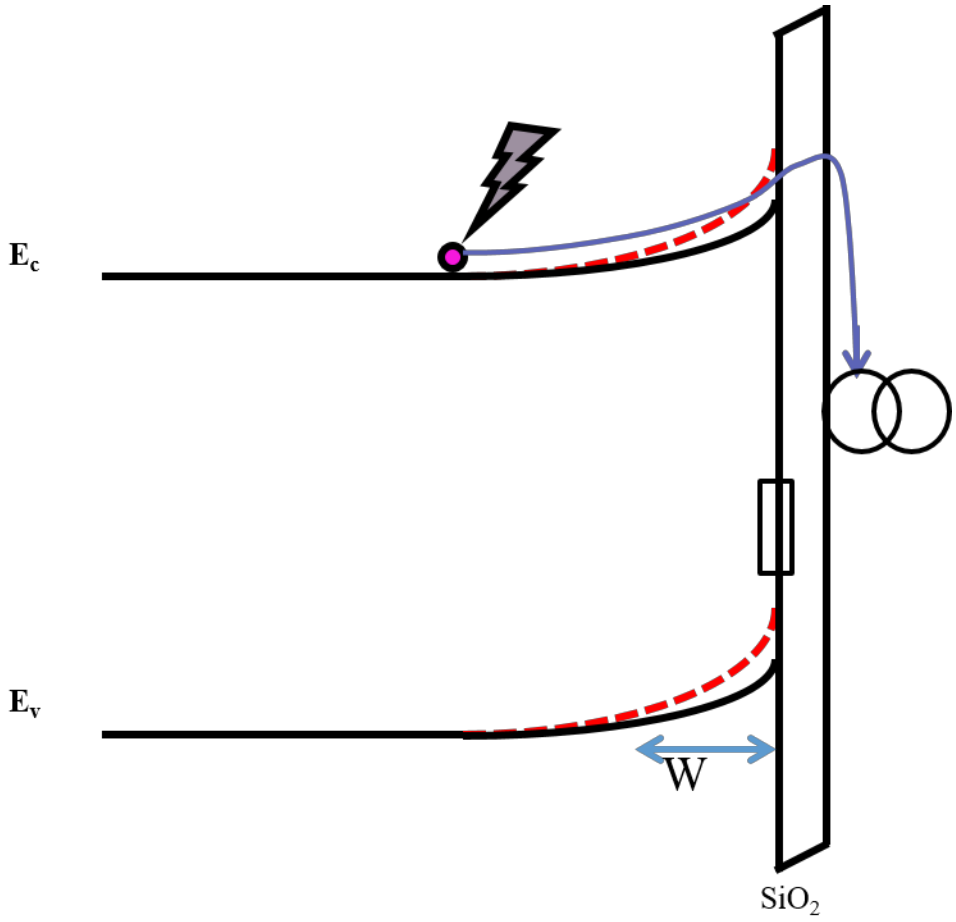

Figure 30 Model band diagram for NPS surface illustrating slow (dominated by phonon-mediated processes) charge redistribution occurring during light-on SPV transient in different environments.

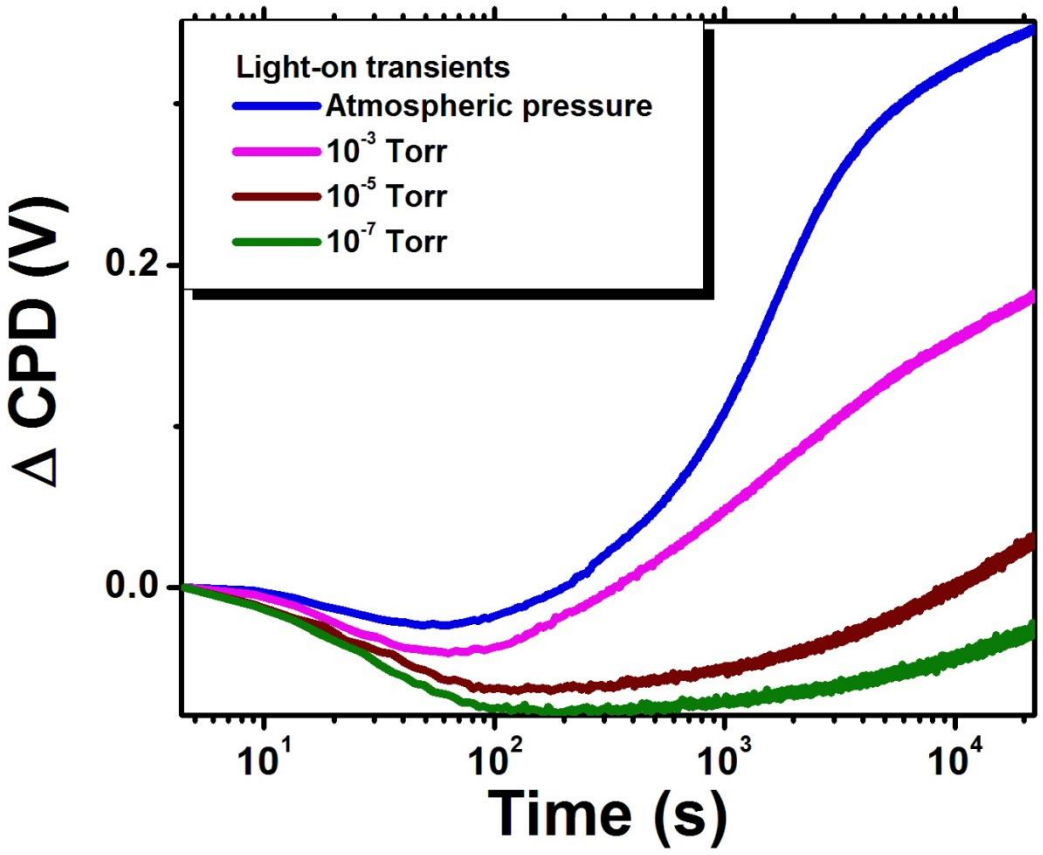

Figure 31 Pressure-dependent SPV in NPS. Slow processes are strongly affected by lowering experimental pressure during illumination.

consistent with our hypothesis that weakening of the slow process contribution with the decreasing pressure should be associated with the removal of the inherited adsorbed surface species from the surface. Even at 10^{-7} Torr not all the adsorbed species were taken away during the evacuation. This result clearly supports the model within which the fast charge recombination process is related to the intrinsic states and the slow to the surface-adsorbed species.

Additional confirmation of this hypothesis was carried out by studying the reversibility of the observed dependencies. The experiments were performed with the nitrogen gas pressure cycled from atmospheric through vacuum back to atmospheric. Fig. 32 shows the results of this cycling. One can clearly see that qualitatively the transient behavior is restored when the pressure returns to atmospheric, although a certain hysteresis is observed, most likely associated with irreversible loss of some surface adsorbates during evacuation.

From the practical point of view, such measurements should be useful in assessing the efficiency of this material for applications in optoelectronic gas sensors.

3.2. Verification of the surface conductivity type of NPS

Depending on the growth conditions, the surface conductivity type of porous silicon might be changed from that of its host material. For example, in [49] both *n*-type and *p*-type surface conductivity was reported for the porous silicon grown on a *p*-type Si. Determining the surface conductivity type of NPS is necessary to correctly ascertain the starting assumptions of the model, which in our case were based on the initially depleted surface of an *n*-type Si. To establish the type of the surface conductivity, we employed the wavelength-dependent

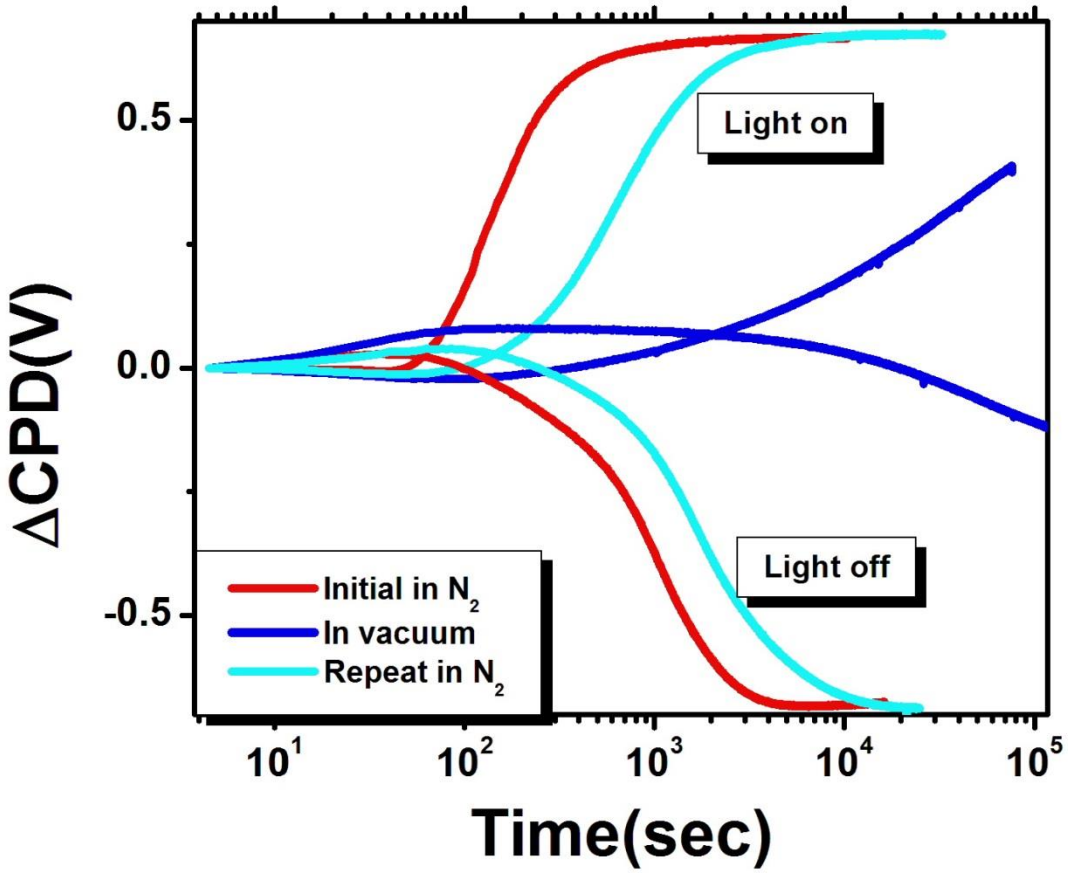

Figure 32 Light-on and light-off SPV transients in gas-vacuum-gas cycle.

measurements, the SPV spectroscopy [6]. Fig. 33 shows a distinct downward transition at ~1.85 eV (most likely related to the NPS bandgap broadening) for both nitrogen and vacuum environments indicating that the NPS layer has an *n*-type conductivity. Since an *n*-doped silicon wafer was used to grow the NPS layer, our result means that the conductivity of the NPS layer has not been changed, and the assumptions for the band diagram alignments were correct.

In most reported studies of transient SPV in porous silicon a broad-spectrum polychromatic light was used. Although only in a few papers a monochromatic excitation was applied, to the best of our knowledge, no work has been performed employing a comparative study using both polychromatic light and the monochromatic light. In our experiments we systematically studied SPV transients in both polychromatic and monochromatic light of several different wavelengths in vacuum and in nitrogen gas environments.

Fig. 34 juxtaposes the light-on and light-off SPV results employing polychromatic light, ultraviolet (325 nm), blue light (442 nm) and red light (632 nm) in N_2 gas. Fig. 35 shows the same set of curves obtained in vacuum.

Qualitatively, in almost all these wavelength-dependent experiments SPV transients with multiple components were obtained, albeit with different relative contributions, with the exception of the near-band edge (632 nm) excitation in vacuum, where only a single SPV transient component was observed. It is possible that during the near band-edge excitation only the sub-bandgap charge separation dominates over the thermal excitation of the bulk electrons reaching the surface. The electrons from interface states which are closer to the conduction band between Si and SiO_2 are promoted to the conduction band and then quickly swept into the bulk due to the strong electric field present at the surface. This might cause the decrease in the band bending and a single component in the CPD evolution. For the super-bandgap excitation the

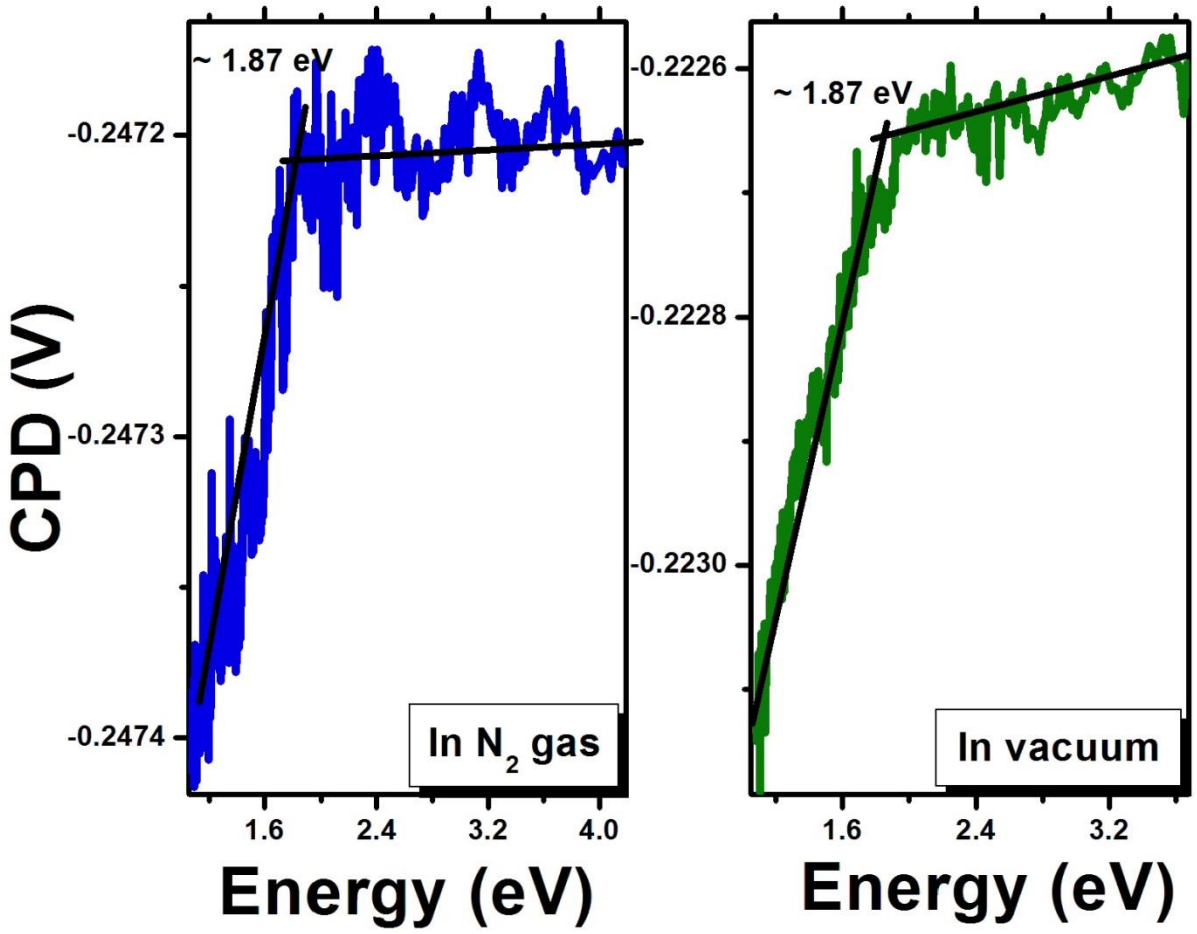

Figure 33 Bandgap of porous silicon measured in nitrogen and in vacuum by SPV spectroscopy.

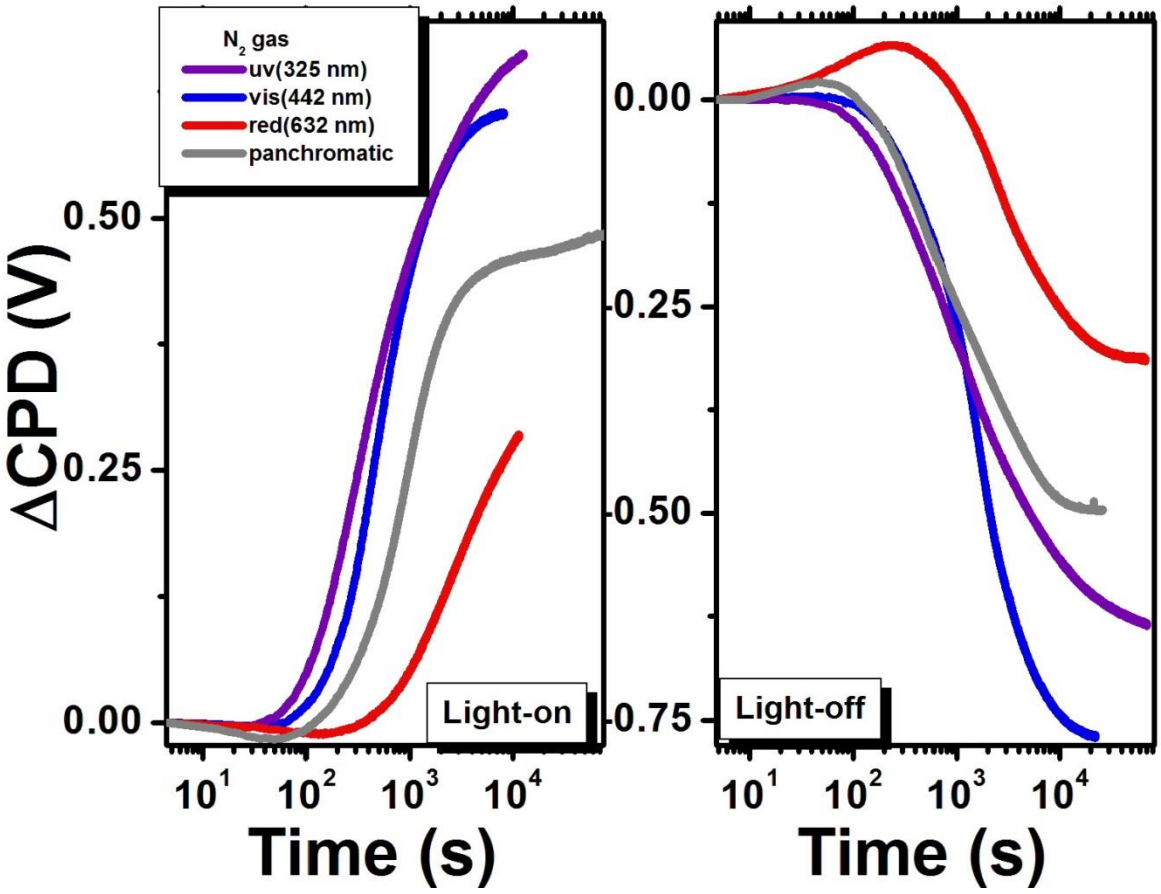

Figure 34 Light-on and light-off transients during excitation by polychromatic, 325 nm, 442 nm and 632 nm illumination in N_2.

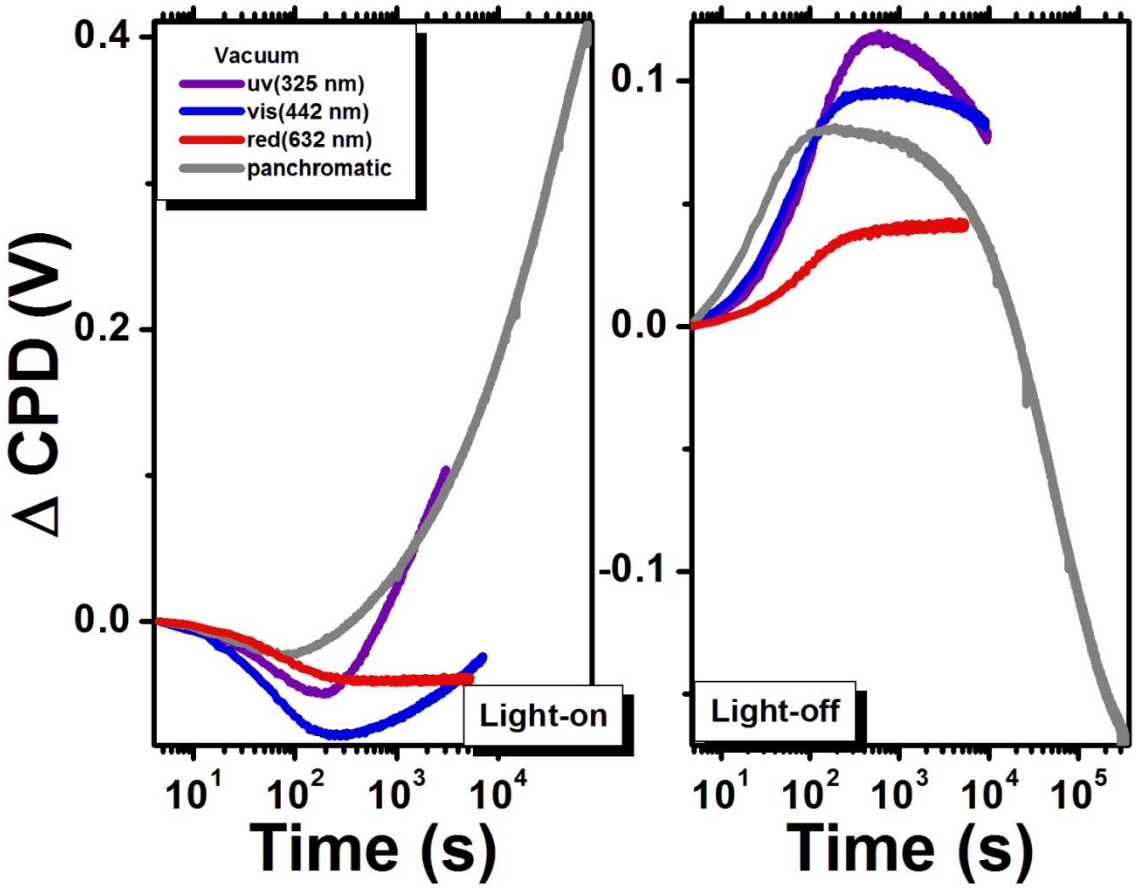

Figure 35 Light-on and light-off transients excited by polychromatic, 325nm, 442 nm and 632 nm illumination in vacuum.

electron-hole pairs are generated in the near-surface region. The flux of holes coming to the surface under the electric field modifies the electron-rich surface states whereas electrons move to the bulk thus giving rise to the fast process. Depletion of the surface electrons reduces the band bending which brings the thermal electrons from the bulk to the surface yielding the slow process. The relative contribution of the slow process is obviously increasing with the increasing energy of the incoming photons.

3.3. Illumination intensity-dependent SPV studies of NPS

The shape and the sign of the SPV transients are sensitive to the light intensity. The rate of change of the surface potential is directly related to the rate of charge transfer to the surface states. One way to measure the dynamics of such transfer is to monitor the slope of initial onset of the SPV transients as a function of light intensity, particularly for the processes related to optical transitions in the absence of thermally-mediated charge transport. For most semiconductors the dependence of such onset vs. light intensity was reported to be linear. In these materials, the underlying bulk serves as essentially an infinite reservoir supplying charge to the surface states. However, in the case of nanoscale materials the relative contribution of the bulk could be substantially reduced, and surface plays a dominating role in many processes. Thus a question arises whether the linear SPV onset vs. light intensity behavior common for bulk materials will be retained by such essentially nanostructured material as NPS. To address this issue we ran a series of light intensity-dependent transient SPV experiments on our NPS specimens.

Laser beams of wavelengths 325 nm, 442 nm, and 632 nm, with incident intensity controlled by neutral density filters, were used to study intensity-dependent SPV in NPS. The

results observed for the 325 nm excitation are shown below on both linear and logarithmic time scales (Fig. 36 and 37). One can clearly see the increase of the of SPV onset slope with the increasing illumination intensity.

Fig. 38 and 39 show SPV transients for the 442 nm excitation with different excitation intensities.

Fig. 40 and 41 show SPV transients for the 632 nm excitation with different intensities.

We employed analytical approach proposed by Reschikov *et*. *al*. [50] for transient SPV results obtained for GaN where the authors evaluated initial slopes of the light-on transients over several decades of photon flux values to calculate surface-related parameters. The onset slopes (the rate of change of surface potential immediately after turning on/off the light) were calculated by using the best linear fit (least squares) for the first five points which are presented in Table 2-4. The error bars for the slopes were calculated by evaluating the propagation of errors from the measured values of the initial rate of the slope change and the calculated slope. The absolute values of the onset slopes thus calculated for our samples for the light-on and light-off cycles plotted as a function of illumination intensities are illustrated in Fig. 42. We found that the slope change during light and dark conditions were approximately the same.

Importantly, for all the three excitation wavelengths, the onset slopes for NPS, were not linear functions of the illumination intensity. Initially $\frac{dV_s}{dt}$ increases with the increasing intensity and later reaches saturation at higher laser intensities for the 325 nm and 442 nm excitations. At lower excitation powers the functional dependencies follow the power law, scaling approximately as a square root of the incident intensity. This strongly non-linear behavior along with saturation at higher powers may be related to the limitations on the increase

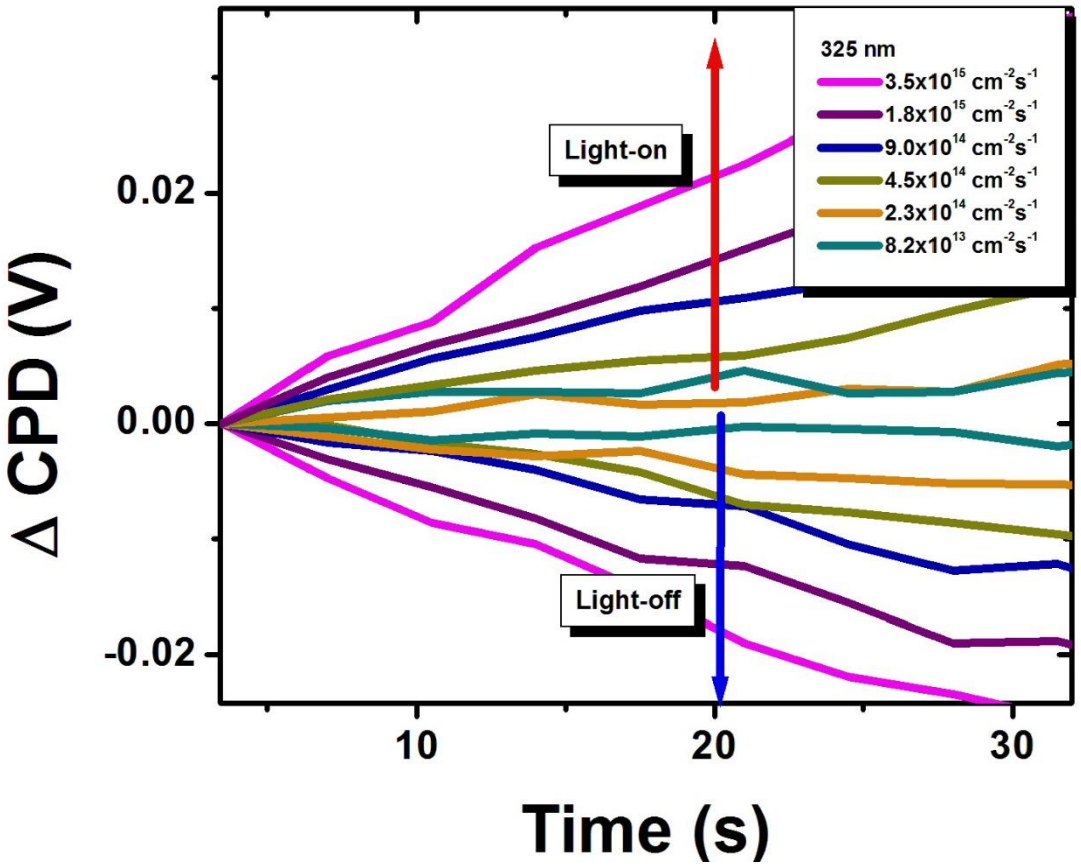

Figure 36 Intensity-dependent SPV transients for excitation by 325 nm light on linear time scale.

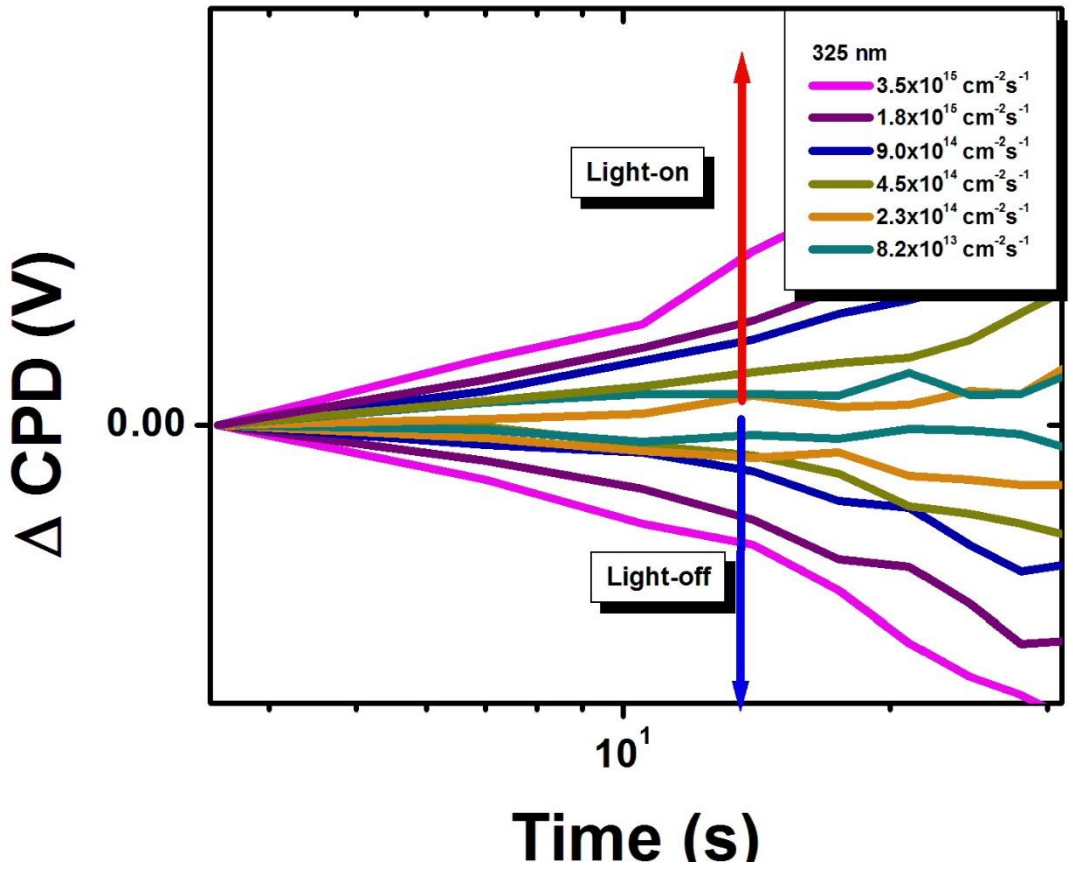

Figure 37 Intensity-dependent SPV transients for excitation by 325 nm light on logarithmic time scale.

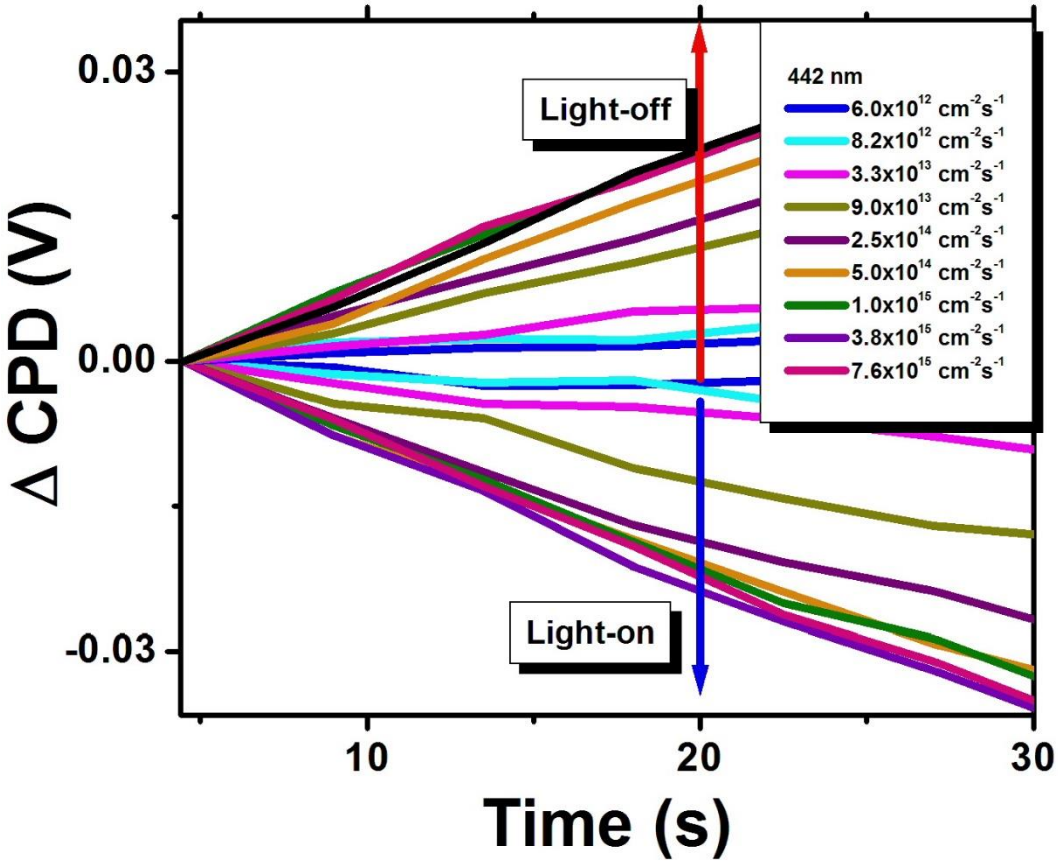

Figure 38 Intensity-dependent SPV transients for excitation by 442 nm light on linear time scale.

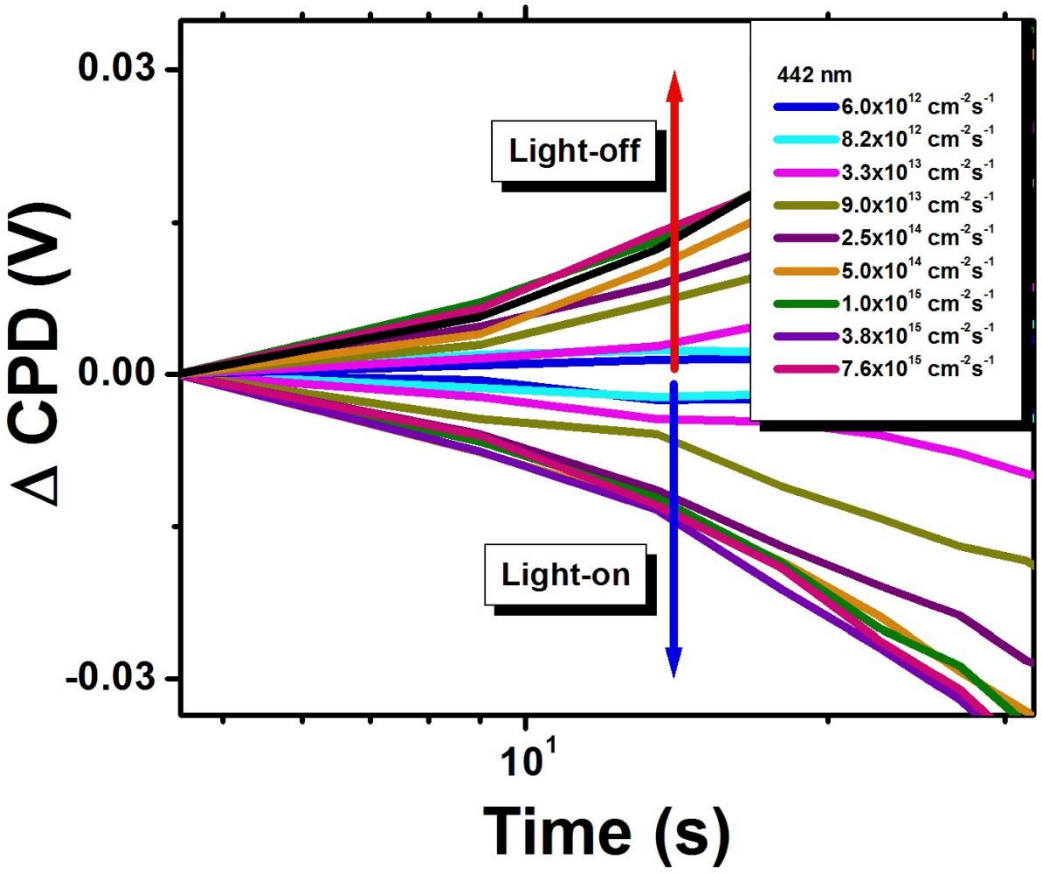

Figure 39 Intensity-dependent SPV transients for excitation by 442 nm light on logarithmic time scale.

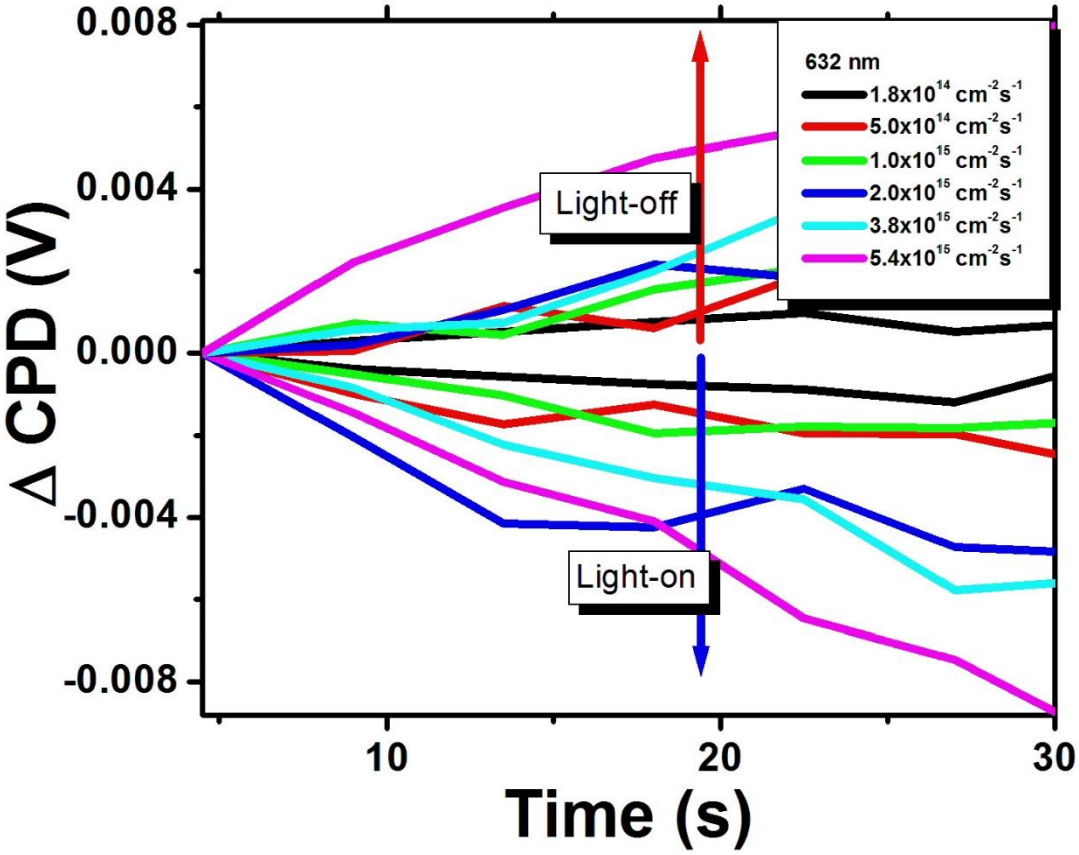

Figure 40 Intensity-dependent SPV transients for excitation by 632 nm light on linear time scale.

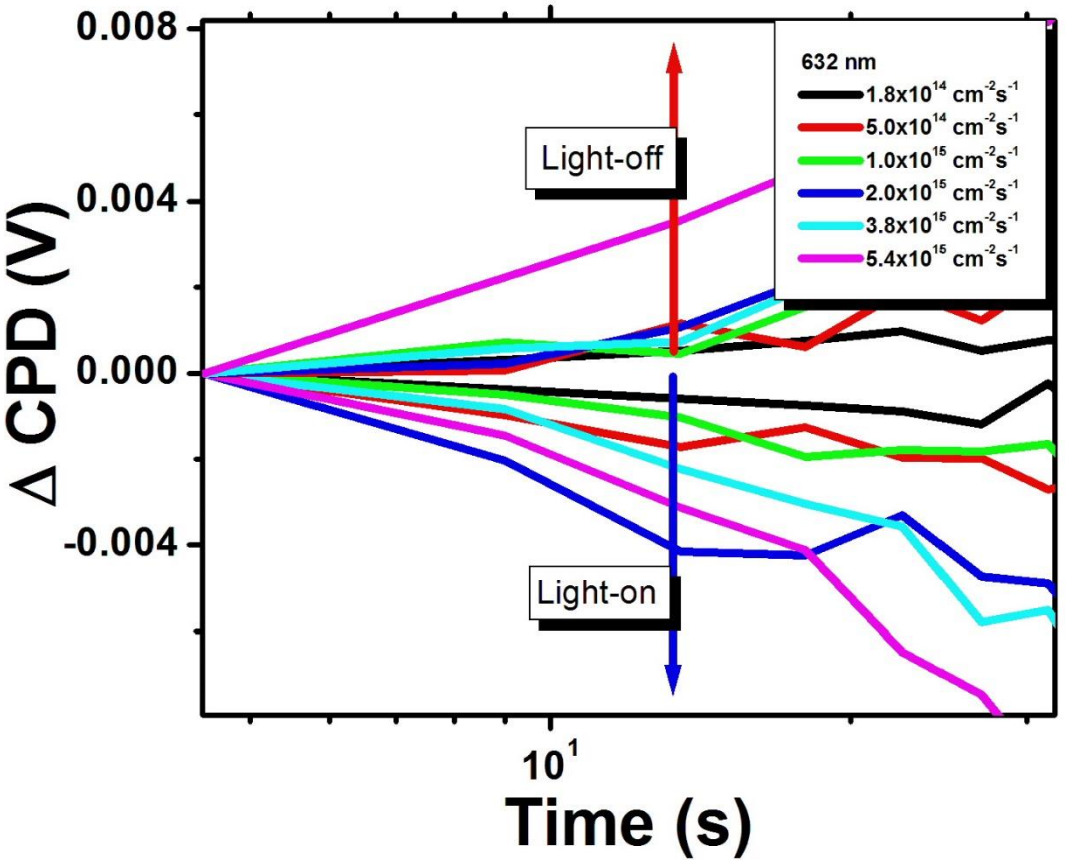

Figure 41 Intensity-dependent SPV transients for excitation by 632 nm light on logarithmic time scale.

Table. 2 Onset slopes of SPV for different 325 nm illumination intensities

325 nm	**Light-on**		**Light-off**	
Intensity $(cm^{-2}\ s^{-1})$	**Onset slope** $(V\ cm^2)$	**Error in slope** $(V\ cm^2)$	**Onset slope** $(V\ cm^2)$	**Error in slope** $(V\ cm^2)$
1.80×10^{13}	7.90×10^{-5}	4.00×10^{-5}	1.00×10^{-4}	5.00×10^{-5}
4.90×10^{13}	1.90×10^{-4}	1.90×10^{-5}	1.50×10^{-4}	2.70×10^{-5}
9.70×10^{13}	3.80×10^{-4}	2.40×10^{-5}	3.80×10^{-4}	2.00×10^{-5}
1.90×10^{14}	4.80×10^{-4}	3.20×10^{-5}	5.50×10^{-4}	4.10×10^{-5}
3.80×10^{14}	7.50×10^{-4}	3.40×10^{-5}	8.00×10^{-4}	1.80×10^{-5}
7.50×10^{14}	9.90×10^{-4}	7.90×10^{-5}	1.20×10^{-3}	2.90×10^{-5}

Table. 3 Onset slopes of SPV for different 442 nm illumination intensities

442 nm	**Light-on**		**Light-off**	
Intensity ($cm^{-2}\ s^{-1}$)	**Onset slope** ($V\ cm^2$)	**Error in slope** ($V\ cm^2$)	**Onset slope** ($V\ cm^2$)	**Error in slope** ($V\ cm^2$)
5.50×10^{12}	1.20×10^{-4}	5.60×10^{-5}	9.20×10^{-5}	1.70×10^{-5}
7.70×10^{12}	2.00×10^{-4}	4.40×10^{-5}	1.50×10^{-4}	3.50×10^{-5}
3.00×10^{13}	3.20×10^{-4}	4.80×10^{-5}	3.30×10^{-4}	3.50×10^{-5}
8.40×10^{13}	7.80×10^{-4}	6.20×10^{-5}	7.80×10^{-4}	2.00×10^{-5}
2.30×10^{14}	1.20×10^{-3}	4.90×10^{-5}	9.50×10^{-4}	1.90×10^{-5}
4.60×10^{14}	1.30×10^{-3}	5.60×10^{-5}	1.20×10^{-3}	4.90×10^{-5}
9.00×10^{14}	1.30×10^{-3}	2.00×10^{-5}	1.40×10^{-3}	4.60×10^{-5}
3.60×10^{15}	1.50×10^{-3}	4.50×10^{-5}	1.40×10^{-3}	6.00×10^{-5}
7.00×10^{15}	1.50×10^{-3}	2.10×10^{-5}	1.40×10^{-3}	3.70×10^{-5}

Table. 4 Onset slopes of SPV for different 632 nm illumination intensities

632 nm	**Light-on**		**Light-off**	
Intensity ($cm^{-2}\ s^{-1}$)	**Onset slope** ($V\ cm^2$)	**Error in slope** ($V\ cm^2$)	**Onset slope** ($V\ cm^2$)	**Error in slope** ($V\ cm^2$)
3.00×10^{14}	4.90×10^{-5}	4.20×10^{-6}	5.40×10^{-5}	1.90×10^{-6}
6.00×10^{14}	7.80×10^{-5}	2.20×10^{-5}	9.70×10^{-5}	3.30×10^{-5}
1.70×10^{15}	1.10×10^{-4}	2.00×10^{-5}	1.00×10^{-4}	2.40×10^{-5}
2.30×10^{15}	2.00×10^{-4}	8.90×10^{-5}	1.30×10^{-4}	2.90×10^{-5}
4.60×10^{15}	2.10×10^{-4}	1.80×10^{-5}	1.90×10^{-4}	3.60×10^{-5}
5.40×10^{15}	3.50×10^{-4}	2.40×10^{-5}	3.00×10^{-4}	3.60×10^{-5}

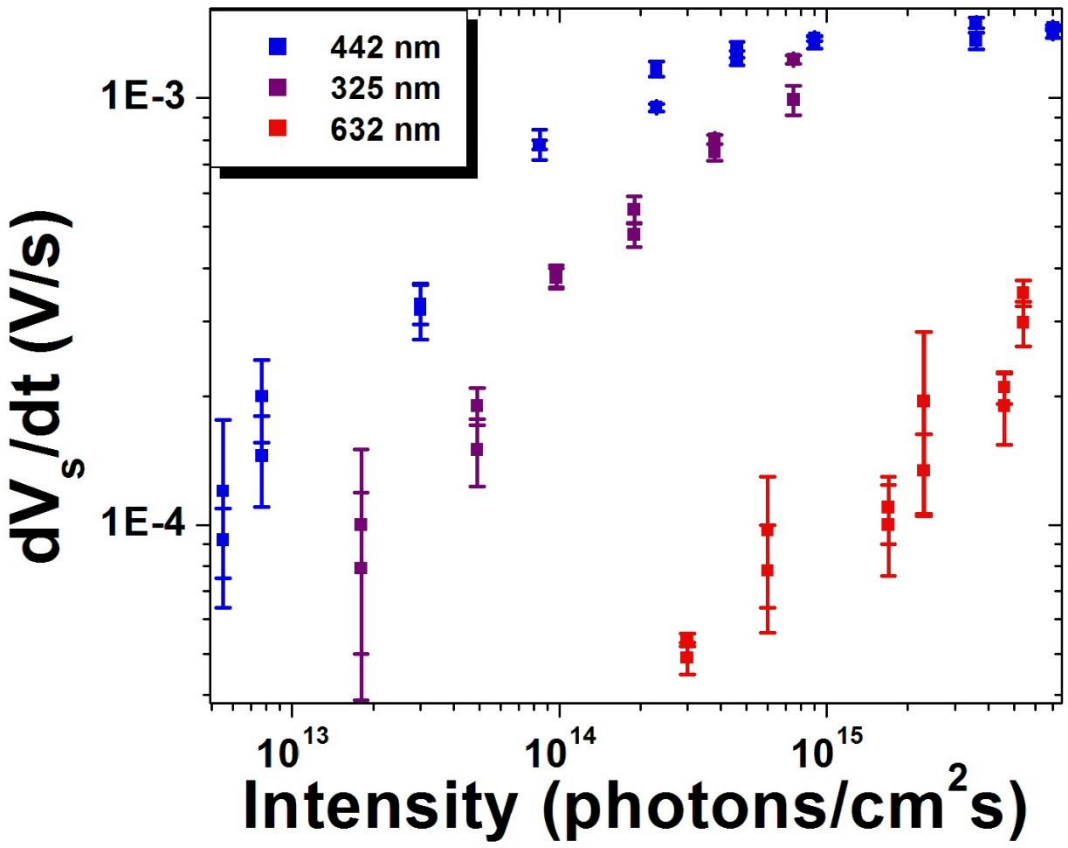

Figure 42 SPV onset values vs. light intensity of incident photons for three different excitation wavelengths.

of the excess carrier concentration in NPS, which can be explained as follows. In our model, we have assumed that for the super-bandgap excitation, electron-hole pairs are generated in the near-surface region through interband transitions and via modification of the interfacial states by holes due to the band bending being reduced by the field. The corresponding reduction in the surface barrier allows electrons from the bulk to tunnel to the surface and become trapped by the surface adsorbates at the oxide surface. This process would effectively increase the barrier. However, there is limitation on the excess hole current change with the excitation intensity as governed by Goodman's relation [6]: $\delta p(w) = \left(\frac{1}{1+\frac{1}{\alpha \mathrm{L}}}\right)\left(\frac{1}{s+\frac{D}{L}}\right) I$ where α is the absorption coefficient, L is the diffusion length for holes, D is the diffusion coefficient for holes, s is the drift velocity for holes at the edge of the space charge region and I is the illumination intensity. According to this model, electron-hole pairs are generated not only in the SCR but also in the quasi-neutral bulk. The excess holes generated in the SCR drift due to the electric field to the surface whereas the holes in the quasi-neutral bulk within the diffusion length of the SCR edge, drift *and diffuse* toward the surface. The values of D and L are affected by the impurity density, and if s is much smaller than D/L, this model will not be valid. Since the depletion width is rather small and absorption decreases almost exponentially from the surface into the bulk, the diffusion from the surface will dominate over the drift and even for an increasing illumination intensity the excess holes diffusing towards the bulk will produce saturation of the SPV values. Also it has been reported that depending on the geometry of NPS, the mobility of electrons can be 2 to 3 orders of magnitude greater than the mobility of holes [93]. The diffusion of the charge carriers may give rise to the Dember effect affecting the initial rate of SPV [6.]. Thus interference of the drift and the Dember effect may cause the non-linearity in the onset slope vs. intensity dependence.

Several additional factors may be involved in limiting the supply of excess carriers such as the ratio of the capture cross-sections of holes and electrons, involvement of multiple surface states [94], as well as interference between super- and sub-bandgap illumination, etc.

3.4. Surface photoresponse studies of NPS embedded with metal nanoparticles

For potential applications of NPS in nanospintronics, its pores could be embedded with nanoparticles of magnetic metals such as Ni and Co [61]. In order to test whether these nanoparticles affect the photoresponse performance, we carried out SPV measurements for metal-filled NPS in N_2 and in vacuum. Figure 43 shows SPV transients for the Ni-filled NPS in the N_2 gas environment. The anomalous voltage spikes were also present in this sample during turning on and off the illumination. In Fig. 44 SPV transients observed for a pristine and Ni-filled NPS are presented for comparison on a logarithmic time scale illustrating similar trends for both samples during the light-on and light-off intervals. SPV transients for the Ni-filled NPS in vacuum also revealed curves similar to those for a pristine NPS in vacuum (not shown here).

As we observed transient SPV behavior of the metal-embedded NPS for both vacuum and non-vacuum environments similar to that of the pristine NPS suggesting that the embedded metal nanoparticles did not play any significant role in the surface photoresponse properties of NPS. The shift in the transient curves for Ni-filled NPS (Fig. 44) can be described as follows. Due to the presence of metal particles the surface potential barrier in the composite material may change relative to that in the pristine NPS. As described in ref. [92], a change in the surface barrier height from 0.4 eV to 1 eV brings multiple orders of magnitude change in the saturation time.

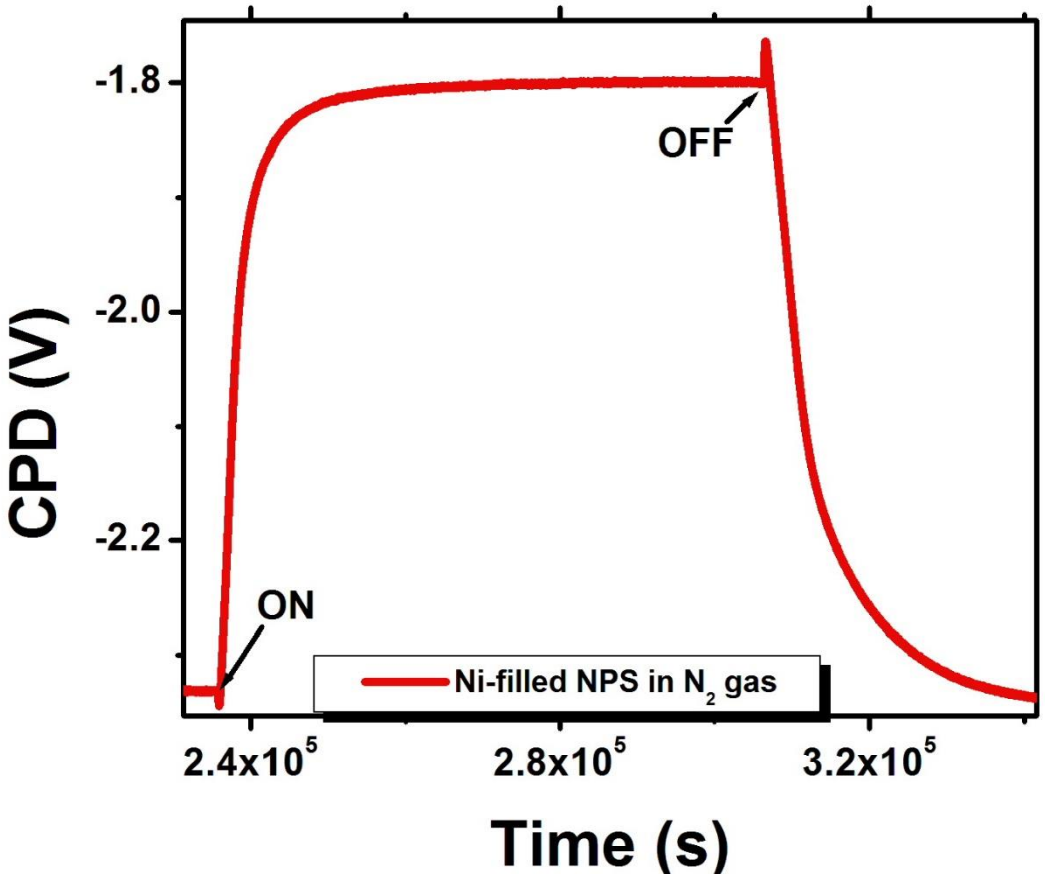

Figure 43 CPD during illumination and in dark in N_2 for Ni-embedded NPS on linear time scale.

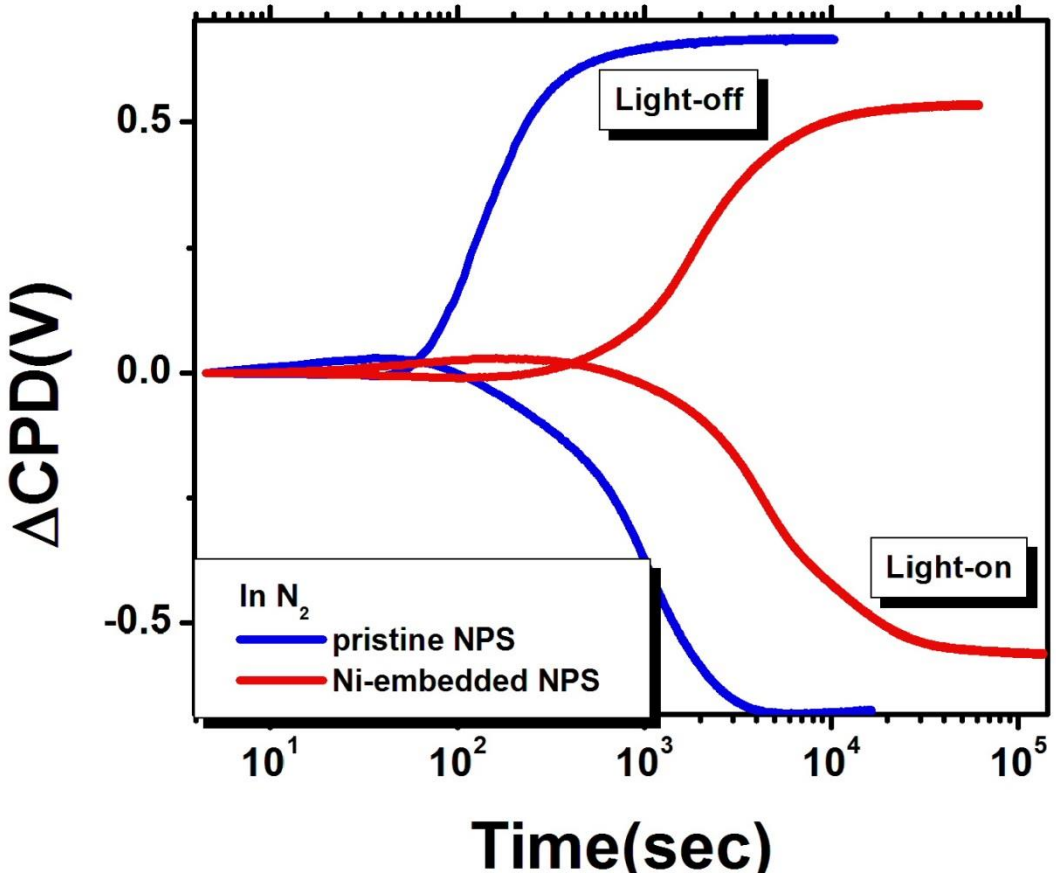

Figure 44 CPD during illumination and in dark in N_2 for both pristine and Ni-filled NPS on logarithmic time scale.

Having established the substantial sensitivity of the SPV transients to the ambient pressure in our experiments we also addressed the question whether the surface photoresponse of NPS is gas selective. In order to tackle this issue, we performed SPV transient experiments of Ni-embedded NPS in such different gas environments as oxygen, helium and argon. We found no significant influence of the type of gaseous ambient on the SPV transient behavior. Figs. 45 and 46 show the results of these measurements, indicating that the surface band bending in NPS is independent of the type of gas environment, yet strongly dependent on the ambient pressure. This behavior observed for the metal-infused NPS could be useful for dual spintronic/sensor applications.

With all the results described above it is important to understand whether the observed behavior of the surface band bending in different ambients is generic for different nanoscale materials or specific to NPS only. Figs. 47 and 48 show SPV transients obtained for SNT with the largest diameter in N_2 gas and in vacuum on a linear and a logarithmic time scale respectively. One can clearly see that the surface photoresponse of SNT during the light-off process is not symmetric with respect to the response during the light-on interval, which is very different from that of NPS thus answering the question on the material-specific nature of transient SPV dependence on the ambient.

We also monitored time evolution of the surface potential in SNT with different diameters in vacuum, and the observed results are illustrated in Fig. 49 on both linear and logarithmic time scales. The light-on transients for the SNT with the largest external diameter revealed multiple processes, as fitted by a superposition of several exponential transient components, and the light-off transients showed only a single exponential component. On the other hand, the SNT samples with smaller external diameters (70 nm and 85 nm) showed only a single transient component both during illumination and in the dark.

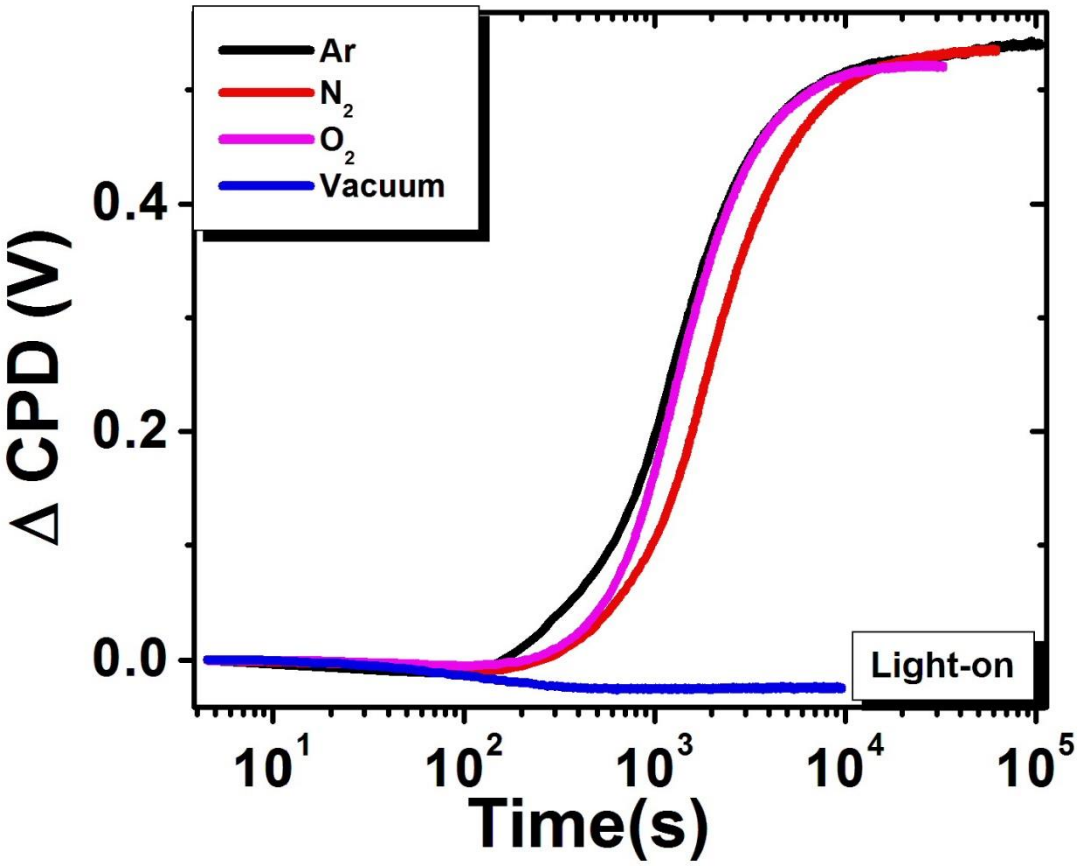

Figure 45 Change in CPD for Ni-embedded NPS in different gas environments for light-on intervals.

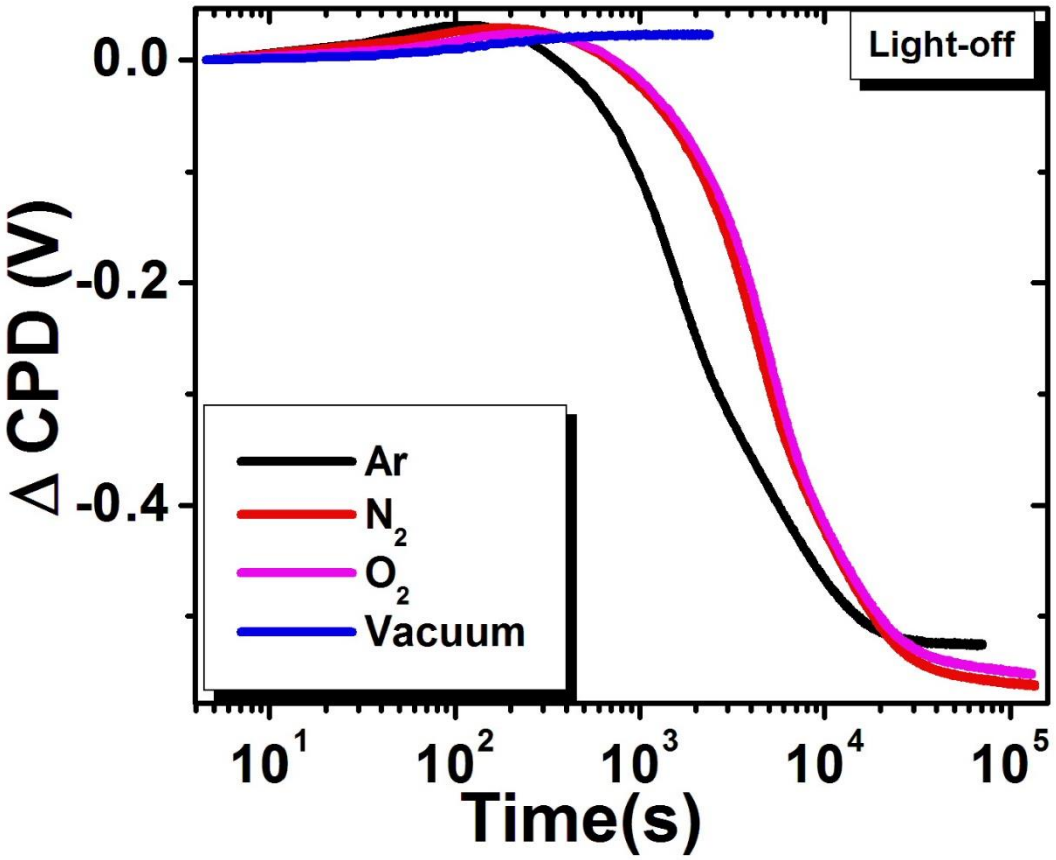

Figure 46 Change in CPD for Ni-embedded NPS in different gas environments for light-off intervals on logarithmic times scale.

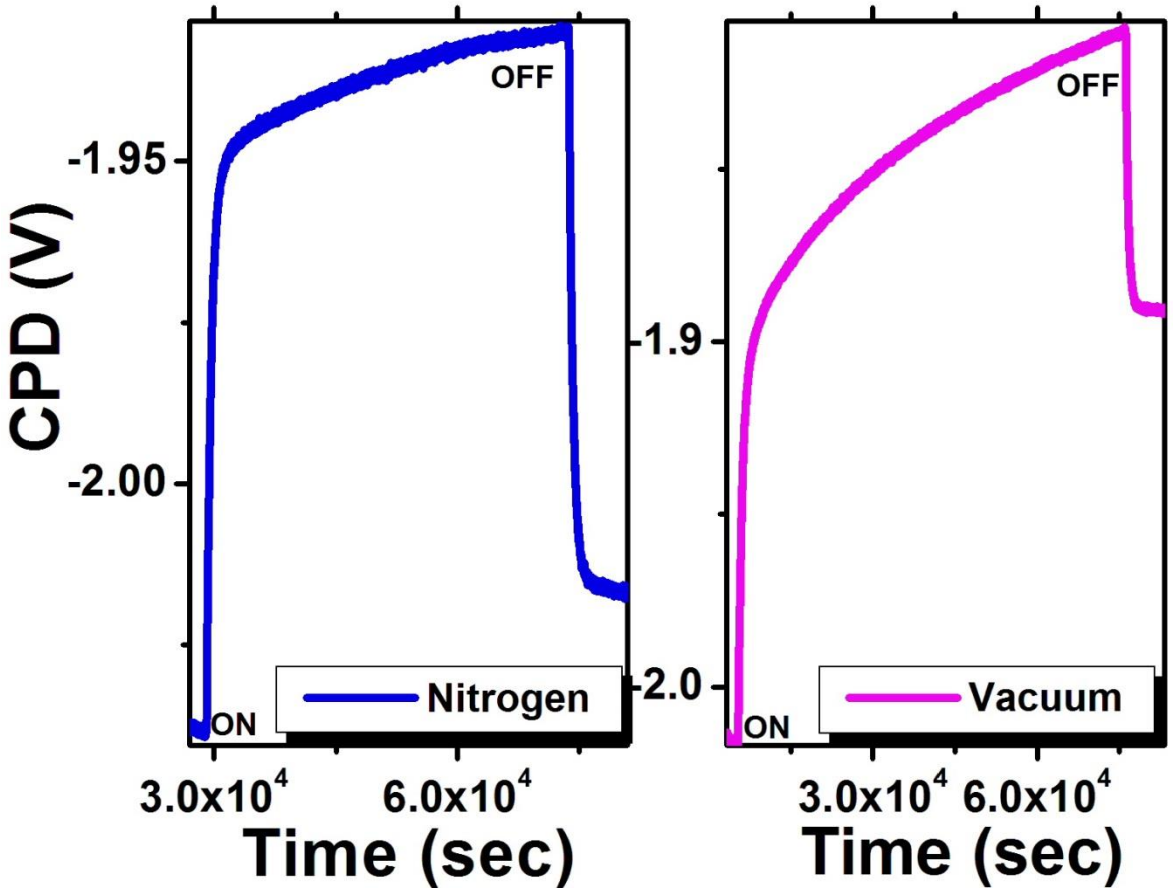

Figure 47 SPV transients for SNT with largest external diameter in N_2 gas and in vacuum on linear time scale.

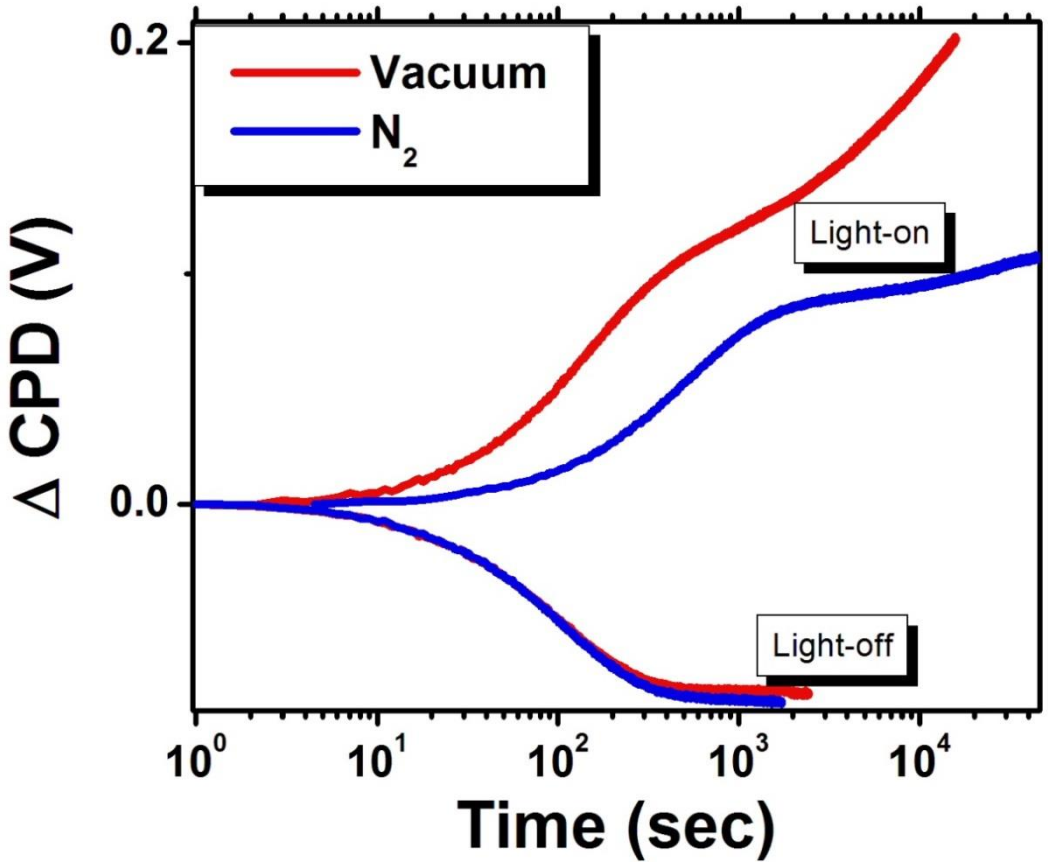

Figure 48 Light-on and light-off transients for SNT with largest external diameter in N_2 gas and in vacuum on logarithmic time scale.

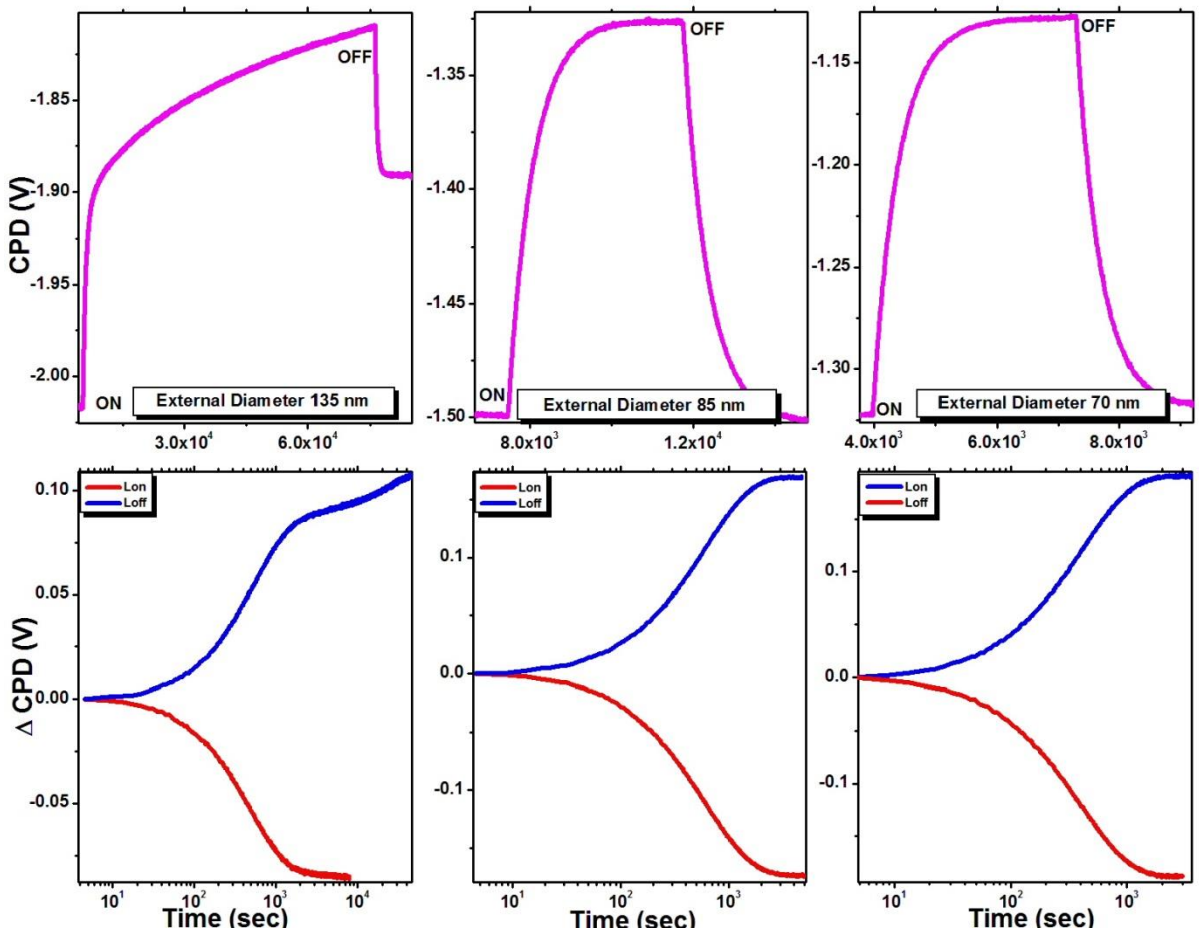

Figure 49 SPV transients for SNT of different external diameters in vacuum (first row – on linear time scale and second row – on logarithmic time scale)

The following possible mechanisms of the observed phenomena could be suggested. In the sacrificial template method, the undoped silicon tubes were grown on a *p*-type silicon substrate. To single out a possible contribution from the substrate, we performed SPV transient measurements separately for the *p*-type silicon wafers, on which the tubes were grown, as shown in Fig. 50. The curves reveal, as expected, a response of an accumulated *p*-type surface (please see p. 33). It is worth noting that whereas the light-on transients have only one component, the light-off transients exhibit most likely multiple components. One can clearly see that the change in the surface potential for both the light-on and light-off intervals is completely opposite for the bare wafers and the specimens with the tubes.

For the observed multiple and single processes in the SPV transients of SNT in nitrogen and vacuum during illumination, we propose three primary competing processes:

i. Trapping of photo-induced electrons at the Si/oxide interface;
ii. Diffusion of excess charge carriers along the nanotube due to the concentration gradient;
iii. Drift of photo-generated charge carriers at the nanotube/bulk silicon interface.

Even though the tubes themselves are intrinsic (undoped), the bands at the Si/SiO_2 interface bend downwards due to the presence of the interface states on the Si side (Fig. 51). The electron-hole pairs are generated in the near-surface region, the holes drift towards the bulk whereas the electrons move towards the surface due to the electric field present at the Si/SiO_2 interface and then trapped at the interface states. This leads to the decrease of the surface band bending. At the same time, due to the non-uniform absorption of light from the surface into the bulk, the diffusion of the carriers occurs along the tubes. For an intrinsic Si, the mobilities of electrons $(\mu_e = 1900\ cm^2/Vs)$ and holes $(\mu_e = 500\ cm^2/Vs)$ are very high [96]. From Einstein's relation the diffusion coefficients for electrons and holes at room temperature are

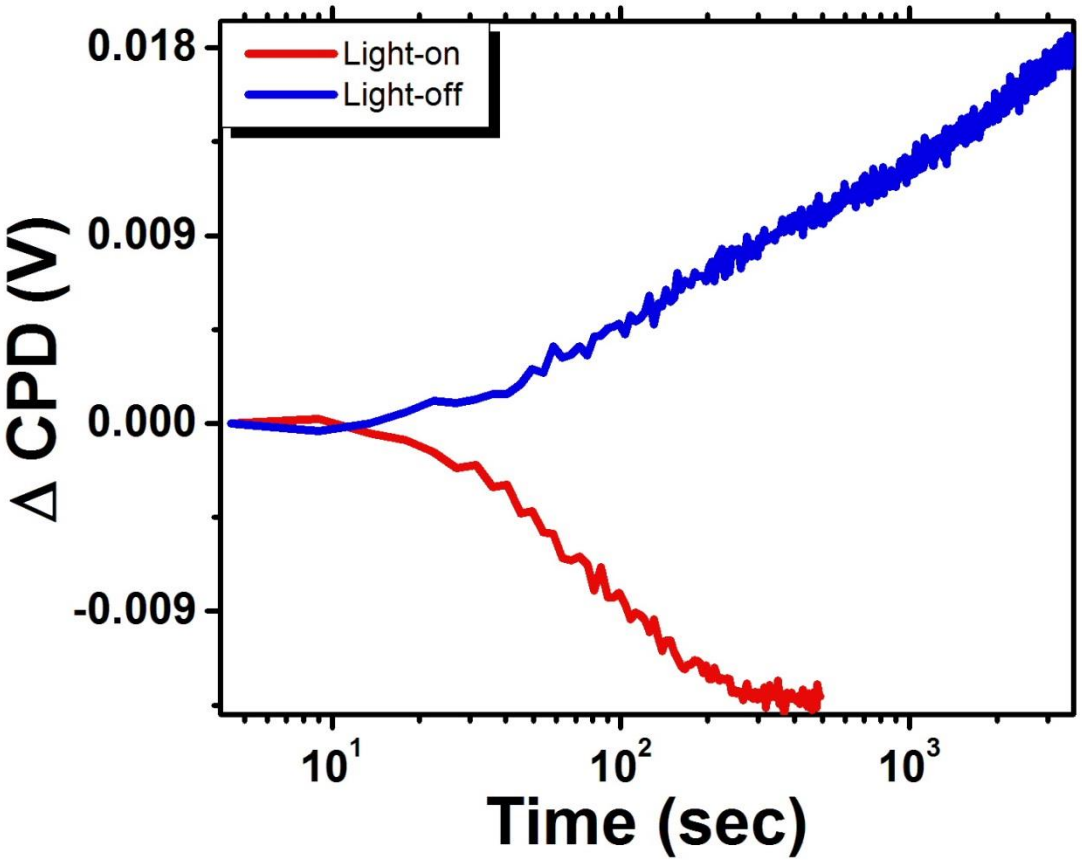

Figure 50 SPV transients for bare *p*-type silicon wafers.

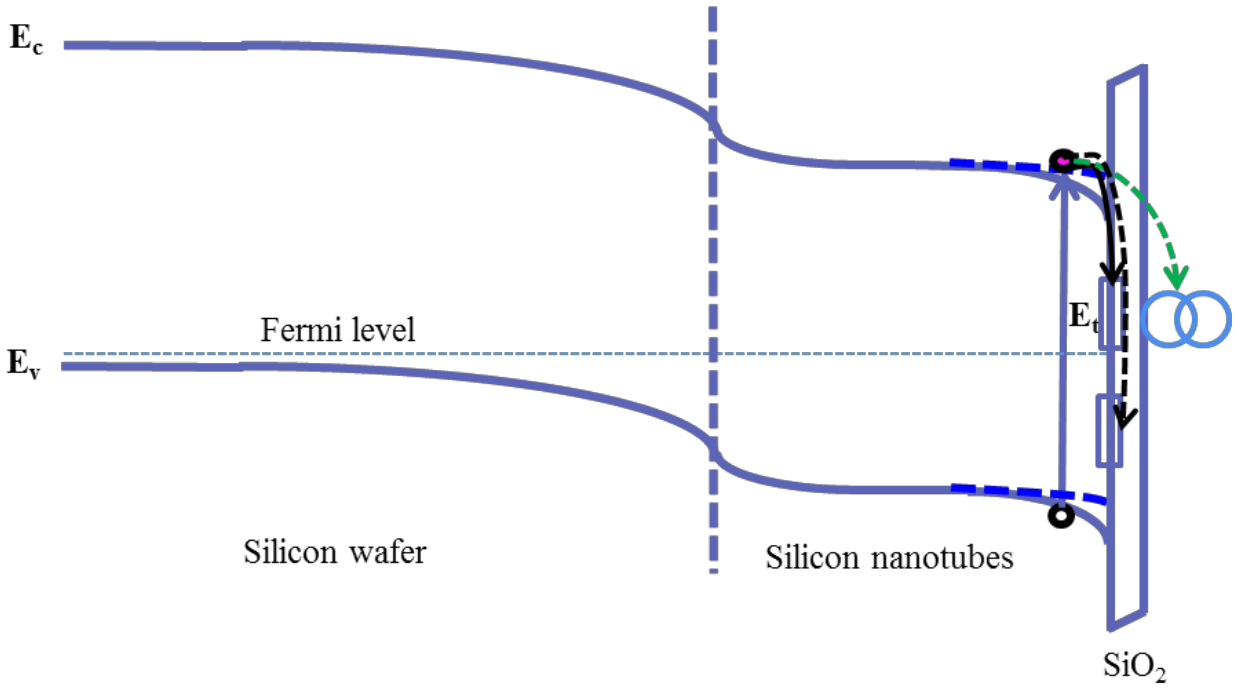

Figure 51 Surface band bending in SNT in nitrogen and in vacuum conditions. Fast process related to charge exchange with shallow interface states and slow process – to charge exchange with surface adsorbates or with deep level interfacial traps (solid lines – initially in dark and dashed lines – illumination).

$D_e = \left(\frac{k_B T}{e}\right)\mu_e = 500\ cm^2/s$ and $D_h = \left(\frac{k_B T}{e}\right)\mu_h = 13\ cm^2/s$, respectively,. For an intrinsic silicon the effective masses for electrons and holes are approximately the same at room temperature. Since the diffusion times for holes (τ_h) and electrons (τ_e) are inversely proportional to the effective mass, we can consider them equal. For the *p*-type and *n*-type silicon, their magnitude at room temperature is below 10^{-3} s [97]. Thus for the diffusion times we have $(\tau_e \approx \tau_h \approx 1\times10^{-6}\ s)$ so the diffusion lengths for electrons and holes are found to be $(L_e = \sqrt{D_e\tau_e} \approx 70\ \mu m,\ L_h = \sqrt{D_h\tau_h} \approx 36\ \mu m)$ [96], which are greater than the lengths of the tubes $(1-2\ \mu m)$. Thereby, both electrons and holes can diffuse into the bulk of the substrate. Because the mobility of the electrons is higher than that of the holes, the electrons may diffuse deeper into the bulk than the holes. However, the electrons are pushed back towards the Si/SiO_2 interface at the nanotube top surface by the electric field present at interface between the nanotubes and the substrate. They could be captured by the states at the Si/SiO_2 interface or by the surface adsorbates, leading to the further decrease of the surface band bending. In this case the deep level traps might be involved in the observed slower processes in the SPV transients or, alternatively, a chemisorption of the physisorbed species takes place. Although all the processes occur simultaneously, the process occurring in the presence of the field dominates in the beginning resulting in the fast SPV component while other processes such as diffusion and trapping by the deep level interface states or the adsorbed species may be responsible for the slower SPV components. The presence of the fast process only in the samples with smaller external diameters might be the consequence of the reduced size of the tubes. It has been found that in nanoscale materials the interface states extend through the edge of the conduction band to the middle of the gap when the size of the nanostructure is reduced [69-70]. Thus, it may be

possible that the fast process is the dominating one in the tubes with the smaller external diameters and it is very difficult to observe the slower components in the light-on transients. These nanotubes are separated from each other by ~ 45 nm, thus there may be a possibility of charge generation along the side of the tubes due to the illumination. We however, neglect the effects of the side surface contribution.

We performed similar measurements on GC specimens described above. Oxygen-containing functional groups in these materials behave as the possible adsorption sites for different species. Figure 52 shows SPV transients for GC in different ambients on the linear time scale in nitrogen gas and in vacuum, clearly indicating an unsymmetrical light-on vs. light-off behavior, which is different from that observed for NPS. The SPV transients in both nitrogen gas and vacuum show a rapid decrease in the CPD response followed by a slow rise opposite to the fast response. On a logarithmic time scale (Fig. 53), we can clearly see that the transients in both environments are similar and reveal fast and slow response during the light-on and light-off cycles. The fast response during the illumination in both environments occurred on approximately the same time scale whereas the slow response in vacuum took longer time to saturate. The transients in the dark didn't saturate even in more than 12 hours.

The multi-component SPV transients observed for GC could be explained by the model developed for NPS. The processes occurring on the shorter time scale might be related to the charge exchange with the intrinsic surface states related to the sp^2-hybridized carbon and the process occurring in the longer run might be associated with the surface species that are physisorbed at the surface of graphene and its derivatives (GO or rGO) thus converting them to chemisorbed in a gaseous environment. For the slow transient process in vacuum it takes longer time to saturate because of the removal of physisorbed species from the surface during

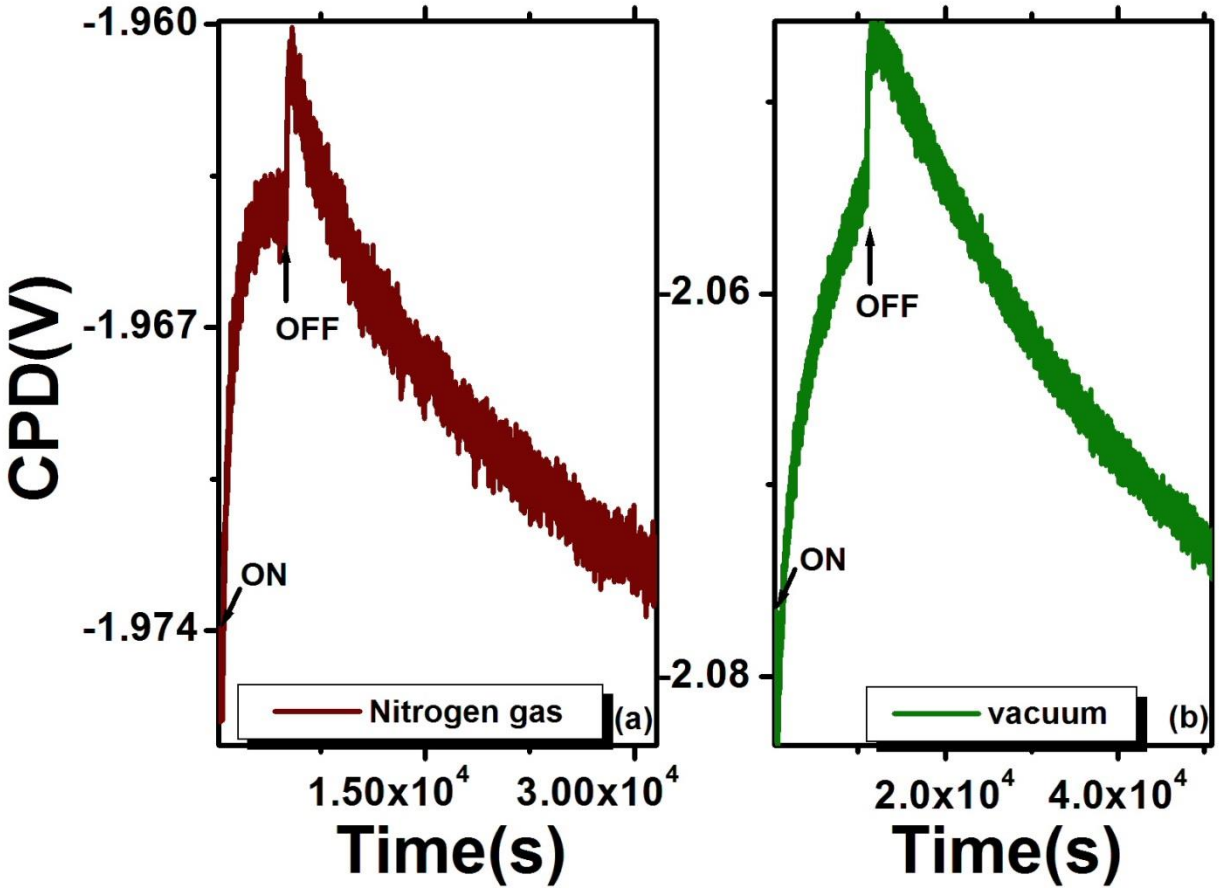

Figure 52 SPV transients for GC in (a) N_2 gas and (b) in vacuum on linear time scale.

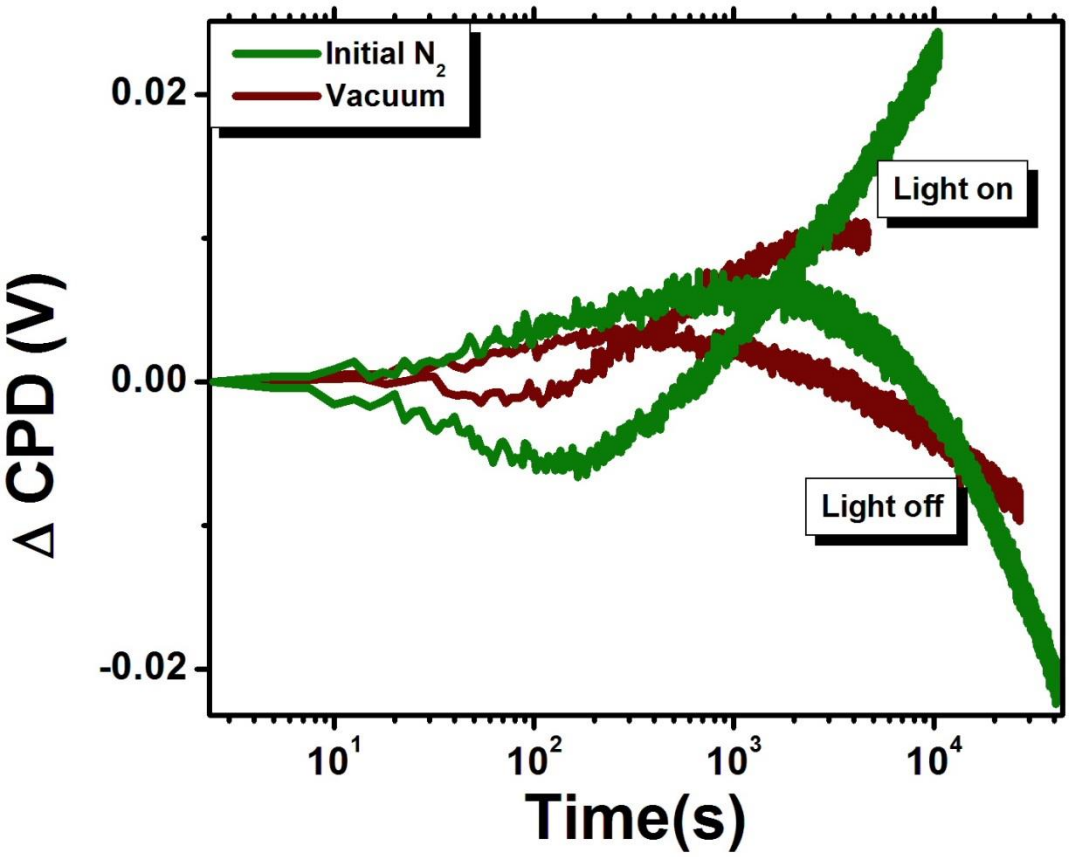

Figure 53 SPV transients for GC during light-on and light-off intervals in N_2 and in vacuum on logarithmic time scale.

evacuation. The lack of saturation in the dark might be due to the persistent photo-response related to surface adsorption and desorption, as suggested for ZnO [98] and GaN [50]. Alternatively, involvement of multiple surface states or the charge exchange between extrinsic states, intrinsic states and the bulk might be involved in the charge dynamics in the dark. These results show that GC could be a potential optoelectronic gas sensor. Furthermore, we performed a reversibility test in a N_2 environment after a nitrogen-vacuum cycle. We observed a reasonable reversibility of the SPV transients (Fig. 54).

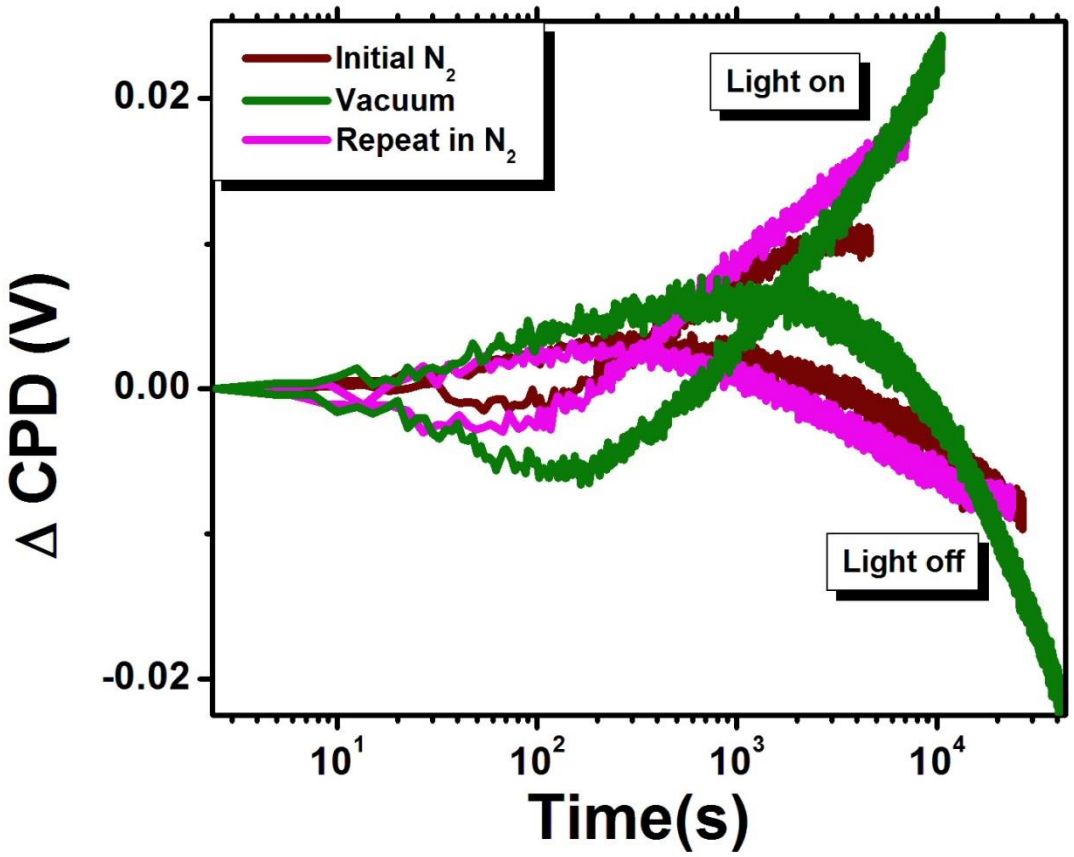

Figure 54 Light-on and light-off SPV transients for GC showing behavior during N_2-vacuum-N_2 cycle.

Chapter 4

4. Conclusions

Using SPV transients, we studied nanoporous silicon specimens in different environments and were able to answer the following questions:

1. How does the ambient affect the surface band bending of NPS?

The surface barrier height of NPS was found to be sensitive to the experimental environment. SPV transients showed fast and slow components during the light-on events in different ambient pressures. The time scale for the fast process remained approximately same but the strength of slow process become weaker with the decrease in pressure. To the best of our knowledge, there were no reports on the systematic studies of SPV sensitivity to the variation of ambient pressure in NPS.

2. What are the possible mechanisms for the observed transient behavior in different environments?

Since the fast process remains unaffected and the slow process is heavily affected by the environment we suggest that the fast process might be related to the recombination of electrons from the states at the Si/SiO_2 interface and photo-generated holes in NPS driven towards the silicon surface by the electric field present in the SCR, whereas the slow process may occur due to the trapping of bulk electrons by the adsorbates at the oxide surface via tunneling through the oxide layer. The slower process becomes weak in vacuum, which may be due to the desorption of the surface species from the oxide surface during evacuation. The fast charge recombination process is not affected by the ambient pressure whereas the slow charge recombination process decreases gradually from high pressure to the very low pressure confirming our hypothesis of the

rapid response and its relation to the intrinsic interface states and the relation of gradual response to the surface-adsorbed species. Fast and slow SPV processes were observed previously in NPS [39-41], where the slow process was attributed to the diffusion between the bulk and the oxide/silicon interface states. We argue that the results of our studies point to another possible explanation of the slow process – namely due to the diffusion between the bulk and the species absorbed at the free surface of the NPS material.

3. What are the effects of the excitation wavelength on the surface band bending in NPS?

Except for a monochromatic near-band edge excitation in vacuum, we observed multiple SPV processes in different ambients for both poly- and monochromatic excitation. It is possible that the near band-edge excitation is sufficient to just depopulate the interface states whereas in the super-bandgap excitation the excess carriers generated in the near-surface region modify the surface sates. The near-band edge excitation directly affects the optical cross section of the surface states and the optical processes are faster than the thermal processes resulting in a single component in the SPV transients. During the super-bandgap excitation, both optical and thermal processes compete with each other resulting in a coexistence of fast (photo-assisted) and slow (phonon-assisted) components in SPV transients, with the relative intensity of the latter decreasing with the decrease of the energy of the photons. Although multi-component transient SPV were reported for both polychromatic or monochromatic excitation [55-58], to the best of our knowledge there were no studies performed on a systematic comparison of SPV transients for different excitation wavelengths for the same material, including NPS.

4. How does the onset slope of SPV in NPS depend on the illumination intensity?

The initial rate of the SPV change with the illumination intensity varies in NPS according to the 1/2-power law for all the wavelengths (325 nm, 442 nm and 632 nm) of a monochromatic excitation. For 325 nm and 442 nm, the dependence reaches a saturation regime at higher intensity values. It is possible that the photo-induced separation of charge carriers occurs not only due to the field present in the SCR but also due to the diffusion from the surface towards the bulk because of a very narrow SCR. Interference between the drift-mediated and the diffusion-mediated processes most likely limits the transport of excess carriers. As a result, the dependence of the slope of the SPV onset vs. light intensity changes from the linear behavior characteristic for bulk semiconductors [12, 55, 59, 60] to nonlinear.

5. Is there an impact on the SPV transients from metal nanoparticles embedded in NPS?

The embedded metal nanoparticles do not affect the SPV transients in NPS. Moreover, the surface photoresponse of the metal-embedded NPS revealed similar trends in the presence of both chemically active and inert gases, suggesting that that charge transport in NPS is pressure-selective and not gas-selective. The charge transport properties in pristine NPS were studied in many cases [38-41, 51-54]. To the best of our knowledge, the surface band bending in metal embedded NPS was not studied before. This kind of study is beneficial for the dual (optoelectronic gas and magnetic) sensor applications of metal-infused NPS-based composites.

6. Are the observed photoresponse phenomena NPS-specific?

We found that the behavior of SPV transients is not generic and varies from one material to the other. The surface barriers in SNT (with the largest diameter) and GC are sensitive to the ambient conditions revealing multiple transient SPV components, although behaving very

different from those in NPS. The surface band bending of SNT was affected by the size of the external diameter of the tubes. The transients associated with the thickest tubes revealed multiple transient SPV components whereas the tubes with smaller diameters showed only a single component during illumination. It is possible that the surface trapping at the Si/SiO_2 interface, the diffusion along the tubes, the drift due to the interface between tube and Si and chemisorption of the physisorbed species at the surface contribute to the multiple transients in the tubes with the largest diameters, whereas the surface trapping at the Si/SiO_2 dominates the charge recombination processes in the tubes with smaller diameters revealing transients with a single characteristic time.

Chapter 5

5. Future Work

There is another interesting type of nanostructured silicon material for which initial transient SPV measurements in different ambients have been carried out by us. This material (courtesy of Dr. Jeffery Coffer, Chemistry, TCU) was synthesized by a magnesiothermic reduction of biogenic silica plant extracts followed by acid treatment. These samples consist of nanocrystallites of Si embedded in silicon dioxide [99]. SPV transients observed for these nanosilicon specimens were different from what we observed for NPS grown by anodization. Both in N_2 gas and in vacuum, SPV transients revealed only one component during illumination and in the dark (Fig. 55). On the other hand, the behavior of the surface in N_2 gas was that of an *n*-type semiconductor with accumulated surface whereas in vacuum it revealed a depleted *n*-type nature. The model we have discussed for the anodized NPS could not explain the observed transient behavior in these NPS materials. Continuation of this study will be helpful to further investigate how the growth method or the change in morphology affects the charge dynamics in nanoscale silicon.

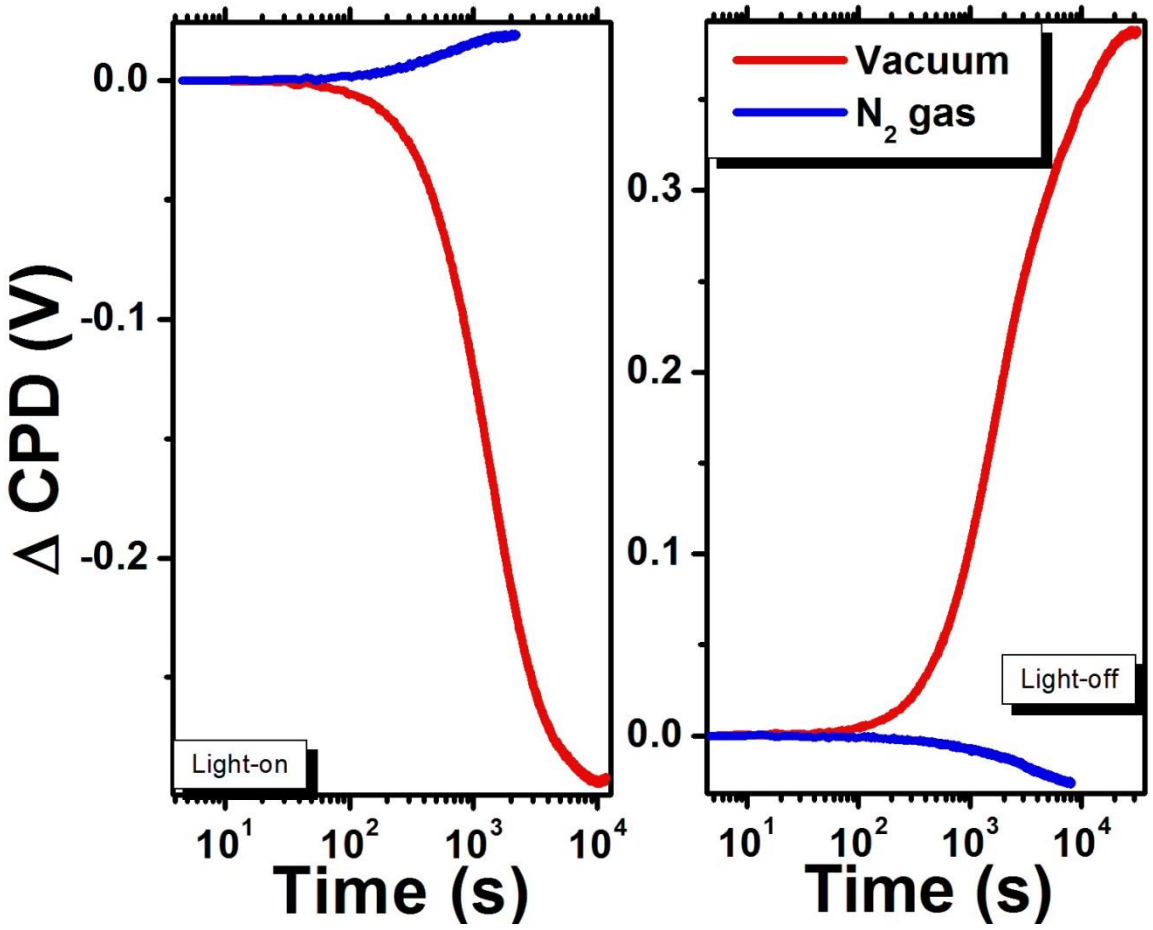

Figure 55 SPV transients for "bio-NPS" during (a) light-on process and (b) light-off process in N_2 gas and in vacuum.

References

1. J. L. Coffer, M. A. Whitehead, D. K. Nagesha, P. Mukherjee, G. Akkaraju, M. Totolici, R. S. Saffie, and L. T. Canham, *Phys*. *Stat*. *Sol*. *(A)* **202**, 8, 1451-1455 (2005).
2. V Lehmann, W Hönlein, H Reisinger, A Spitzer, H Wendt, and J Willer, *Thin Solid Films* **276**, 138-142 (1996).
3. A. Bratkowski, A. Korcala, Z. Lukasiak, P. Borowski, and W. Bala, *Opto-Electron Rev*. **13**, 35 (2005).
4. M. Casalino, G. Coppola, M. Iodice, I. Rendina and L. Sirleto, *Sensors* **10**, 10571-10600 (2010).
5. A. G. Cullis, L. T. Canham, and P. D. J. Calcott, *J*. *Appl*. *Phys*. **82**, 909 (1997).
6. L. Kronik and Y. Shapira, *Surf*. *Sci*. *Rep*. **37**, 1 (1999).
7. J. T. Yates, Jr., P. Hrvoje, *Chem*. *Rev*. **106**, 4113 (2006).
8. G. Polisski, D. Kovalev, G. Dollinger, T. Sulima, and F. Koch, *Physica B* 273, 951 (1999).
9. E. Rucavado, J.P. Badilla, and A. Ramírez-Porras, *ECS Transactions* 16, 299-303 (2008).
10. K. Q. Peng, X. Wang, and S-T. Lee, *Appl*. *Phys*. *Lett*. 95, 243112 (2009).
11. G. Amato, L. Boarino, and F. Bellotti, *Appl*. *Phys*. *Lett*. **85**, 4409 (2004).
12. S. C. Dahlberg, J. R. Chelikowsky and W. A. Orr, *Phys*. *Rev*. *B* **15**, 3163 (1977).
13. Z. Zhang and J. T. Yates, Jr., *Chem*. *Rev*. **112**, 5520-5551 (2012).
14. N. M. Kalkhoran, F. Namavar, and H. P. Maruska, *Appl*. *Phys*. *Lett*. **63** (19), 2661-2663 (1993).
15. E. Pastor, E. Matveeva, V. Parkhutik, J. Curiel-Esparza, M.C. Millan, *Phys*. *Stat*. *Sol (C)* **4**, 2136-2140 (2007).
16. K. Rumpf, P. Granitzer and P. Poelt, *Nanoscale Res*. *Lett*. **5**, 379 (2010).

17. A. Uhlir, Jr., *Bell System Tech*. *J*. **35**, 333-347 (1956).

18. L.T. Canham, *Appl*. *Phys*. *Lett*. **57**, 1046–1048 (1990).

19. E. G. Barbagiovanni, D. J. Lockwood, P. J. Simpson, and L. V. Goncharova, *J*. *Appl*. *Phys*. **111**, 034307 (2012).

20. A. J. Read, R. J. Needs, K. J. Nash, L. T. Canham, P. D. J. Calcott, and A. Qteish, *Phys*. *Rev*. *Lett*. 69, 1232 (1992).

21. J. F. Harvey, M. Shen, R. A. Lux, M. Dutta, J. Pamulapti, and R. Tsu, *Mater*. *Res*. *Soc*. *Symp*. *Proc*. 256, 175 (1992).

22. L. Tsybeskov, Yu V. Vandyshev, and P. M. Fauchet, *Phys*. *Rev*. *B* **49**,7821 (1994).

23. M. K. Lee and K. R. Peng, *Appl*. *Phys*. *Lett*. **62**, 3159 (1993).

24. S. M. Prokes, W. E. Carlos and O. J. Glembocki, *Phys*. *Rev*. *B: Condens*. *Matter Mater*. *Phys*. 50, 17093 (1994).

25. D. T. Jiang, I. Coulthard, T. K. Sham, J. W. Lorimer, S. P. Frigo, X. H. Feng and R. A. Rosenberg, *J*. *Appl*. *Phys*. 74, 6335 (1993).

26. H. Tamura, M. Ruckschloss, T. Wirschem and S. Vepek, *Appl*. *Phys*. *Lett*. **65**, 1537 (1994).

27. V. Lehmann and U. Gosele, *Appl*. *Phys*. *Lett*. **58**, 856 (1991).

28. T. V. Buuren, T. Tiedie, J. R. Dahn, and B. M. Way, *Appl*. *Phys*. *Lett*. **63**, 2911 (1993).

29. S. M. Prokes, *J*. *Appl*. *Phys*. **73**, 407 (1993).

30. L. R. Tessler, F. Alvarez, and O. Tbschke, *Appl*. *Phys*. *Lett*. **62**, 2381 (1993).

31. H. P. Maruska, F. Namavar, and N. M. Kalkhoran, *Appl*. *Phys*. *Lett*. **61**, 1338 (1992).

32. H. P. Maruska, F. Namavar, and N. M. Kalkhoran, *Appl*. *Phys*. *Lett*. **63**, 45 (1993).

33. K. Peng, X. Wang and S. Lee, *Appl*. *Phys*. *Lett*. **95**, 243112 (2009).

34. H. Ouyang, P. M. Fauchet, *Proc*. *SPIE*. **6500**, (2005).

35. P. Granitzer, K. Rumpf, and H. Krenn, *J*. *Nanomater*. **2006**, 1-7 (2006).

36. V.E. Primachenko, S.I. Kirillova, V.A. Chernobai, E.F. Venger, *Semiconductor Physics, Quantum Electronics & Optoelectronics* **8**, 38-54 (2005).

37. B Hamilton, *Semicond. Sci. Technol.* **10** 1187-1207 (1995).

38. P.K. Kashkarov, E.A. Konstantinova, A.B. Matveeva, V.Yu. Timoshenko, *Appl. Phys. A* **62**, 547-551 (1996).

39. V. Yu. Timoshenko and E. A. Konstantinova and T. Dittrich, *Semiconductors*. **32**, 1063-7826 (1998).

40. G. Faglia, C. Baratto, G. Sberveglieri, Z. Gaburro, L. Pavesi, *Proc. SPIE*. **5222**, (2003).

41. V. Duzhko, F. Koch, and Th. Dittrich, *J. Appl. Phys.* **91**, 9432 (2002).

42. S. Zhao, X. Lu, F. Zhang, H. Jiang, W. Wang, X. Hou and X. Wang, *J. of Phys. D-Appl. Phys.* **29**, 1326-1328 (1996).

43. V. Yu. Timoshenko, Th. Dittrich, V. Lysenko, M. G. Lisachenko, and F. Koch, *Phys. Rev. B* **64**, 085314 (2001).

44. V. Lehmann, F. Hofmann, F. Moeller, and U. Gruening, *Thin Solid Films* **255**, 20 (1995).

45. G. Polisski, D. Kovalev, G. Dollinger, T. Sulima, and F. Koch, *Physica B* **273**, 951 (1999).

46. L. A. Balagurov, D. G. Yarkin, and E. A. Petrova, *Mater. Sci. Eng., B* **69-70**, 127 (2000).

47. E. H. Poindexter, P. J. Caplan, B. E. Deal, and R. R. Razouk, *J. Appl. Phys.* 52, 879 (1981).

48. E. Rucavado, J.P. Badilla, and A. Ramírez-Porras, *ECS Transactions* **16**, 299-303 (2008).

49. L. Burstein, Y. Shapira, J. Partee, J. Shinar, Y. Lubianiker and I. Balberg, *Phys. Rev B.* **55**, 1829 (1997).

50. K. Q. Peng, X. Wang, and S-T. Lee, *Appl. Phys. Lett.* **95,** 243112 (2009).

51. L. Boarino, C. Baratto, F. Geobaldo, G. Amato; E. Comini, A.M. Rossi, G. Faglia, G. Lerondel, G. Sberveglieri, *Mater. Sci. Eng. B* **69–70**, 210–214 (2000).

52. T. Ozaki, M. Araki, S. Yoshimura, H. Koyama, and N. Koshida, *J*. *Appl*. *Phys*. **76**, 1986 (1994).

53. N. J. Pulsford, G. L. J. A. Rikken, Y. A. R. R. Kessener, E. J. Lous, and A. H. J. Venhuizen, *J*. *Appl*. *Phys*. **75**, 636 (1994).

54. J. P. Zheng, K. L. Liao, W. P. Shen, W. A. Anderson, and H. S. Kwok, *Appl*. *Phys*. *Lett*. **61**, 459 (1992).

55. M. A. Reschikov, M. Foussekis, and A. A. Baski, *J*. *Appl*. *Phys*. **107**, 113535 (2010).

56. E. Beyreuthera, A. Thiessena, J. Becherera, S. Grafströma, K. Dörrb, L.M. Enga, *Mater*. *Sci*. *Eng*. *B* **176**, 446–452 (2011).

57. E. Beyreuther, D. Paparo, A. Thiessen, S. Grafstrom, and L. M. Eng, *J*. *Appl*. *Phys*. **114**, 243709 (2013).

58. E. Beyreuther, J. Becherer, A. Thiessen, S. Grafström, L.M. Eng, *Surf*. *Sci*. **612** 1–9 (2013).

59. J. Lagowski, E. S. Sproles, and H. C. Gatos, *J*. *Appl*. *Phys*. **48**, 3566 (1977).

60. J. Lagowski, C. L. Balestra and H. C. Gatos, *Surf*. *Sci*. **29**, 203-212 (1972).

61. P Granitzer and K Rumpf, Semicond. *Sci*. *Technol*. **31** 014004 (2016).

62. X. Huang, R. Gonzalez-Rodriguez, R. Rich, Z. Gryczynskib and J. L. Coffer, *Chem*. *Commun*. **49**, 5760-5762 (2013).

63. S. B. Fagan *et*. *al*, *Phys*. *Rev*. *B* **61**, 9994 (2000).

64. M.-H. Park, M. G. Kim, J. Joo, K. Kim, J. Kim, S. Ahn, Y. Cui and J. Cho, *Nano Lett*. **9**, 3844 (2009).

65. J. Sha, J. Niu, X. Ma, J. Xu, X. Zhang, Q. Yang and D. Yang, *Adv*.*Mater*. **14**, 1219. (2002).

66. C. Mu, Y. X. Yu, W. Liao, X. S. Zhao, D. S. Xu, X. H. Chen and D. P. Yu, *Appl*. *Phys*. *Lett*. **87**, 113104 (2005).

67. J. Lan, D. Cheng, D. Cao and W. Wang, *J*. *Phys*. *Chem*. *C* **112**, 5598. (2008).

68. A. Soudi, P. Dhakal, and Y. Gua, *Appl*. *Phys*. *Lett*. 96, 253115 (2010).

69. A. Motayed, M. Vaudin, A. V. Davydov, J. Melngailis, M. He, and S. N. Mohammad, *Appl*. *Phys*. *Lett*. **90**, 043104 (2007).

70. Afsoon Soudi, Cheng-Han Hsu, and Yi Gu, *Nano Lett*. 12, 5111−5116 (2012).

71. W. Strek, B. Cichy, L. Radosinski, P. Gluchowski, L. Marciniak, M. Lukaszewicz, and D. Hreniak, *Light-Sci Appl*. **4**, 237 (2015).

72. S. Basu and P. Bhattacharyya, *Sensors and Actuat*. *B-Chem*. **173**, 1 (2012).

73. K. Toda, R. Furue, and S. Hayami, *Analytica Chimica Acta*. **878**, 43 (2015).

74. K. R. Raitinac, W. Wang, S. P. Ringer, F. Braet, *Environ*. *Sci*. *Technol*. **44**, 1167–1176 (2010).

75. J. T. Robinson et. al, *Nano Lett*. **8**, 3137-31401 (2008).

76. J. T. Robinson, J. S. Burgess, C. E. Junkermeier, S. C. Badescu, T. L. Reinecke, F. K. Perkins, M. K. Zalalutdniov, J. W. Baldwin, J. C. Culbertson, P. E. Sheehan, and E. S. Snow, *Nano Lett*. **10**, 3001 (2010).

77. J. Wang, B. Singh, J.-H. Park, S. Rathi, I.-y. Lee, S. Maeng, H.-I. Joh, C.-H. Lee, and G.-H. Kim, *Sensors and Actuat*. *B-Chem*. **194**, 296 (2014).

78. S. Prezioso, F. Perrozzi, L. Giancaterini, C. Cantalini, E. Treossi, V. Palermo, M. Nardone, S. Santucci, and L. Ottaviano, *J*. *Phys*. *Chem*. *C* **117**, 10683 (2013).

79. M. Cittadini, M. Bersani, F. Perrozzi, L. Ottaviano, W. Wlodarski, and A. Martucci, *Carbon* **69**, 452 (2014).

80. L. Kronik, N. Ashkenasy, M. Leibovitch, E. Fefer, and Yoram Shapira, *J*. *Electrochem*. *Soc*. **145**, 5, (1998).

81. R. M. Peters, Ph. D thesis, Texas Christian University, Fort Worth, 2010.

82. S.M. Sze, *Physics of Semiconductor Devices*, 2nd ed., Wiley, New York, 1981.

83. D. Gal, Y. Mastai, G. Hodes, L. Kronik, *J*. *Appl*. *Phys*. **86**, 5573 (1999).

84. L. Kore and G. Bosman, *Sol*. *Energy Mater*. *Sol*. *Cells* **57**, 31 (1999).

85. E. Kamieniecki, *J*. *Appl*. *Phys*. **54**, 6481 (1983).

86. B.I. Bednyi, M.I. Vasilevskii, I.A. Karpovich, *Sov*. *Phys*. *Semicond*. **23**, 223 (1989).

87. M. Foussekis, A. A. Baski, and M. A. Reshchikov, *Appl*. *Phys*. *Lett*. **94**, 162116 (2009).

88. H. Luth, *Solid Surfaces, Interfaces and Thin Films* (Springer, 2010).

89. L.J. Brillson, *Surfaces and Interfaces of Electronic Materials* (Wiley-VCH, Weinheim, 2010).

90. E. Fefer, L. Kronik, M. Leibovitch, Y. Shapira, W Riedl, *Appl*.*Surf*.*Sci*. **104**, 61-67 (1996).

91. H. C. Gatos and J. Lagowski, *J*. *Vac*. *Sci*. *Technol*. **10**, 130 (1973).

92. M. A. Reshchikov, S. Sabuktagin, D. K. Johnstone, and H. Morkoc, *J*. *Appl*. *Phys*. **96**, 2556 (2004).

93. E. A. Lebedev, E. A. Smorgonskaya and G. Polisski, *Phys*. *Rev*. *B* **57**, 14 607 (1996).

94. O. B Aphek *et*. *al*, *Surf*. *Sci*. **409**, 485-500 (1998).

95. D. Alamo, J. A. and R. M. Swanson, *Solid State Electron*. **30**, 11 1127-1136. (1987).

96. M. S Tyagi and R. Van Overstraeten, *Solid State Electron*. **26**, 6 577-598 (1983).

97. E. G. Barbagiovanni, D. J. Lockwood, P. J. Simpson, and L. V. Goncharova, *J*. *Appl*. *Phys*. 111, 034307 (2012).

98. J. C. Moore and C.V. Thompson, *Sensors* **13**, 9921-9940 (2013).

99. L. Batchelor, A. Loni, L. T. Canham, M. Hasan and J. L. Coffer, *Silicon*. **4**, 259–266 (2012).

VITA

Personal Background	Puskar Raj Chapagain Son of Khem Nath Chapagain and Laxmi Chapagain
Education	Master of Science, Physics University of Minnesota, Duluth, MN, 2009 Doctor of Philosophy, Physics Texas Christian University, Fort Worth, 2015
Experience	Teaching Assistantship, Texas Christian University Fort Worth, 2011-2015
Professional Memberships	Materials Research Society

ABSTRACT

SURFACE PHOTOVOLTAGE STUDIES OF ENVIRONMENTAL INFLUENCE ON CHARGE DYNAMICS IN NANOSTRUCTURED SILICON

By Puskar Raj Chapagain, Ph.D., 2015
Department of Physics and Astronomy
Texas Christian University

Dissertation Advisor:
Dr.Yuri M. Strzhemechny, Associate Professor of Physics

Optoelectronic properties of nanoscale materials are significantly affected by their surfaces because of the presence of intrinsic and extrinsic electronic states in the bandgap. Thermally or optically driven charge exchange between the bulk and these states directly affects the surface band bending of these materials. Physisorption, chemisorption or desorption of environmental species at the surface also bring in additional modifications to the surface electronic structure, thereby, changing the surface potential barrier. The focus of this work was to investigate the influence of the environmental conditions on the surface band bending in nanoporous silicon (NPS), as well as some other nanostructured materials, using transient surface photovoltage – a non-destructive and highly surface-sensitive experimental probe.

The potential barrier in NPS was monitored in a wide range of pressures, going down to high vacuum, and in a variety of gases. Due to the different rates of physisorption and chemisorption processes, we observed a coexistence of multiple components in the SPV transients occurring on different time scales and under different ambient conditions. We suggested a model elucidating the roles of intrinsic or extrinsic states in the surface transport

properties of NPS. The importance of results is discussed in relation to potential applications of the studied materials in optoelectronic gas sensors.

In order to distinguish between different surface charge transport processes affected by adsorption/desorption, we employed monochromatic illumination using several different wavelengths for selective excitation of these processes and compared these results with the ones observed for a polychromatic illumination containing both super- and sub-bandgap wavelengths. The scaling of transient SPV onset slopes in NPS vs. the excitation intensity was found to deviate from the linear dependence commonly observed in conventional bulk semiconductors. Considering drift- and diffusion-mediated surface charge redistribution, we discuss possible reasons for such discrepancy in nanoscale materials. We also performed transient SPV measurements for NPS filled with magnetic metal nanoparticles, in vacuum and non-vacuum environments, and found that the embedded filler does not affect the photoresponse of the material, a finding beneficial to potential dual spintronic/sensor applications.

Finally, using similar approaches, we compared results obtained for some other nanomaterials with those described above, and demonstrated that the behavior observed for NPS is not generic, but rather unique and germane to NPS.